The Institute of Paper Chemistry

Appleton, Wisconsin

Doctor's Dissertation

A Study of the Resistance
of Woven Wool Felts to Liquid Flow

James E. Macklem

June, 1960

A STUDY OF THE RESISTANCE OF WOVEN WOOL FELTS TO LIQUID FLOW

A thesis submitted by

JAMES E. MACKLEM

B.S. 1949, Beloit College
M.S. 1956, Lawrence College

in partial fulfillment of the requirements
of The Institute of Paper Chemistry
for the degree of Doctor of Philosophy
from Lawrence College,
Appleton, Wisconsin

June, 1960

TABLE OF CONTENTS

INTRODUCTION

An important process in the manufacture of paper on the commercial paper machine is the dewatering of the wet paper web in the press section. The wet web supported by a woven wool felt passes through the nip of the press rolls where water is caused to flow from the wet sheet into the felt and from the felt into the surrounding atmosphere. Before the complicated mechanism of water removal in the nip of the press rolls can be completely understood, the nature of the resistance presented by the woven wool felt to the flow of water through it must be considered.

The complex yarn and fiber orientation of the woven felt exclude it from the classes of porous media for which flow relationships have been established. The effect of such structural felt properties as weave, napping, and the number and size of the yarns per inch is not well understood. Commercial felt design has been largely a trial and error procedure aimed at finding the best combination of the above factors for a particular paper machine.

Flow normal to the felt and flow along the felt in the machine direction are both of importance in the nip of the press rolls. Because of the complex fiber and yarn orientation of woven felts, the resistance to flow is generally different in these two directions. Therefore, the flow resistance in each direction must be considered.

Because viscous, single-phase flow through porous media is understood better than other types, it was the only kind considered here. An understanding of viscous, single-phase flow through woven wool felts is certainly basic to any investigation of turbulent or two-phase flow.

HISTORICAL REVIEW

Previous work directly concerned with woven wool felts is limited. Studies concerned with flow through ordinary open-weave textiles are not applicable to the close weave and less highly twisted yarns of woven felts. Of interest to the present study, however, is the considerable amount of work done in recent years on the flow through porous beds of fibers with a random or a known orientation.

Previous work on the air permeability of woven textiles is concerned primarily with the inertial resistance of open-weave fabrics. Robertson (1), Backer (2), and Penner and Robertson (3) assumed that flow was mainly through the interyarn pores and considered them to behave like orifices. They worked out correlations between a modified Reynolds number and calculated discharge coefficients. Because the orificelike behavior of a fabric pore was dependent not only on the yarn diameter and yarns per inch but also upon the weave, difficulty was experienced in finding a characteristic pore dimension to generalize the correlation for all fabrics.

Goglia, et al. (4), studying the air permeability of parachute cloth, assumed the pressure gradient at an interior point of flow was due to the presence of inertial and viscous contributions combined linearly. They developed a correlation relating permeability to the effective pore diameter, the plane porosity, and the fabric thickness which fits data for screens and open-weave fabrics but not close-weave fabrics. Because the present investigation is concerned with viscous resistance in close-weave fabrics, the above work will not be considered further.

Cunningham, et al. (5) studied the flow of air, water, and oil through several porous filter media of a textile type including nonwoven and woven felts. A linear relationship between a Darcy-type resistance coefficient and the cloth weight was observed for viscous flow of air through the nonwoven, but not the woven, felts. The complex geometry of the weaves was believed to be the governing factor determining the resistance of the latter. Differences between air, water, and oil permeabilities were observed and attributed to wetting phenomena and degree of aeration of the liquid. The liquid flow data were correlated by a Reynolds-number-friction-factor-type relationship that did not include geometrical factors.

In the broad field of flow through porous media, generalized correlations of a modified friction factor and a modified Reynolds number have been proposed for streamline and turbulent flow. One of the more recent of these (6) uses as a basis the Reynolds-number-friction-factor plot for flow through smooth pipe. To use this correlation, values of the modified Reynolds number and the modified friction factor must be multiplied by suitable parameters that are functions of the bed porosity and the particle shape. Because correlations of this type are useful mainly in the turbulent-flow region, they will not be considered further here.

In the streamline-flow region, better characterization of flow in relation to the physical properties of the medium is possible. The resistance of the material to fluid flow, obtained from rate and driving-force relationships can be related to the shape, size, and orientation

of the particles comprising the bed. Particularly useful in this connection is the familiar Kozeny-Carman equation which expresses the viscous flow resistance of a porous material in terms of its porosity and the specific surface and orientation of the particles comprising the bed. This equation has been derived for the streamline flow of a noncompressible fluid through a porous bed under the following conditions. (1) The pore space may be regarded as a bundle of parallel capillaries with a common hydraulic radius and a cross-sectional shape representative of the average shape of a pore cross section. (2) The path of a streamline through the bed is tortuous, the average length being greater than the bed length. (3) The basic mechanism is capillary flow. (4) No pores are sealed off. (5) The pore size is uniform. (6) The pores are randomly oriented. (7) Diffusion and surface effects are absent.

Because of the importance of this equation to the field of flow through porous media and to the present work, a brief summary of its derivation will be given here. The original relationship was derived by Kozeny (7) and later modified by Carman (8). The derivation has been summarized by others, for example, Ingmanson (9), Scheidegger (10), and Whitney, Ingmanson, and Han (11).

Darcy's permeability equation for viscous flow through porous media modified to include the fluid viscosity may be stated as follows:

$$q = K \frac{A\Delta P}{\mu L} \qquad (1)$$

where q is the volumetric flow rate through a bed of cross-sectional area A and thickness L; ΔP is the frictional pressure drop across the bed; μ is the fluid viscosity, and K is the permeability coefficient.

Kozeny observed a similarity between this equation and Poiseuille's expression for the rate of streamline flow of a noncompressible fluid through a long, straight channel of constant, circular cross section. Poiseuille's law,

$$q = r_e^2 \frac{A_e \Delta P}{8 \mu L_e} , \tag{2}$$

where A_e is the cross-sectional area of a tube of length L_e and radius r_e, can be generalized for single channels of various cross-sectional shapes by substituting the mean hydraulic radius m for $r_e/2$ and k_o for the resulting numerical factor 2. (The hydraulic radius is defined as the ratio of the volume of channel to the area of wetted surface and for a circular pore is therefore equal to $r_e/2$.) Making these substitutions, the generalized form of Poiseuille's equation becomes

$$q = m^2 A_e \frac{\Delta P}{k_o \mu L_e} \tag{3}$$

where k_o, the channel shape factor, depends upon the shape of the pore cross section.

If one considers a randomly packed, porous bed, the cross-sectional area of the pore space is constant throughout the bed and equal to ϵA where ϵ is the porosity or void fraction of the bed. If an equivalent system of parallel similar capillaries is assumed per unit volume of the bed, the total volume and internal wall surface of the channels are

equivalent, respectively, to the void space and surface area of the material. The mean hydraulic radius is then equal to

$$\underline{m} = \frac{\epsilon}{\underline{S}_o} \tag{4}$$

where $\underline{S}_o$ is the effective surface area of the particles per unit bed volume.

If $\underline{u}$ is the superficial linear fluid velocity, the pore velocity parallel to the flow direction would be $\underline{u}/\epsilon$. Carman (8) pointed out that because the path taken by an element of fluid is tortuous, the correct pore velocity is given by

$$\frac{\underline{q}}{\underline{A}_e} = \underline{u}_e = \left(\frac{\underline{u}}{\epsilon}\right)\left(\frac{\underline{L}_e}{\underline{L}}\right) \tag{5}$$

because in a given time interval the fluid must move the tortuous distance $\underline{L}_e$, greater than $\underline{L}$.

Combining this concept of the pore velocity with Equations (1), (3), and (4), one obtains the following:

$$\underline{u} = \frac{\underline{q}}{\underline{A}} = \underline{K}\,\frac{\Delta \underline{P}}{\mu \underline{L}} = \left[\frac{\epsilon^3}{\underline{k}_o\left(\frac{\underline{L}_e}{\underline{L}}\right)^2 \underline{S}_o^2}\right]\left[\frac{\Delta \underline{P}}{\mu \underline{L}}\right]. \tag{6}$$

Thus, the permeability coefficient $\underline{K}$ is given by

$$\underline{K} = \frac{\epsilon^3}{\underline{k}_o\left(\frac{\underline{L}_e}{\underline{L}}\right)^2 \underline{S}_o^2}. \tag{7}$$

If the area of contact between particles is assumed negligible in comparison with the total effective surface area of the particles, the surface area per unit volume of particles, $\underline{S}_v$, will be given by

$$\underline{S}_o = \underline{S}_v(1 - \epsilon). \tag{8}$$

The product of the channel shape factor $\underline{k}_o$ and the tortuosity $(\underline{L}_e/\underline{L})^2$ is usually called the Kozeny constant $\underline{k}$. Substituting for $\underline{S}_o$ and $\underline{k}_o(\underline{L}_e/\underline{L})^2$ in Equation (7), one obtains the Kozeny-Carman equation,

$$\underline{K} = \frac{\epsilon^3}{\underline{k}\underline{S}_v^{\,2}(1 - \epsilon)^2}. \tag{9}$$

This equation has been experimentally verified for viscous fluid flow through unconsolidated beds of many different shaped particles including spheres, sands, powders, various textile fibers, and glass fibers by a great number of workers. Recent monographs by Carman (12) and Scheidegger (10) discuss in detail some of the significant findings of this previous work and therefore a review of this type will not be given here. The general conclusions of significance to the present work will be discussed, particularly those relating to beds of fibers.

In recent years the Kozeny-Carman theory has been used successfully to relate the specific filtration resistance of wood pulp fibers to the bed structure for conditions of both constant-pressure and constant volume filtrations (9, 13). In a recent review of filtration theory, Miller (14) states that "...the validity of the porosity-surface-resistance relationship as correlated by the Kozeny-Carman law is well established at least within the limits of engineering accuracy."

Some work has also been done on the application of the Kozeny-Carman equation to viscous fluid flow through consolidated porous media (15, 16). Consolidated media refer to those materials in which the

solid portion forms a continuous and permanent structure. These media, unlike randomly packed, unconsolidated beds, usually have nonuniform pore textures, high tortuosities, and different permeabilities in different directions. Because consolidated beds usually do not conform to the requirements of a random pore structure and a uniform pore size assumed in the derivation of the Kozeny-Carman equation and are characterized by high tortuosity, values of the Kozeny constant $\underline{k}$ are different from those observed for random, unconsolidated beds and in some cases become quite large.

For cases of more uniform pore texture, the effect of high tortuosity has been evaluated by an electrical conductivity technique (15, 16, 17). As a basis for this treatment, $\underline{k}_o$, the channel shape factor, is assumed to be constant for all pores in the consolidated bed and a tortuosity factor, $\underline{T}$, obtained by electrical conductivity measurements is equated to $(\underline{L}_e/\underline{L})$. Thus, for consolidated media, the Kozeny constant is given by the expression

$$\underline{k} = \underline{k}_o \underline{T}^2. \tag{10}$$

Studies (15, 16, 17) have shown good agreement between experimental and calculated permeabilities based on these assumptions for some consolidated media. This assumed relationship between electrical and hydraulic tortuosities is somewhat questionable, however, as one investigator (18) presents data for porous rocks that indicate the expression for the Kozeny constant should be

$$\underline{k} = \underline{k}_o \underline{T}. \tag{11}$$

Unfortunately, the technique has not been applied to beds of fibers, and the correct relationship, if it exists, is unknown.

Of particular interest to the present investigation is the work concerned with the application of the Kozeny-Carman theory to the permeability of fibrous beds. Those studies of importance to the present investigation will be briefly reviewed here.

In an investigation of the water permeability of wood pulp, rayon, and cotton fibers, Robertson and Mason (19) point out that the void fraction, ϵ, represents that portion of the bed volume available to the flowing liquid. Because their fibers were of irregular cross section and swell in water, the bed porosity was expressed as

$$\epsilon = 1 - \underline{v}\underline{c} \qquad (12)$$

where $\underline{c}$ is the mass of the fibers per unit volume of the bed and $\underline{v}$ is the effective specific volume of the fibers. Since the void fraction could not be determined directly from the bed density, $\underline{c}$, they rearranged the Kozeny-Carman equation in such a manner that a graphical treatment of permeability data taken at different bed densities would yield directly the values of effective specific volume, $\underline{v}$, and the product of the Kozeny constant and the square of the specific surface, $\underline{S}_w$, defined on a mass basis. The equation that they used, obtained by substituting the expression for ϵ given by Equation (12) in the Kozeny-Carman equation, is

$$(\underline{K}\underline{c}^2)^{1/3} = \left(\frac{1}{\underline{k}\underline{S}_w^{\,2}}\right)^{1/3} (1 - \underline{v}\underline{c}) \qquad (13)$$

where S_w, the surface area per unit mass is equal to vS_v. A plot of $(Kc^2)^{1/3}$ against c will be linear if the Kozeny-Carman equation applies, and the slope and intercept will yield respectively values of kS_w^2 and v.

Carroll and Mason (20) compared values of the specific volume of nylon, acetate, and viscose rayon fibers obtained by a displacement technique with those calculated from permeability data obtained with a nonswelling liquid and observed good agreement. Specific volumes, determined on the same fibers using water as the permeating liquid showed fair agreement with values calculated from moisture regain and centrifuging measurements.

Deviations of the data from the linear relationship predicted by Equation (13) were observed by Robertson and Mason (19) for porosities greater than 0.8, which they attributed to increasing values of the Kozeny constant with increasing porosity. Deviations of water permeability data from the predicted linear relationship at porosities below 0.5 were observed for bleached sulfite wood pulp by Carroll and Mason (20) and Mason (21). They believed this deviation was due to deformation of the fiber either by collapse of the lumen or deswelling of the fiber wall by the applied compressive load.

These same investigators (19-21) observed a decay in permeability with continued flow of liquid through the fibrous bed. Systematic experiments by Carroll and Mason (20) showed that the decay was most serious with highly swollen or very flexible fibers and was accelerated by liquid flow. They believed the decrease in permeability was caused

by a relaxation of internal stresses in the compressed pads causing a movement of fibers which would cause the Kozeny constant to increase. To minimize decay, they measured the flow rate as quickly as possible, released the stress on the pad, and momentarily reversed the flow direction before proceeding with the next measurement, Ingmanson, et al. (22) have stated that pressure drops in excess of 1% of the applied stress cause a mat deformation that results in a nonlinear relationship between pressure drop and flow rate.

Another form of the Kozeny-Carman equation found useful in analyzing flow through compressible porous beds is given by Fowler and Hertel (23). If one considers a porous bed so highly compressed that its void volume is zero, then the effective particle density and the bed density are the same and equal to $\underline{W}/\underline{AL}_o$ where $\underline{L}_o$ is the bed thickness at zero porosity and $\underline{W}$ is the mass of particles in the bed. Since the solid fraction of the bed is $\underline{L}_o/\underline{L}$, the porosity is given by

$$\epsilon = 1 - \underline{L}_o/\underline{L}. \qquad (14)$$

If this value of ϵ is substituted in Equation (9), the following form is obtained

$$(\underline{KL})^{1/3} = \left(\frac{1}{\underline{kS}_v^{\,2}\,\underline{L}_o^{\,2}}\right)^{1/3} (\underline{L} - \underline{L}_o) \qquad (15)$$

A plot of $(\underline{KL})^{1/3}$ against $\underline{L}$ will be linear if the Kozeny-Carman equation applies--that is, if $\underline{k}$, $\underline{S}_v$, and $\underline{L}_o$ are constant. Permeability values at different bed thicknesses can be used to evaluate $\underline{kS}_v^{\,2}$ and $\underline{L}_o$ simultaneously from which the effective particle density may be calculated.

A plot of Brown's (24) air-permeability data for beaten sulfite pulp fibers in the above form is linear for porosities of 0.56 to 0.88 but deviates from linearity for porosities lower than 0.56. Extrapolations of this curved portion of the plot gives a fiber density very nearly the same as that obtained for cellulose by displacement means. Brown believed that the Kozeny constant increased with decreasing porosity in the low-porosity range. Mason (21) pointed out that under the high compressive pressures used by Brown the effective specific volume of the fibers may decrease and gradually approach the specific volume of cellulose determined by gas displacement.

Several investigations have indicated the effect of fiber orientation and porosity variation on the value of the Kozeny constant. Fowler and Hertel (23), studying the air permeability of several randomly packed beds of different textile fibers, found excellent agreement between specific surface values calculated from microscopic measurements and those calculated from the Kozeny-Carman equation using an average value of the Kozeny constant of 5.55.

Sullivan and Hertel (25) studied the air permeability of carefully oriented beds of glass spheres and glass fibers for which the specific surface had been determined microscopically. For surfaces oriented at random, a value of the Kozeny constant of 4.5 ($\epsilon = 0.39$) was observed. For fibers parallel to the direction of flow, the Kozeny constant was equal to 3.0 ($\epsilon = 0.87$) and for fibers oriented perpendicular to the flow direction, k was 6.0 ($\epsilon = 0.81$).

From Emersleben's (26) mathematical treatment of flow parallel to uniform cylinders in square array, a decrease in the Kozeny constant with porosity may be predicted. Sullivan (27), in an investigation of flow through compact bundles of circular fibers oriented parallel to flow, observed an initial rapid decline in the Kozeny constant with porosity from 10.6 at a porosity of 0.98 to 3.0 at a porosity of 0.88 and a more gradual decline thereafter, to a value of 0.99 at a porosity of 0.35. Cotton fibers possessing an irregular cross section showed a much smaller decline in the Kozeny constant with porosity than the circular fibers. Incomplete parallel orientation of the fiber surfaces caused by convolutions and other irregularities was believed responsible for this difference. A decline in the Kozeny constant from 3.46 at a porosity of 0.93 to 2.31 at a porosity of 0.55 was observed for cotton fibers.

In an investigation of the air permeability of wool fibers oriented parallel to flow, Anderson and Warburton (28) observed that the Kozeny constant was fairly independent of porosity in the range 0.47 to 0.68 and had an average value of 2.0. Using fibers of different diameters, they observed values of the Kozeny constant ranging from 1.6 for coarse fibers to 2.5 for fine fibers. Since the coarse fibers were more easily straightened, they were probably more nearly straight and parallel. For the same fibers cut into short lengths and packed into random beds at a porosity of 0.7, they observed an average value of 6.1 for the Kozeny constant for all diameter fibers.

Roy and co-workers (29), studying the air permeability of fibers oriented parallel to flow, observed a variation in the Kozeny constant

with porosity for wool fibers very nearly the same as that observed by Sullivan for circular fibers in the porosity range 0.45 to 0.95.

An increase in the Kozeny constant with porosity was observed by Lord (30) for the flow of air through carefully randomized and uniformly distributed beds of textile fibers in the porosity range 0.77 to 0.99. Relatively higher values of the Kozeny constant were obtained for wool fibers than for cotton fibers under similar conditions. Differences in fiber cross section were believed responsible for the difference.

Studies of the air permeability of fibers oriented normally to the flow direction indicate an increase in the Kozeny constant with porosity at porosities greater than 0.80. Sullivan (31) observed such a variation for fibers parallel to each other and normal to flow. Davies (32) obtained an empirical equation for the variation in the Kozeny constant with porosity based on air-permeability data for filters formed from different fibrous materials. Davies' fibers were oriented primarily normal to flow but randomly in the x-y plane. Brown (24) observed an increase in the Kozeny constant with porosity from air-permeability data for glass fibers oriented normal to flow. He found that k varied less with porosity in a randomized bed than in the oriented bed. Ingmanson, et al. (22) observed an increase in the Kozeny constant with porosity from water-permeability measurements on beds of nylon and glass fibers oriented normally to the flow direction but randomly in the x-y plane.

Happel (33) presents a solution of the Navier-Stokes equations for viscous flow normal and for viscous flow parallel to a square array of circular cylinders. For each case, a derived expression for the variation in the Kozeny constant with porosity predicts a decrease in $\underline{k}$ with ϵ. Also on the basis of his analysis, the predicted value of the Kozeny constant for flow normal to the cylinders was about twice that for flow parallel to the cylinders at a given value of porosity. Happel points out that his analysis is probably not applicable at porosities lower than 0.4 to 0.5, but showed fair agreement with the results of others in the higher porosity range.

In a theoretical study of viscous flow normal to an infinite array of circular cylinders arranged in a hexagonal pattern, Shearer (34) used an electric resistance network analog to solve the Navier-Stokes equations. Although the values of the Kozeny constant he obtained were about four times those observed for beds of real fibers, the percentage variation of the Kozeny constant with porosity appeared to be the same as that obtained for randomly packed fiber beds at porosities greater than 0.8. Therefore, Shearer concluded that the variation in Kozeny constant with porosity was not due simply to a shift of the pore-size distribution with the degree of packing of the fibers.

Carman (35) points out that the assumption of flow through channels used in deriving the Kozeny-Carman equation no longer applies at high porosities. As the particles move farther apart, the situation becomes one of a fluid in relative motion to the particles.

The variation in Kozeny constant with porosity for flow parallel to beds of fibers can be attributed to a change in the channel shape factor, because the tortuosity $(L_e/L)^2$ would be unity for this case. Carman (35) points out that the very low values of Kozeny shape factor observed by Sullivan for flow parallel to beds of fibers of low porosity are reasonable from geometrical considerations. When the capillary walls approach to form relatively narrow spaces with sharp angles, shape factors near 1.0 are to be expected. In a bed of closely packed parallel fibers, channels of this shape would be expected to extend the length of the bed. However, in a randomly packed bed the flow channels are continually breaking up, dividing and reconnecting along the flow direction. Therefore, one may speak of an average channel shape which would vary little with porosity. Carman believes the average value of the shape factor for most porous beds should be about 2.5. Fowler and Hertel (23) believe an average value of 3.0 applies to the rather elongated cross sections present in fibrous beds.

Scheidegger (10) criticizes the Kozeny-Carman theory as being an oversimplified approach to the problem of flow through porous media, and proposes a statistical theory. However, as Ingmanson, et al. (22) point out, this approach is not sufficiently advanced for direct application to problems of interest, and the Kozeny-Carman theory, though oversimplified for flow through fiber beds of high porosity, does lead to intelligible results that can be related to experimental observations. The present investigation is not concerned with the high-porosity region, and the type of deviations from the Kozeny-Carman equation associated with highly porous fibrous beds are not expected to be too important.

Until recently no attempt had been made to test the applicability of the Kozeny-Carman theory to flow through woven filter media. Because woven wool felts possess a definite but complex orientation, they cannot be treated as random fibrous beds. Felts also do not strictly belong to the class of consolidated porous media because the solid portion of the fabric does not form a continuous and permanent structure. Grace (36) made a start toward the study of the flow resistance of woven textile filter media. In his study he observed good agreement between the average pore size of a woven felt calculated from the simple Kozeny-Carman equation from permeability data (obtained with a nonswelling liquid) and the modal pore size in the bulk of the felted structure obtained by a mercury intrusion technique. He assumed a value of 5 for the Kozeny constant. Because his work was concerned with a study of the pore-size distribution of different types of filter media, he obtained data for only one woven felt under one set of conditions. His results also indicated that 30 to 50% of the pore volume of many woven textiles consists of interfiber pores even for fabrics woven with high-twist yarns. These results indicate that the interfiber pores of textiles may be more important to fluid flow than was believed heretofore. Grace's work was concerned with woven textiles under no compressive load.

In an investigation published near the end of the present study, Ginn (37) compared the permeabilities of different commercial woven felts at various stages of compression. Air and water permeabilities for each sample were determined for the case of flow parallel to the warp yarns (lateral direction) as well as for flow normal to the felt.

The data were plotted on double logarithmic paper in the form permeability constant against Kozeny-Carman porosity function, and the deviation of the data for each felt from the predicted line of 45° slope was interpreted as an indication of the changing pore-size distribution of the felt. He concluded that the largest pores were affected most by compression initially, and as compression proceeded, the smaller pores changed more than the larger ones. A greater permeability was shown by all felts in the lateral direction than in the normal direction, which was believed due to a wider distribution of pore sizes in the lateral direction. Used felts showed a higher permeability and wider pore-size distribution than new felts, and fine felts had a lower permeability and narrower pore-size distribution than ordinary felts.

PRESENTATION OF THE PROBLEM

The review of the literature revealed that the validity of the Kozeny-Carman equation is well established for randomly packed fibrous beds of porosities 0.5 to 0.8. Several investigations have demonstrated the dependence of the Kozeny constant on the fiber orientation and the porosity of the bed. Investigations by Grace (36) and Ginn (37) have indicated that the Kozeny-Carman theory may be useful in the analysis of flow through woven wool felts.

In the present investigation, the effect of certain structural characteristics of woven felts on their flow properties was to be studied. It was expected that these structural characteristics would affect the flow resistance mainly through differences in fiber orientation. If the Kozeny-Carman theory could be established for flow through woven wool felts, the effect of the different fiber orientations on the flow resistance could be determined by comparing calculated values of the Kozeny constant for different felts with the values reported in the literature for fibrous beds of known structure.

Thus, the first objective of this investigation was to extend the Kozeny-Carman theory to flow through woven wool felts. Then if an independent measurement of the specific surface and the specific volume of the water-swollen wool fibers were made, these data in conjunction with the permeability results could be used to calculate values of the Kozeny constant for different felts at various values of pad density. Then the effect of the structural properties on the flow resistance could be evaluated.

Eleven felts were specially constructed to evaluate the contribution of four structural felt properties to the resistance of the felt to the flow of water. The experimental objectives were: (1) To measure the permeability of each felt sample at several pad densities for flow normal to the bed, (2) to measure the lateral permeability of each felt at several pad densities, (3) to measure the specific volume of the water-swollen wool fiber, and (4) to measure the specific surface of the water-swollen wool fiber for each sample. The data could then be used to validate the application of the Kozeny-Carman theory to flow through woven felts, and to ascertain the effect of the structural properties as well as different compressive loads on their resistance to flow.

EXPERIMENTAL SAMPLES

A discussion of the felt structures studied should be preceded by a brief description of the steps in the manufacture of a felt. The following paragraphs outline the manufacturing processes used to convert wool fibers into a felt.

Cleaned and dried wool fibers are laid down to form a thin, uniform sheet which is condensed into a cylindrical sliver. The fibers are then spun into a yarn by stretching and twisting this cylinder. Operations designed to align the fibers more or less parallel to each other may precede the spinning.

Following the spinning operation, the base structure of the felt is formed by weaving. Weaving consists of interlacing warp and fill yarns at right angles to form a fabric. The warp yarns extend lengthwise on a loom, and fill yarns (often termed picks) are passed between them in a definite pattern called the weave. The properties of the felt can be controlled by using warp and fill yarns of different diameter, varying the number of yarns per inch, and choosing different weaves.

After the basic wool fabric is formed, it is subjected to a long series of alternating compressions and relaxations in warm, soapy water of a controlled pH. The wool fibers migrate and become entangled. The felt may shrink as much as 50%, and a denser and more compact structure is obtained. This process is referred to as fulling.

If a felt is desired that will impart a smoother finish to the paper, it is napped by raising fibers on the surface. Napping is done on machines

with large cylinders equipped with small spindles covered with teazles. The spindles and teazles revolve in the direction opposite to that taken by the felt. Individual fibers are gently pulled up from the felt surface.

In the present investigation, it was desired to study the effect of basic weave, the number of picks per inch, the yarn size, and the felt finish (i.e., napped or natural) on the resistance of the felt to the flow of water. To observe the contributions of each of these variables to the flow resistance, it was desirable to have pairs of felts of known structure which were identical in all these properties but one. Differences in flow resistance between each pair could then be associated with the known structural difference.

With the co-operation of a local felt company, special felts were designed and manufactured which made possible the type of comparisons referred to above. Eleven felt samples were constructed which made possible the investigation of three weaves, three yarn sizes, napped and natural finishes, and two pick counts. In all felts, the number of warp yarns per inch, the yarn twist, and wool fiber type were the same. All samples were fulled. In any one felt, the warp yarn and fill yarn size were the same.

The structural properties of the eleven felt samples studied are given in Table I. Yarn sizes are given in the American cut system, the cut being the number of 300-yard hanks per pound. The weave patterns are shown diagrammatically in Fig. 1. The 5 & 1 sateen weave gives a cloth characterized by predominantly fill yarns on one surface and warp yarns on the other. The 3-3 plate weave is characterized by predominantly

TABLE I

STRUCTURE OF FELT SAMPLES

(All felts have 48 warp ends per inch.)

Sample Number	Basis Weight, g./sq. cm.	Weave Pattern	Picks per Inch	Yarn Size, American Cut System	Finish
1	0.0704	5 & 1 sateen	70	16	natural
2	0.0702	3-3 plate	70	16	natural
3	0.0552	3-3 plate	48	16	natural
4	0.0512	5 & 1 sateen	48	16	natural
5	0.0692	duplex	70	16	natural
6	0.0727	3-3 plate	48	11	natural
7	0.0514	3-3 plate	70	20	natural
8	0.0752	5 & 1 sateen	70	16	nap
9	0.0752	3-3 plate	70	16	nap
10	0.0545	duplex	48	16	natural
11	0.0595	3-3 plate	48	16	nap

fill yarns on both surfaces which envelop the warp yarns in the center. The duplex weave results in a cloth that appears to have a 5 & 1 weave on one surface and a broken twill weave on the other. The yarn orientation is therefore irregular with one surface predominantly fill yarn and the other approximately equally divided between fill and warp yarn.

The felt samples were not designed to attempt an investigation of all types presently manufactured. Those designs chosen are typical of many wet press felts, and most press felts now in use would be similar in most characteristics to one of the samples studied here.

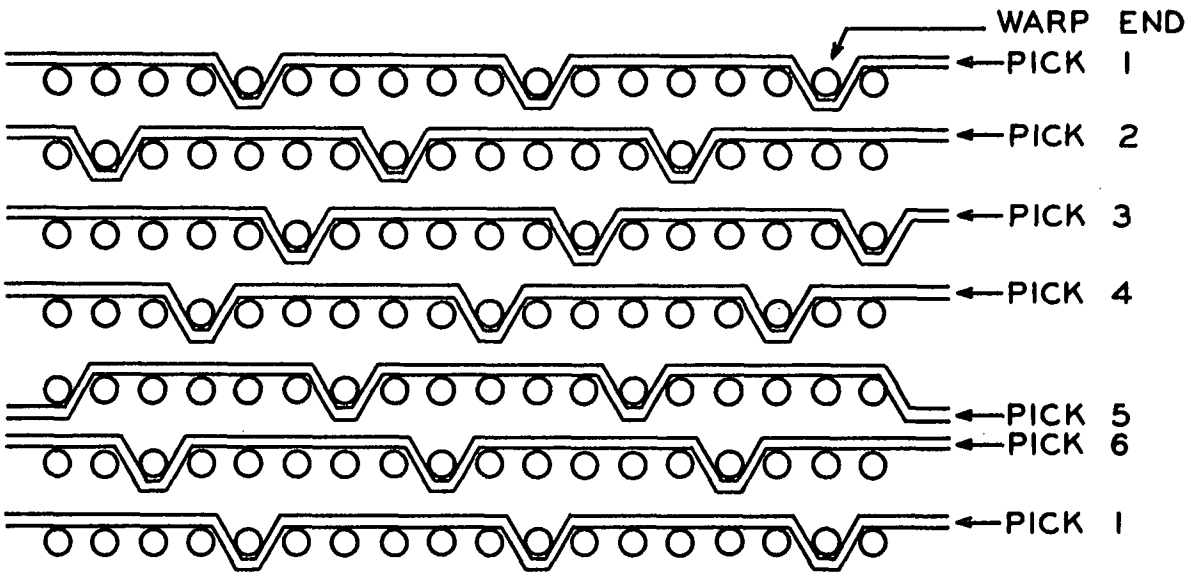

5 & 1 SATEEN WEAVE

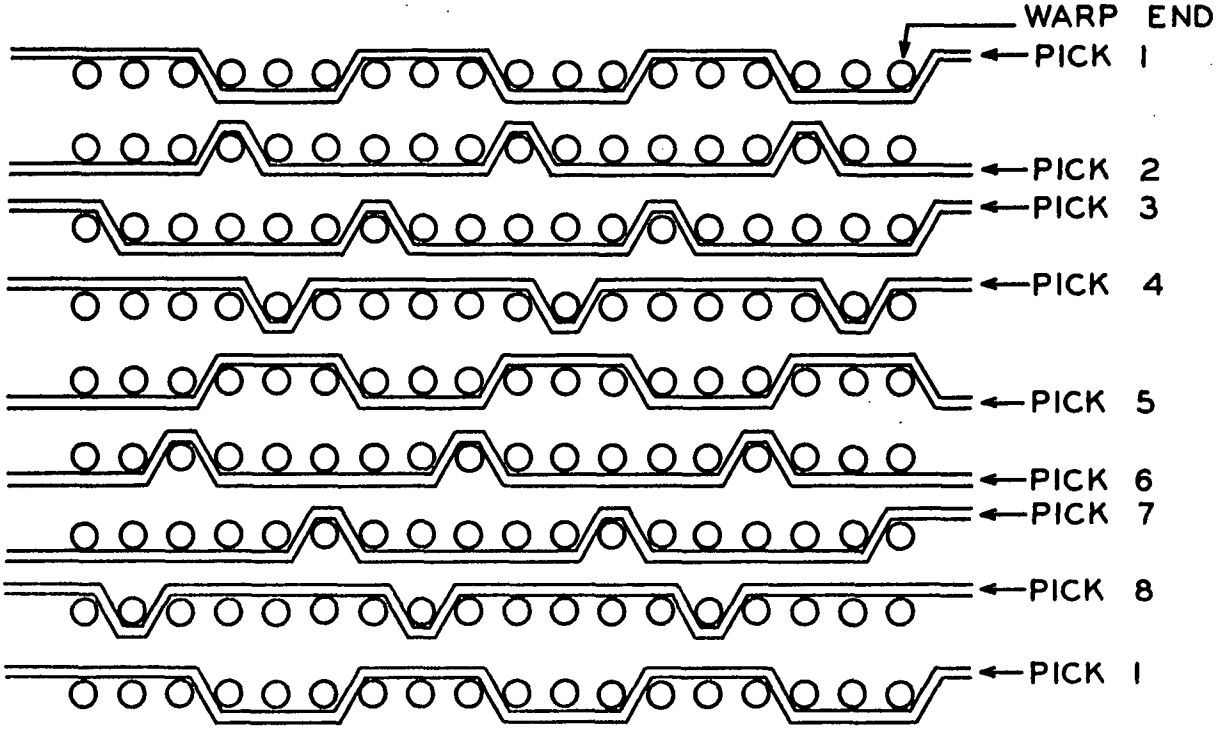

DUPLEX WEAVE

Figure 1. Weave Patterns

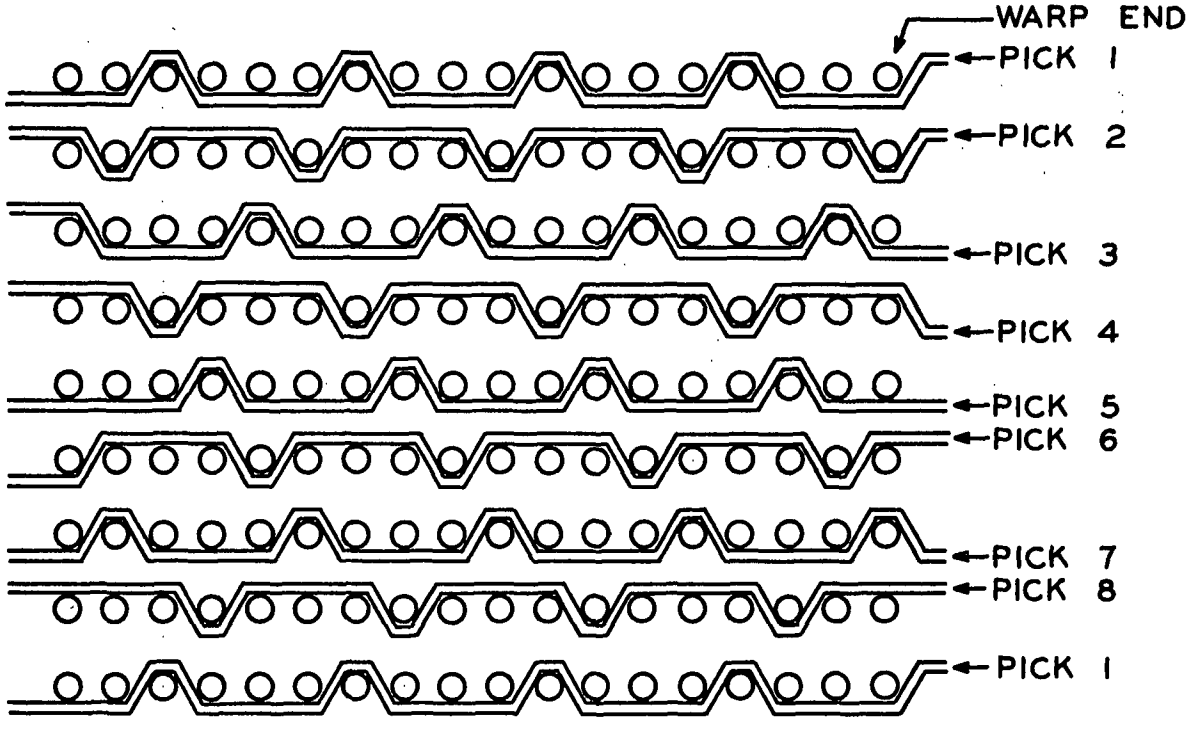

3 - 3 PLATE WEAVE

Figure 1 (Continued). Weave Patterns

EXPERIMENTAL EQUIPMENT

TRANSVERSE PERMEABILITY APPARATUS

The transverse permeability apparatus, shown in Fig. 2, incorporates some of the features of the filtration tube of Ingmanson (9). The major modifications in design required for this work were concerned with the necessity of applying large, constant compressive loads to the sample; the addition of a guarded zone to eliminate from consideration the decreased resistance around the edges of the precut pad; and the measurement of very small pad thicknesses.

The upper portion of the permeability tube consisted of a 4 1/2-inch inside diameter Plexiglas tube. To the top of this tube was cemented a Plexiglas flange, and to the top of this flange was cemented a 6 1/2-inch inside diameter Plexiglas tube. Two holes were drilled through this flange, and to each were cemented 1/2-inch plastic tubes, one of which was the water inlet and the other a constant-level overflow tube. A plastic scale was affixed to the inside of the 6 1/2-inch tube to permit reading of the water level. A Plexiglas cover was provided for the top of this tube to prevent contamination of the water supply during the course of the permeability determination.

The septum consisted of a 1-inch thick brass plate perforated over the flow area with 3/16-inch diameter holes on 1/4-inch centers, and faced with a 150-mesh screen backed by a 48-mesh screen. The septum was designed to provide the largest flow area consistent with the necessary strength required to transmit large pressures to the pad. A brass retaining ring was used to draw the 150-mesh screen tight and hold it in place.

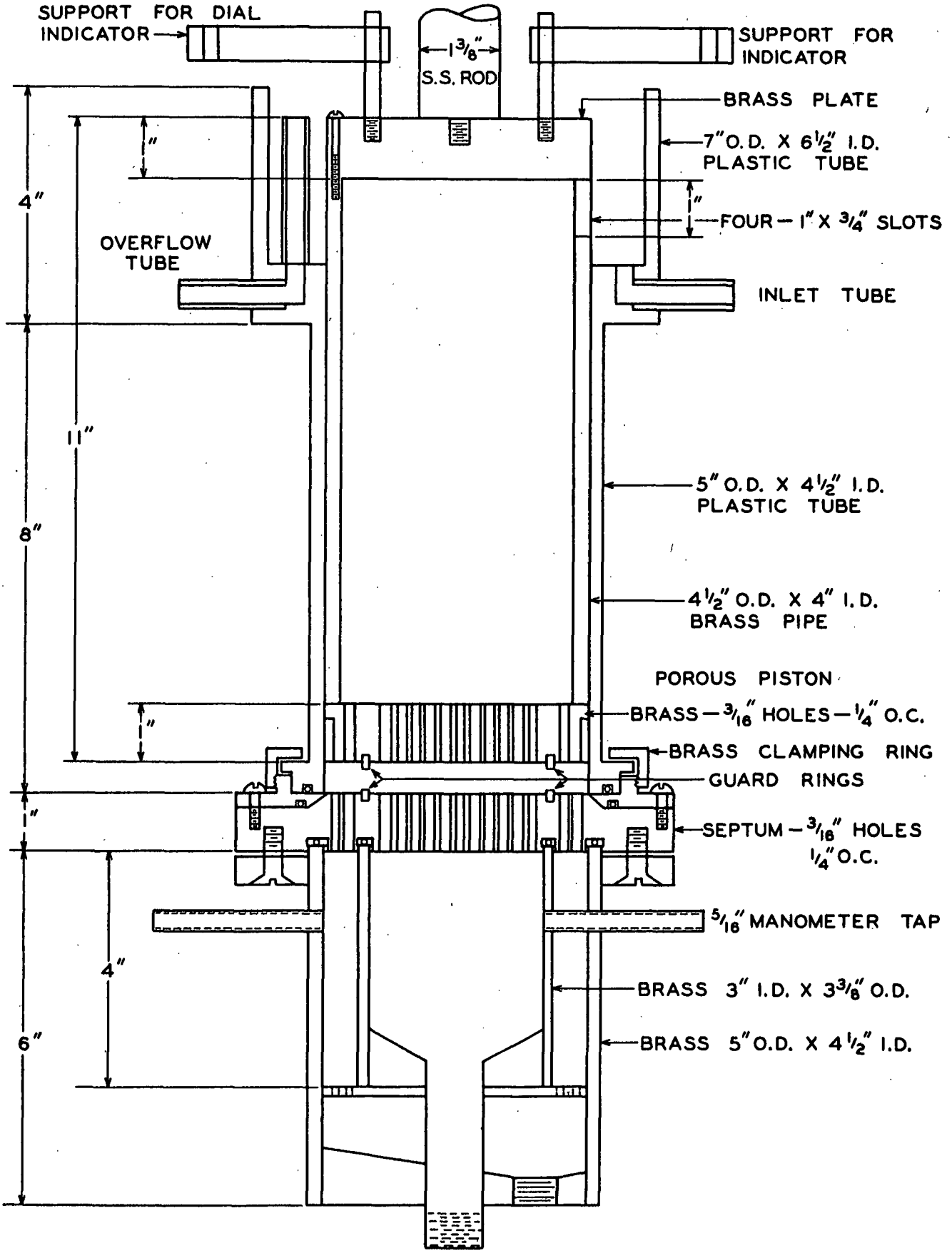

Figure 2. Transverse Permeability Cell

The plastic permeability tube was equipped with a brass clamping ring which screwed to the septum. A water-tight seal between the permeability tube and the septum was provided by a rubber "O" ring.

The piston consisted of an 11-inch length of 4 1/2-inch outside diameter brass pipe to one end of which was soldered a 1-inch brass disk perforated in the same manner as the septum. A 3/4-inch brass disk was attached to the opposite end of the piston to permit connection to the 1 3/8-inch stainless steel rod which transmitted the compressive pressure to the piston. Four 1 by 3/4-inch slots around the top circumference of the piston tube helped maintain the constant water level above the sample.

To prevent inaccuracies in the permeability determination caused by a decreased resistance at the pad edges and a resulting lateral flow, the apparatus was constructed in accordance with the annular guard ring principle of Carson (38), which has previously been used in permeability studies on paper (24, 39, 40). Therefore, provision was made to separate the flow through a center test area (guarded zone) of the pad from flow through the outer annulus of the pad. Formation of these two zones in the pad was accomplished by installing a narrow clamping ring on the face of the septum and on the face of the piston. These rings, exactly opposite each other, protruded slightly above their respective surfaces. Separate collection chambers and piping systems below the septum permitted separate flow control and, therefore, equalization of the pressure in the two chambers. Because the head of water above the sample was the same for both zones and the pressure below the sample was equalized in each zone, no lateral flow from the center section of the pad toward the edges would occur.

The guarded zone was constructed as follows: A groove, 3 inches inside diameter by 1/8-inch wide, was cut into the face of the septum and also into the face of the piston. The grooves were properly centered and were exactly opposite each other when the apparatus was assembled. Into each groove was placed a brass ring 3.000 inches inside diameter by 1/8-inch wide of a depth sufficient to protrude 0.005 inch above the adjacent finished surface. Another similar pair of brass rings designed to protrude 0.035 inch above the adjacent finished surface was provided for use at small compressive loads. Five countersunk brass screws were used to hold the rings in place.

A 1/8-inch annulus was cut from the 48-mesh backing screen to allow insertion of the brass ring. The 150-mesh screen was allowed to pass under the ring. The portions of the septum and piston directly beneath the rings were not perforated.

Flow from the inner guarded zone was kept separated from flow through the outer zone by means of a divided collection chamber below the septum. The inner portion of the chamber was constructed of a 3-inch inside diameter brass pipe 4 inches long, and was mounted inside a 4 1/2-inch inside diameter brass pipe 6 inches long. The bottom of each portion of the discharge chamber consisted of a brass plate soldered to the pipe and beveled toward a 1/2-inch outlet to which was soldered a short section of copper tubing. Screws were used to connect the septum to a brass flange soldered to the outer wall of the divided collection chamber. Rubber "O" rings, recessed in the lower side of the septum at the points of connection with the divided collection chamber, prevented leakage of water from either section.

A pressure tap was provided for each chamber at a point 1 inch below the bottom of the septum. To each pressure tap was connected a U-tube water manometer, one end of which was open to the atmosphere. The manometers were constructed by mounting 10-millimeter glass tubing on meter sticks. The water level in the manometer could easily be read to the nearest millimeter and estimated to the nearest 0.1 mm.

The transverse permeability cell was mounted in a heavy-duty frame so designed that the piston and septum remained parallel during compression. The compressive load was provided by a Blackhawk number 540, 4-ton hydraulic cylinder attached to the top of the frame and connected to the piston by means of the 1 3/8-inch stainless steel rod. This rod passed through a hole in the top steel bar of the frame. This hole, slightly larger than the rod, was placed in the center of a 3/16-inch wide by 10-inch long slot in the 4-inch by 1 1/2-inch steel bar. Machine bolts on either side of the hole at right angles to this slot, when tightened, caused the stainless steel rod to be held firmly in place. Therefore, when the desired pad thickness was reached and the bolts were tightened, continued compression or expansion of the pad was prevented. The separation of the piston face and the septum was obtained with dial indicators reading to 0.001 inch. Two indicators were mounted rigidly on opposite sides of the solid brass disk forming the top of the piston. The reference levels for the indicators were two 3/8-inch stainless steel rods mounted rigidly to each side of the base upon which the permeability cell rested; thus, the deflection of this beam during compression was automatically accounted for. The above features of the apparatus are shown in Fig. 3.

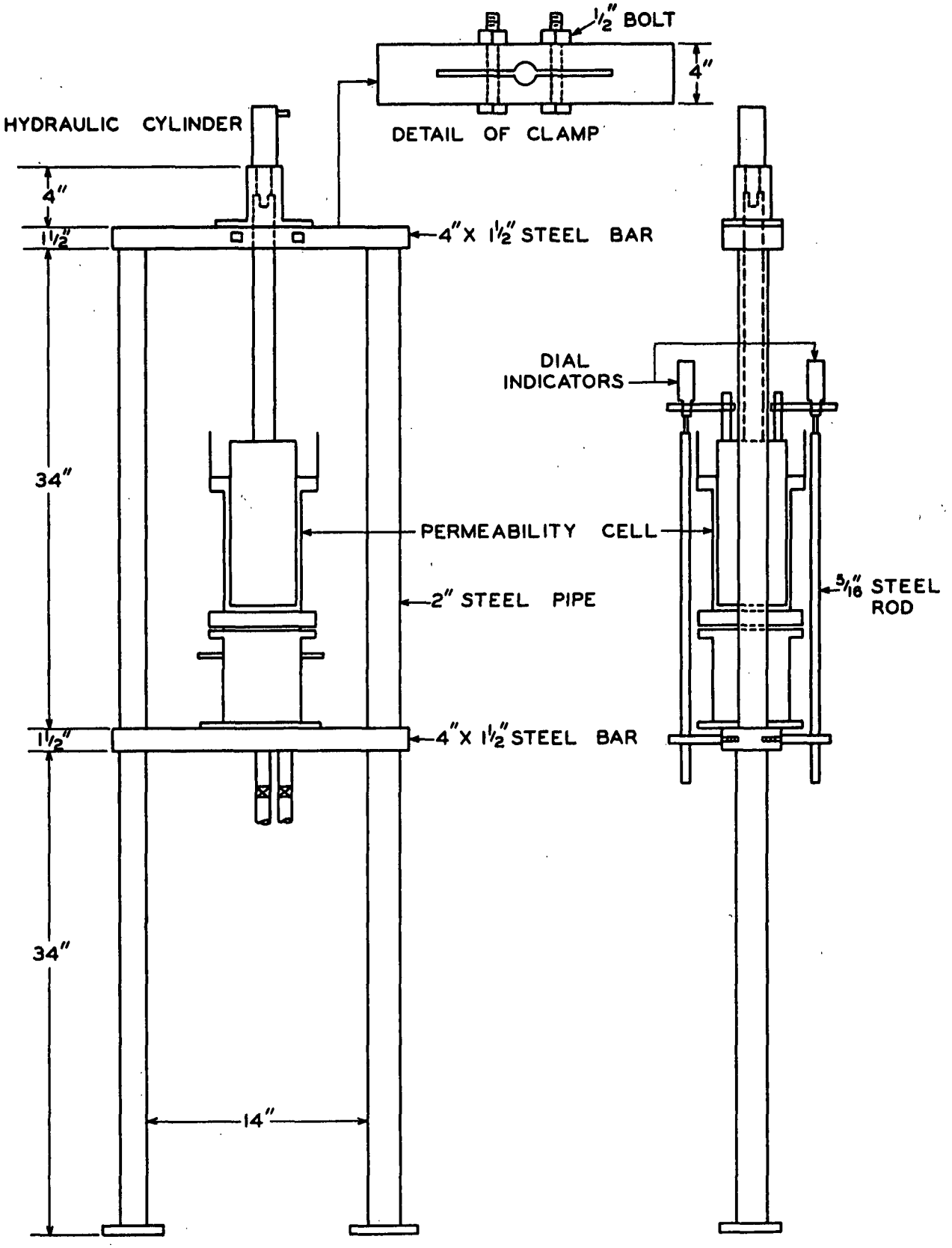

Figure 3. Stand for Permeability Cell

Separate piping systems were provided for each section of the discharge chamber of the permeability apparatus. Suction was applied to each chamber by means of a Roth model 020 turbine-type centrifugal pump (Roy E. Roth Co., Rock Island, Ill.) in each piping system. These pumps were provided with 1150-r.p.m. electric motors and were capable of providing small constant flow rates. The flow rate from each chamber could be regulated by means of needle valves in the discharge line from each pump and by means of needle valves in the by-pass lines connecting the suction and discharge of each pump.

Purified water, stored in glass containers, flowed by gravity into the permeability tube. The flow rate was adjusted with a pinch clamp on the rubber inlet hose. Water from the discharge side of the two pumps passed through Fulflo number BR-8 filtering units (Commercial Filters Corp., Melrose, Mass.) and was returned to the supply bottle. The flow rate through the test zone was measured with a Fischer and Porter rotameter (Fischer & Porter Co., Hatboro, Pa.) installed in the line between the septum and the suction side of the pump. Two meters of different capacities, numbers B4-22-10/77 and 2F-1/2-16-5/70, were connected in parallel with appropriate shut-off valves so that either meter could be used, and flow rates from 0.05 to 4000 cc./sec. could be measured. Thermometers reading to 0.1°C. were installed in the inlet and discharge lines. The piping layout is shown in Fig. 4.

LATERAL PERMEABILITY APPARATUS

The essential features of the lateral permeability apparatus are shown in Fig. 5. The permeability cell consisted of three main portions, namely, the head chamber, the compression jaws, and a divided

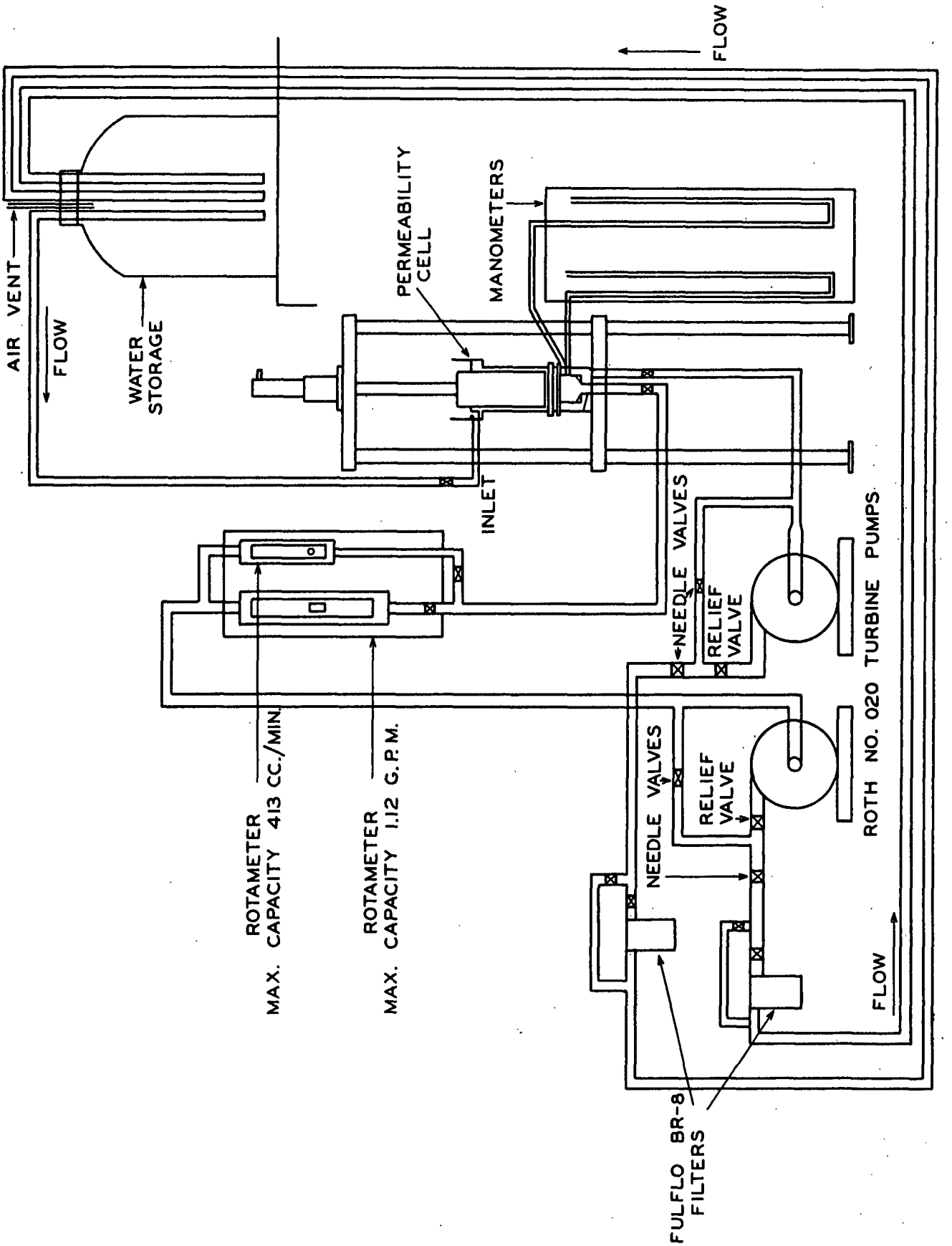

Figure 4. Permeability Apparatus Layout

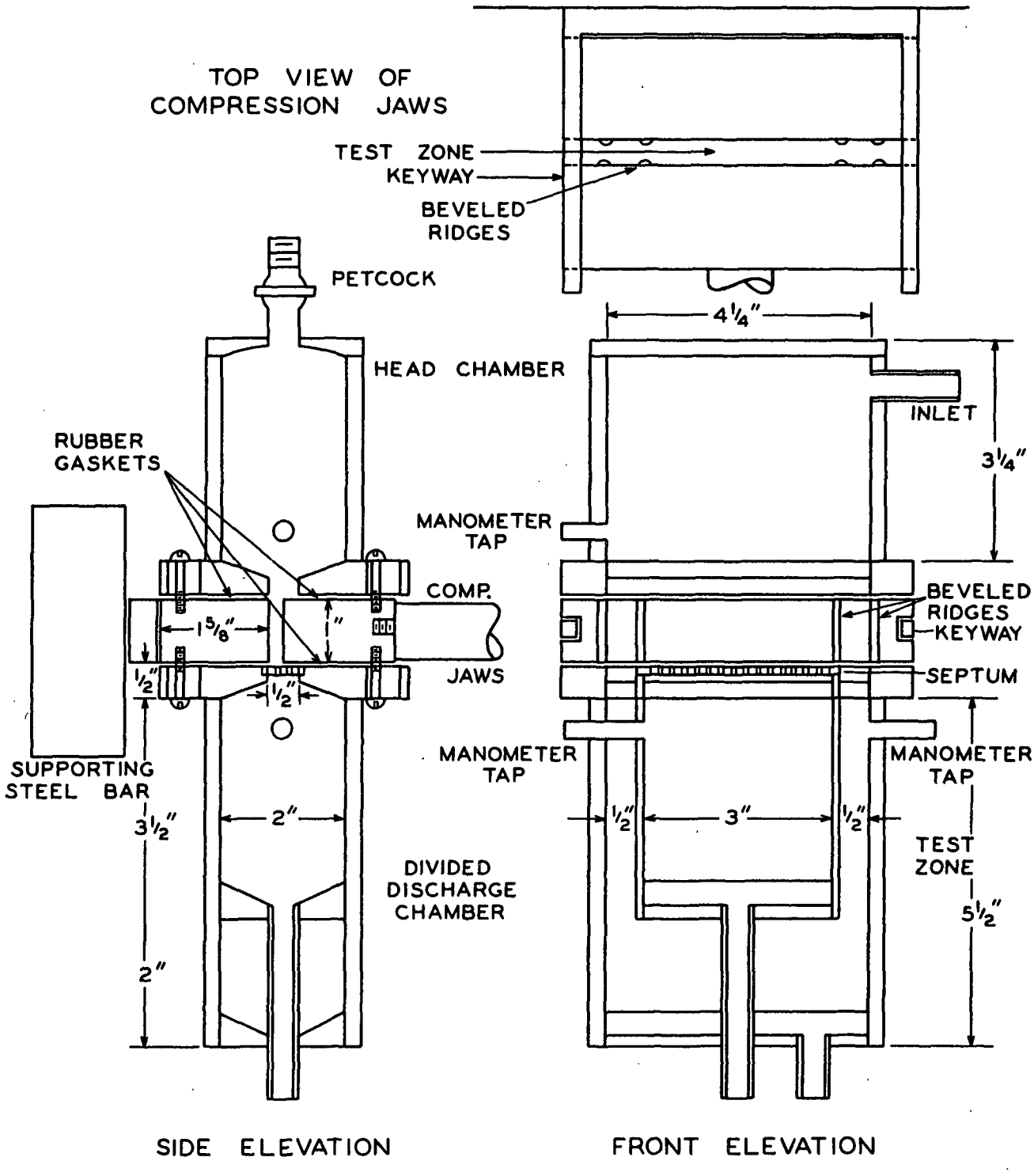

Figure 5. Lateral Permeability Cell

discharge chamber. As in the design of the previous apparatus, provision was made to eliminate sidewise flow to the pad edges. Flow through the center test area of the rectangular pad was separated from flow through the outer pad edges by constructing narrow, protruding ridges on the faces of the rectangular compression jaws. Separate flow collection chambers and piping systems below the sample permitted separate flow control from each zone and permitted equalization of the pressure in the two chambers. Because the pressure above the sample was the same for each zone and the pressure below the sample was equalized in each zone, sidewise flow from the center section of the pad toward its edges was prevented.

The compression jaws were constructed of solid pieces of brass, 1 by 5-3/4 by 1-5/8 inches, between which a 1 by 4 5/8-inch sample was compressed. Four vertical, beveled ridges, 1/8-inch wide by 1-inch long, which protruded 0.035 inch above the face of each jaw divided the flow area into a 3-inch center test zone and two 1/2-inch wide outer guard zones. The ridges at each end of the jaws caused the felt to act as a gasket to prevent leakage. Another set of jaws with ridges protruding 0.005 inch above the jaw face was used together or in combination with the above jaws for smaller pad widths. The opposing jaws operated on accurately aligned brass keyways, 1/4-inch square, fastened to a 4 by 1 1/2-inch steel base that acted as a support for the rear jaw. The sample was compressed by applying hydraulic pressure to the front jaw by means of the 7/8-inch stainless steel rod. The alignment and clamping arrangement provided for the 7/8-inch rod were the same as that described previously for the transverse permeability apparatus.

Accurately ground chromium-plated steel spacers, inserted between the jaws beyond the flow chamber, were used to set the desired sample width.

When the sample had been compressed to the desired width and the compression jaws were locked in place, the divided discharge chamber and the head chamber were fastened to the bottom and top sides, respectively, of the jaw pair. The rectangular head chamber, 4-1/4 inches by 2 inches by 3 inches inside dimensions, was constructed from 1/4-inch brass plate formed into a box and soldered to a 1/2-inch brass plate, 4 inches by 6 inches, provided with a center slot 4-1/4 inches by 1/2 inch. At each corner of this 1/2-inch plate, slots were provided for screws which were used to hold the head chamber to the compression jaws. A gasket of 1/32-inch rubber placed between the jaws and the head chamber prevented leakage. The inside surface of the 1/2-inch Plexiglas top of the head chamber was concave and was provided with a petcock at its highest point to allow air to leave the chamber as it was filled with water. The top of the petcock was provided with a screwed fitting to allow insertion of a Bourdon-type pressure gage. Screws were used to fasten the Plexiglas top to the brass head chamber. The head chamber was provided with a manometer tap and a water inlet connection.

The discharge chamber was constructed entirely of brass plate to the same over-all dimensions as the head chamber. It differed from the latter in having two compartments--one for collection of flow from the center test zone and one for collection of the flow from the two outer guard zones. Separate piping connections were provided for each chamber. A brass septum with countersunk 1/8-inch holes on 3/16-inch centers was

fitted into the slot in the top of the discharge chamber to prevent vertical deformation of the pad during flow. A 1/32-inch rubber gasket cut to fit the upper surface of the partitioned discharge chamber was installed between the compression jaws and this chamber to prevent leakage. Elongated openings for screws were cut at each corner of the slotted 4-inch by 6-inch by 1/2-inch brass plate forming the upper surface of the discharge chamber to permit the attachment of the compression jaws.

The discharge side of a Roth model 020 centrifugal pump was attached to the water-inlet connection of the head chamber. Pressure in the head chamber was controlled by adjustment of a needle valve in a by-pass line connecting the suction and discharge sides of the pump. The flow rate from each section of the discharge chamber was controlled with a needle valve located in the piping leading from each compartment. The rate of flow from the test zone was measured with the Fischer and Porter rotameters, previously described. Water from each section of the discharge chamber passed through a Fulflo BR-8 filtering unit before returning to the supply bottle. A thermometer reading to 0.1°C. was installed in the inlet line. The piping layout is shown in Fig. 6.

A pressure tap was provided for each section of the discharge chamber at a point 1 inch below the septum. To each of these pressure taps and to the pressure tap in the head chamber was connected a U-tube mercury manometer, one end of which was open to the atmosphere. The manometers were constructed by mounting 10-millimeter glass tubing on meter sticks. The mercury level in the manometer could be read to the nearest millimeter and estimated to the nearest 0.1 mm. Pressures in the head

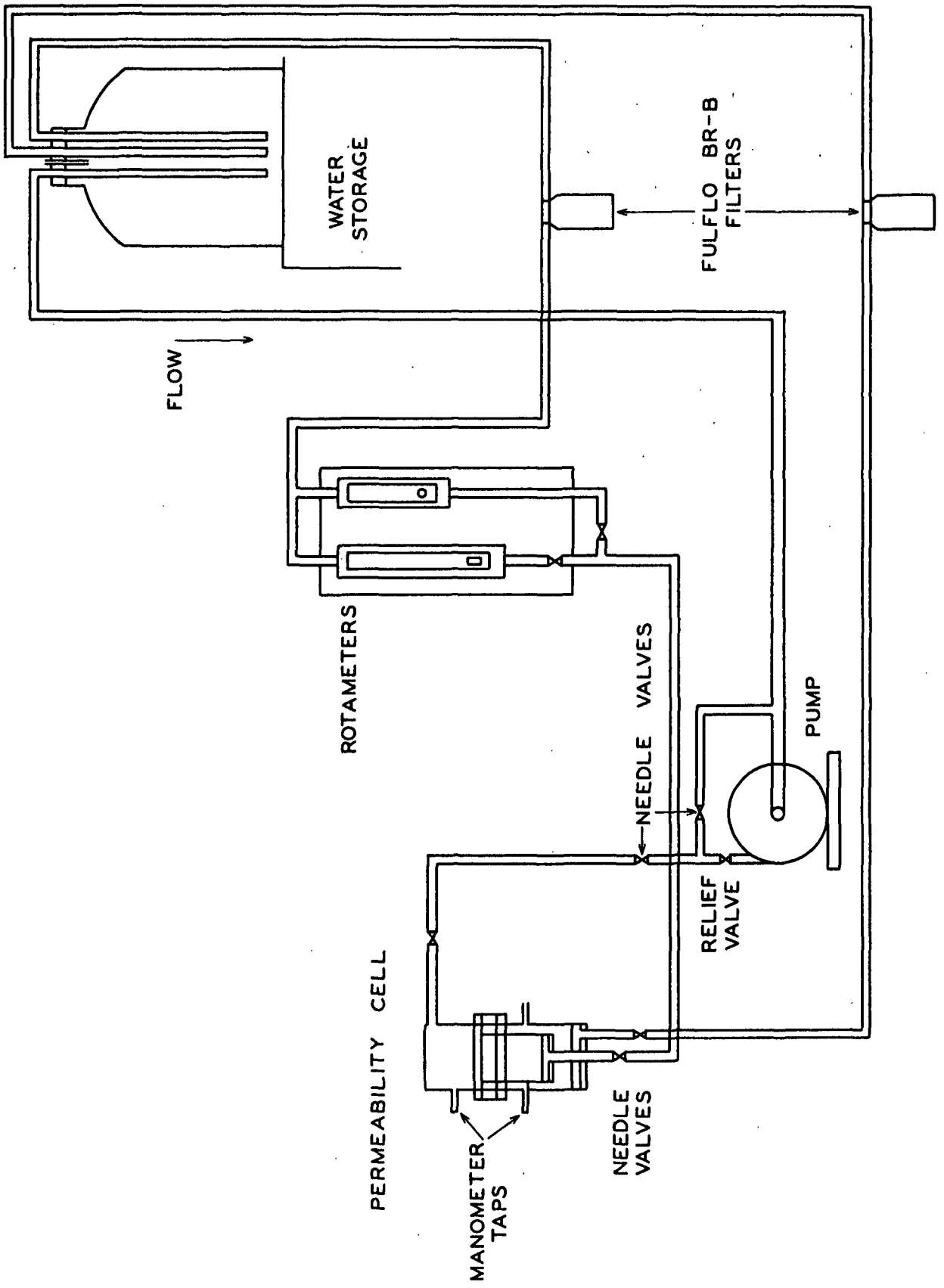

Figure 6. Lateral Permeability Piping Layout

chamber greater than 140 cm. of mercury were obtained with a calibrated Bourdon-type gage.

The permeability apparatus and the water storage bottles were maintained at a constant temperature of 25°C. $\pm$ 1°. Large temperature variations during the operation of the permeability apparatus and in the water storage bottles were thereby avoided, and corrections for viscosity changes were small.

EXPERIMENTAL PROCEDURES

WATER PURIFICATION

To obtain meaningful, reproducible permeability data, the purity of the water was found to be of great importance. Tap water was allowed to pass through a Fulflo model BR-8 cotton yarn filter and then through a Culligan (Culligan Co., Northport, Ill.) water-softening unit. The mineral used in the latter was very effective in filtering out the organic material present in the water. Following the Culligan unit, the water passed through a column of Amberlite MB-3 ion-exchange resin (Rohm and Haas Co.). This resin was a mixture of Amberlite IRA-140 anion exchanger, hydroxide form, and Amberlite IR-120, an acidic cation exchanger in hydrogen form. One pound of resin and a flow rate of 4 gallons per hour were used. The purified water was deaerated by boiling under vacuum in 5-gallon glass solution bottles. Water treated in this manner was found to have a specific resistivity greater than 250,000 ohm-cm. Water prepared in the above manner was used in all the experimental work.

PREPARATION OF SAMPLES FOR EXPERIMENTATION

Before the permeability of a felt sample could be determined, it had to be cut to size, cleaned, and completely saturated with deaerated water. Pieces of felt sample of suitable size were boiled in purified water under vacuum in a vacuum desiccator at 50°C. for 4-6 hours. The sample, while wet, was cut to exactly fit the appropriate apparatus. The circular sample was cut with a punch-type cutter consisting of an accurately machined steel disk around which was clamped a flexible steel

blade. The rectangular sample was cut with a similar cutter consisting of an accurately machined rectangular bar to which was clamped a flexible steel blade. The force needed to cut the felt was applied to the top of the sample cutter by means of a hydraulic press. Cutting the samples while wet avoided any change in dimensions between dry and wet samples. After being cut to size, the felt samples were again boiled under vacuum in clean, purified water at 50°C. for 4 to 6 hours. The last step was repeated to insure that the sample was clean and water-saturated.

TRANSVERSE PERMEABILITY DETERMINATION

DETERMINATION OF THE SEPTUM AND PISTON RESISTANCE

The septum and piston were designed to have as small a resistance to flow as was consistent with their required strength. This resistance was not negligible at the highest flow rates used, particularly where the felt resistance being measured was small. Therefore, careful evaluation of the piston and septum resistance was necessary to permit correction of the permeability data for it.

If flow through the septum and piston is streamline, the permeability (reciprocal of resistance) may be defined by Darcy's equation

$$\underline{K} = \frac{\underline{q}\mu}{\underline{A}\Delta\underline{P}} . \qquad (16)$$

A plot of the frictional pressure drop across the septum and piston versus the flow rate will be linear, and the permeability may be obtained from the slope of the line. Considering the felt sample and the piston and septum as resistance in series, the total resistance would be equivalent to their sum. Therefore, at any flow rate where the resistance of the

piston and septum is not negligible, the true resistance of the felt sample would be the difference of the experimentally observed resistance and the resistance of the piston and septum at that flow rate.

The procedure for determining the flow resistance of the piston and septum was the same as that used in the determination of transverse permeability. Since only the resistance of the center test-zone portion of the piston and septum was desired, the guard-zone portion was not used. A constant water level was maintained in the constant head chamber by adjusting the pinch clamp on the rubber inlet hose until a small steady stream of water flowed out the overflow tube. The needle valves in the pump discharge and by-pass lines were adjusted until the desired flow rate through the test zone was observed on the rotameter. The frictional pressure drop was obtained as the difference in the water level in the manometer when no flow occurred and when flow proceeded at the desired rate. Because the pressure differences were small, the levels in the manometer were obtained with a cathetometer reading to $\pm$ 0.01 cm. The data are plotted in Fig. 7.

PERMEABILITY MEASUREMENT

Before introducing the water-saturated felt sample into the permeability tube, the guard rings were removed from the septum and piston; the dial indicators were securely fastened to their supports on the head of the piston; and with the aid of a Bourdon-type gage, installed on the hydraulic pump, indicator readings were obtained as a function of the compressive load applied to the piston. Having obtained the zero indicator readings, the piston was removed from the permeability tube; the guard rings

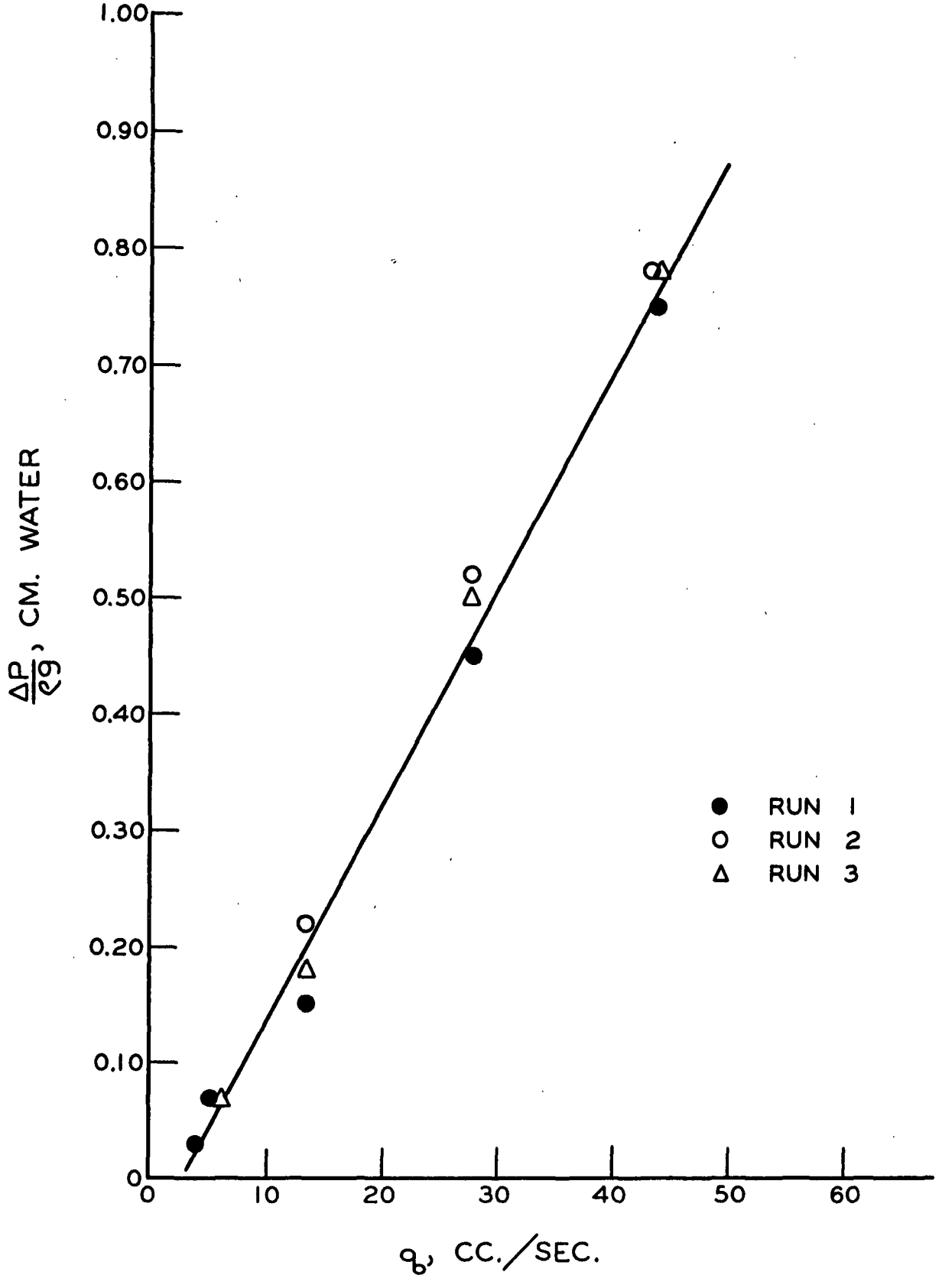

Figure 7. Resistance of Septum and Piston at 25°C.

were installed on the septum and piston; the tube was filled with purified water; the water-saturated sample was quickly transferred to the septum from the vacuum desiccator in which it had been boiled; and the piston was carefully replaced in the permeability tube. In this procedure it was important to remove all air bubbles adhering to the surface of the sample or the piston. Such air bubbles were removed by alternate compressions and relaxations of the sample, accomplished by manually moving the piston up and down in the permeability tube. Air bubbles were removed from the septum before insertion of the sample by slowly filling the septum with water from below.

The sample was compressed to the desired thickness by applying hydraulic pressure to the piston. The felt thickness was obtained as the difference between the indicator readings with the sample in place and the zero indicator readings at the same applied compressive load. After the sample had been compressed, the stainless steel rod connecting the piston and the hydraulic cylinder was secured by tightening the bolts in the clamping device described previously. Continued compression or relaxation of the sample was thus prevented.

With the sample in place, flow was initiated by starting the pump connected to the test zone. The needle valves in the discharge and by-pass lines were adjusted until the desired constant flow could be observed on the appropriate rotameter. The pinch clamp on the rubber inlet hose was adjusted to permit a somewhat larger flow to enter the permeability tube. The pump connected to the guard zone was started, and the needle valves in its discharge and by-pass lines were adjusted until the pressure in each compartment of the discharge chamber was the same. Flow

to the constant head chamber was readjusted as needed until a slight flow proceeded through the overflow tube and the constant water level used in all determinations was observed on the scale. Readjustment of the needle valves in each discharge line was made as needed to obtain the desired flow rate and keep the pressure equal in both discharge compartments. Lateral flow from the test zone to the guard zone was thereby minimized. The reference level for all pressure-drop measurements was the water level in the manometers when no flow proceeded through the sample and conditions in the constant head chamber were the same as during a run. The pressure drop at a given flow rate was the difference between this reading and the manometer reading at the given flow rate minus the pressure drop across the septum and piston. Manometer readings were estimated to the nearest 0.1 mm.

Readjustment of the various flow-control valves discussed above permitted the determination of the pressure drop across the sample at several different flow rates. A series of such flow rate-pressure drop data were obtained for each felt sample at several different values of pad density.

Pad decay (that is, an increase in the pressure drop across the pad with a continued constant flow) was found to be serious under certain conditions. Permeability decay of fibrous beds has been observed by others (19-21) and has been attributed to a movement of the fibers with flow causing an increase in the length of the tortuous path taken by the liquid through the bed. In the present study, decay was minimized by using flow rates as small as possible and reading the manometer as soon as equilibrium conditions had been reached. Pressure drop-flow rate data

were obtained at a given pad density by starting with low flow rates and advancing to higher flow rates. As soon as the manometer was read at a given flow rate, the flow was increased quickly to the next desired flow rate to minimize the time during which flow proceeded through the pad, To further minimize decay, the load on the sample was removed at the end of a series of flow rate-pressure drop determinations at a given pad density, and the pad was allowed to expand to its original uncompressed depth. After a period of twenty to thirty minutes, the pad was compressed to a new pad density and another series of flow rate-pressure drop data were obtained.

Immediately following the series of flow rate-pressure drop readings at different pad densities, the pad was removed from the apparatus, transferred to a tared weighing bottle, and dried at 105°C. to constant weight. This value was used to calculate the pad density at each pad thickness.

Using the above procedure, the reproducibility of the flow rate-pressure drop data at different pad densities was determined on a single felt pad from Felt Sample no. 1. A series of flow rate-pressure drop measurements were taken at a given pad density. At the conclusion of the run, the loading was removed from the pad, and it was allowed to expand to its original thickness. The sample was then compressed to the same pad density and the run repeated. Three separate runs were made at a given pad density in this manner, and the average deviation of the pressure-drop readings at each flow rate was computed. This procedure was repeated at two other values of pad density. The average deviation of the pressure drop values at a given flow rate and pad density was 2%. A summary of the results is given in Table II.

TABLE II

REPRODUCIBILITY OF TRANSVERSE PERMEABILITY DATA

L = 0.153 cm. c = 0.460 g./cc.

q, cc./sec.	$\Delta P/\rho g$, cm. of water				Av. Dev., %
	Run 1	Run 2	Run 3	Av.	
0.89	0.70	0.70	0.75	0.72	2.8
1.89	1.60	1.40	1.55	1.52	5.3
2.88	2.40	2.20	2.55	2.38	5.0
3.90	3.50	3.20	3.55	3.42	4.1
4.91	4.50	4.50	4.55	4.52	0.4
6.00	5.55	5.60	5.65	5.60	0.5
				Av.:	3.0

L = 0.127 cm. c = 0.555 g./cc.

0.89	1.65	1.65	1.65	0.0
1.41	2.60	2.55	2.57	0.6
1.89	3.50	3.45	3.47	0.6
2.39	4.60	4.45	4.52	1.5
2.88	5.60	5.70	5.65	0.9
3.40	6.80	6.90	6.85	0.7
			Av.:	0.7

L = 0.104 cm. c = 0.675 g./cc.

0.15	0.70	0.70	0.70	0.0
0.48	2.35	2.55	2.45	3.9
0.89	4.80	4.65	4.73	1.5
1.41	7.45	7.40	7.42	0.3
1.89	10.55	10.45	10.50	0.5
2.39	14.15	13.50	13.82	2.3
			Av.:	1.4

Duplicate or triplicate runs at each pad density were made using different pads from the same felt sample to insure results representative of that type of felt.

LATERAL PERMEABILITY DETERMINATION

DETERMINATION OF THE CELL RESISTANCE

The resistance of that portion of the lateral permeability cell containing the test sample was determined to estimate its significance to the lateral-permeability measurement. Small pieces of felt were placed between the compression jaws across the 1/2-inch guard chamber at either end of the test zone and with the aid of the chromium-plated spacers the jaws were positioned to leave an opening in the center test zone of 0.107 cm. The discharge chamber was filled with water and screwed to the bottom of the compression jaws. The head chamber was screwed to the top surface of the jaws, connected to the piping system, and filled with water, using the petcock to remove entrapped air. The valve controlling flow from the center test zone was opened, and the valve controlling flow from the guard zone was closed. The pump was started, and the needle valves in the discharge and by-pass lines at the pump were adjusted until the desired flow rate was observed on the rotameter. The fluid pressures in the head chamber and in the discharge chamber were obtained from the appropriate mercury manometers. Since the manometer tap in the discharge chamber was 11 cm. below the manometer tap in the head chamber, the pressure drop across the test area was the difference in the fluid pressure in the two chambers minus the difference in fluid head between the two points where the pressure was measured. A

series of flow rate-pressure drop readings were made in the above manner to determine the resistance of the sample holder from Equation (16). The data are plotted in Fig. 8.

At the small flow rates and large pressure drops used in the lateral permeability determinations, the cell resistance was insignificant and was therefore neglected in the calculations.

PERMEABILITY MEASUREMENT

To insert the water-saturated felt sample, the head chamber had to be removed and the discharge chamber had to be loosened to permit movement of the compression jaws. After placing the accurately cut sample between the jaws, spacers of the desired size were placed at each end of the jaws; and the jaws were brought together with the aid of the hydraulic cylinder. The stainless steel rod connecting the front jaw and hydraulic cylinder was held in place by the clamping arrangement described previously. The discharge chamber, previously filled with water, was tightened to the jaws. The head chamber was screwed to the top of the compression jaws, connected to the piping system and filled with water.

Valves in the inlet and discharge lines were opened, the pump started, and the needle valve in the pump by-pass line was adjusted until the desired flow rate was observed on the rotameter. The needle valves below the divided discharge chamber were adjusted until the pressure in each section of the discharge chamber was the same. The needle valve in the pump by-pass line was readjusted if necessary to return to the desired

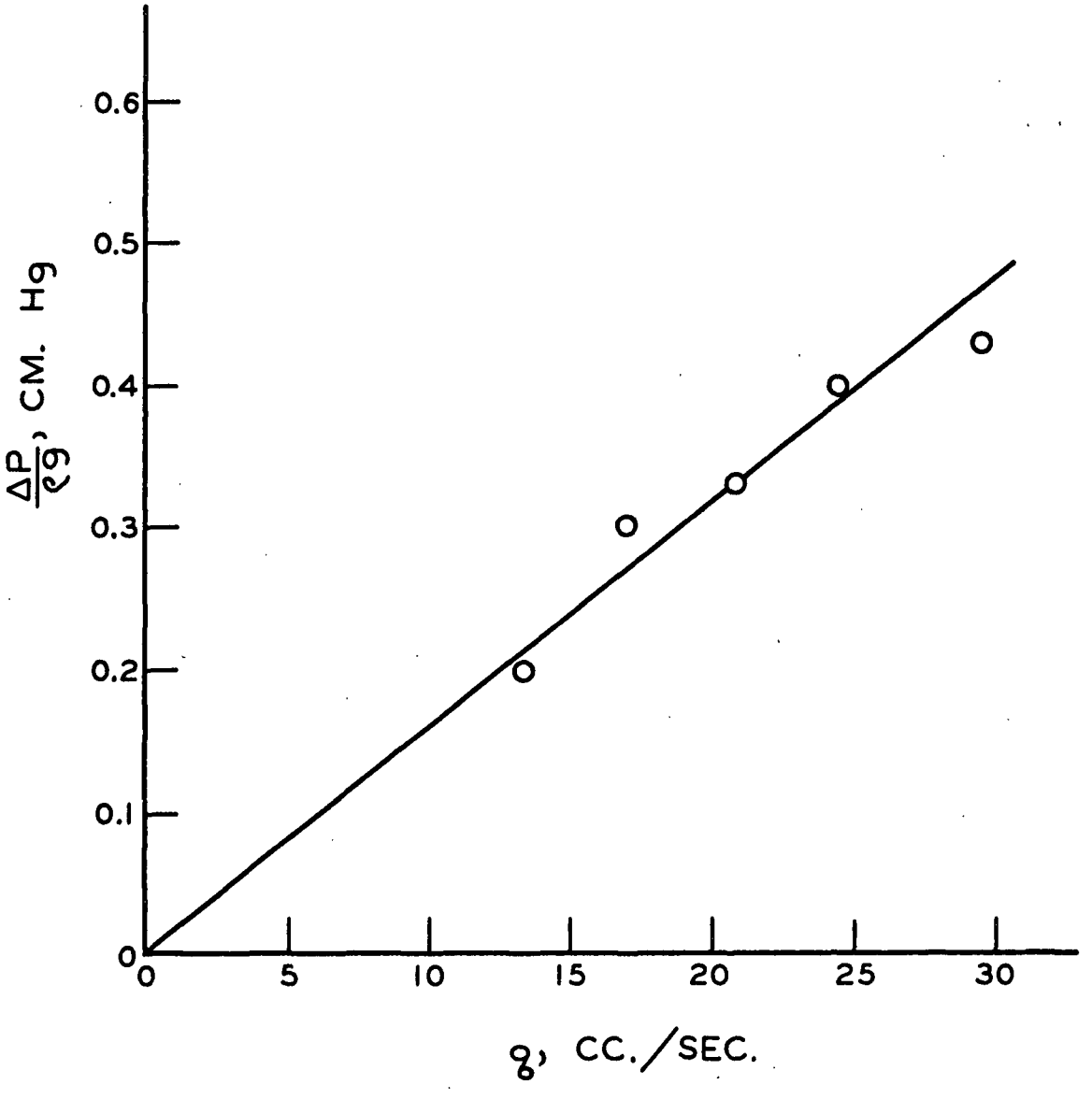

Figure 8. Resistance of Lateral Permeability Cell

flow rate. Since the pressure below and above the sample was the same in the test zone and guard zone, the tendency toward sidewise flow was minimized. The pressure drop across the sample was obtained as the difference in pressure between the head and discharge chamber minus the difference in fluid head between the points where the pressure was measured.

Readjustment of the flow-control valves permitted the determination of the pressure drop across the sample at several different flow rates. As in the determination of transverse permeability, permeability decay was minimized by using flow rates as small as possible, reading the manometers as soon as equilibrium conditions had been attained, advancing from low flow rates to higher flow rates during a run and by proceeding as rapidly as possible from flow rate to flow rate to minimize the total time during which water passed through the pad.

Varying the pad density with this apparatus was more difficult than with the transverse permeability apparatus. The permeability cell had to be disassembled before the compressive load could be released and different spacers inserted between the compression jaws. During this procedure, the sudden expansion of the pad would cause air to enter some of the pore spaces. Therefore, before the pad could be compressed to a new pad density, it had to be removed from the compression jaws and resaturated with water by boiling for several hours under vacuum.

Because such a procedure would require a great deal of time for each run, a simpler and more rapid method was used to obtain the lateral permeability of each felt sample. Because the main interest of this

investigation was the relationship of the felt structure to its permeability and the several test samples had been very carefully manufactured to specifications designed to study this relationship, the structural variance within any given sample would be small. Therefore, several accurately cut, water-saturated pads were prepared from a given sample and a new pad was used for the permeability determination at each pad density. To eliminate the influence of minor fluctuations in structure within a sample on the measured value of the permeability at any one pad density, three determinations on three different pads were made at each pad density, and the average of three measurements at a given pad density was taken as the representative permeability value for the sample at that density. The experimental procedure was further simplified by making the three permeability measurements at the same pad density in succession before preparing the apparatus for the determination at a different pad density.

The average deviation observed for the lateral permeability constant determined at each pad density varied from 3 to 7%. This value is greater than the 2% average deviation noted for transverse permeability measurements made on the same pad at the same density, and about the same as that observed for transverse permeability measurements made on different pads from the same sample at equal densities. Of the 3 to 7% observed variation, 2% appears to be procedural in nature, and 1 to 5% appears to be the result of unavoidable fluctuations in structure within the felt sample.

DETERMINATION OF SPECIFIC SURFACE AND SPECIFIC VOLUME

To test the application of the Kozeny-Carman theory to the flow through woven wool felts, an independent measurement of the water-swollen specific

surface and the water-swollen specific volume of the wool fiber was required. A microscopic procedure was used for these determinations.

Originally it was planned to make fiber cross sections by embedding the yarn in collodion or paraffin and sectioning with the microtome. Photomicrographs of the cross section could be used to measure the perimeter and cross-sectional area of several fibers from which an average value of the specific surface could be calculated. Good cross sections were made by using collodion as the embedding material. Microscopic examination of these cross sections revealed a nearly circular fiber cross section but a rather wide variation in diameter.

On the basis of these observations, it was decided that instead of using the more laborious procedure mentioned above, a sufficiently reliable estimate of the specific surface of the fiber could be calculated from fiber diameter measurements if a circular cross section was assumed. Because the fibers are not perfectly circular, such an estimate would give a specific surface somewhat less than the true value. An idea of the reliability of a specific surface value based on the assumption of a circular cross section may be obtained from the work of Lord (30). Lord wished to estimate the specific surface of a fiber from its cross-sectional area, a, obtained as the product of the specific volume, v, and the weight per unit length, H, of the fiber. Because the perimeter, p, of the fiber would be somewhat larger than the perimeter of a circle of equal area, Lord determined a correction factor, C, equal to the ratio of the area of a circle with a perimeter equal to that of the fiber to the area of fiber cross section. The following relationship was used by Lord.

$$\underline{S_v}^2 = \frac{\underline{p}^2}{\underline{a}^2} = \left(\frac{\underline{p}^2}{4\pi \underline{a}}\right)\left(\frac{4\pi}{\underline{a}}\right) = \underline{C}\left(\frac{4\pi}{\underline{Hv}}\right). \qquad (17)$$

The value of $\underline{C}$ was determined from perimeter and area measurements made on fiber sections projected at a magnification of 1000X. The factor, $\underline{C}$, may be considered as a measure of the circularity of sectional shape, being equal to unity for circular fibers and becoming larger as the shape deviated more and more from circularity. For different samples of solid fibers of the same type, the correction factor was reasonably constant. For dry wool fibers having diameters of 20-22 microns, Lord observed a constant value of $\underline{C}$ of 1.04. Considering this value as an estimate of the roundness of the wool fiber, the aasumption of circularity of cross section in the present investigation probably gives a specific surface value approximately 2% low.

To determine the specific surface of the water-swollen wool fiber, several segments of wool yarn were removed from the felt sample and were saturated with water. A one-eighth-inch length of the wet yarn was placed on a microscope slide; several drops of water were added; and with the aid of a stereoscopic binocular microscope, the fibers were separated from the yarn and were lined up as nearly parallel as possible. The slide was then transferred to the stage of a compound microscope. Using an eyepiece micrometer and a magnification of 200, approximately 200-230 individual fiber diameter measurements were made. Since some variation in specific surface between samples was possible, fiber diameter measurements were made on about 200-230 water-swollen fibers from each felt sample.

The specific surface of the water-swollen fibers was calculated from the following expression (27).

$$S_v = \left(\frac{4\Sigma d}{\Sigma d^2}\right) \qquad (18)$$

where d is the measured fiber diameter. Values of S_v were calculated for each felt sample.

The specific volume of the water-swollen wool fiber could be calculated from the known pycnometric density of dry wool if the increase in volume of the fiber from the dry state to the water-swollen state could be measured. Since the wool fiber increases only 1% in length in water (41), the major contribution to the increased fiber volume in water is a change in the cross-sectional area. The increase in cross-sectional area may be calculated from the change in the fiber diameter if a circular cross section is assumed.

To determine the increase in fiber diameter in water, adjacent, similar yarn specimens were prepared by cutting a yarn segment with a razor blade in three places at intervals of about 1/8 inch. The yarn segments, obtained from Sample 1, had been previously dried over calcium chloride. One of the 1/8-inch specimens was placed on a microscope slide; several drops of xylene were added; and the fibers were separated and aligned as described previously. The other one-eighth-inch specimen was mounted as described previously using water to swell the fibers. Fiber diameters were measured as described before, using yarn specimens to obtain in excess of 200 fiber-diameter measurements for both the dry fibers and the water-swollen fibers.

COMPRESSIBILITY MEASUREMENT

To relate the pad density to the compressive load applied to the pad, load-deformation curves for each felt sample were obtained with a Baldwin-Southwark Universal Tester using a compression rate of 0.0125 inches per minute. Water-saturated samples from which the excess water had been removed were accurately cut to an area of one square inch for the test.

EXPERIMENTAL RESULTS AND DISCUSSION

TRANSVERSE PERMEABILITY DATA

Permeability results have been expressed in terms of the permeability constant, K, defined by Equation (1), rather than its reciprocal, the specific permeation resistance. To determine the permeability constant at a given pad density, pressure-drop measurements were made at 8 different flow rates. Permeability constants were determined at 8 or 9 different pad densities for each felt sample. Figure 9 shows a plot of the pressure drop-flow rate data at several pad densities for Sample 6, which is representative of all runs with respect to the deviation of the points from a linear relationship. At flow rates greater than those shown, the data deviated from the linear relationship, with the deviation becoming progressively greater at larger and larger flow rates.

Carman (8) defines the Reynolds number, Re, for flow through porous beds as

$$\underline{Re} = \frac{q\rho}{A\mu S_o} \qquad (19)$$

and characterizes a Reynolds number numerically less than 2 as the criterion for streamline flow. In these transverse permeability measurements, the maximum Reynolds number observed was 0.086. Therefore, the determinations were made well within the viscous flow range. If, at any constant flow rate, flow was continued over a long period of time (20-60 minutes), a gradual increase in the pressure drop across the pad (i.e., a decay in the permeability) was observed. The magnitude of this increase in the pressure drop was a function of the total flow

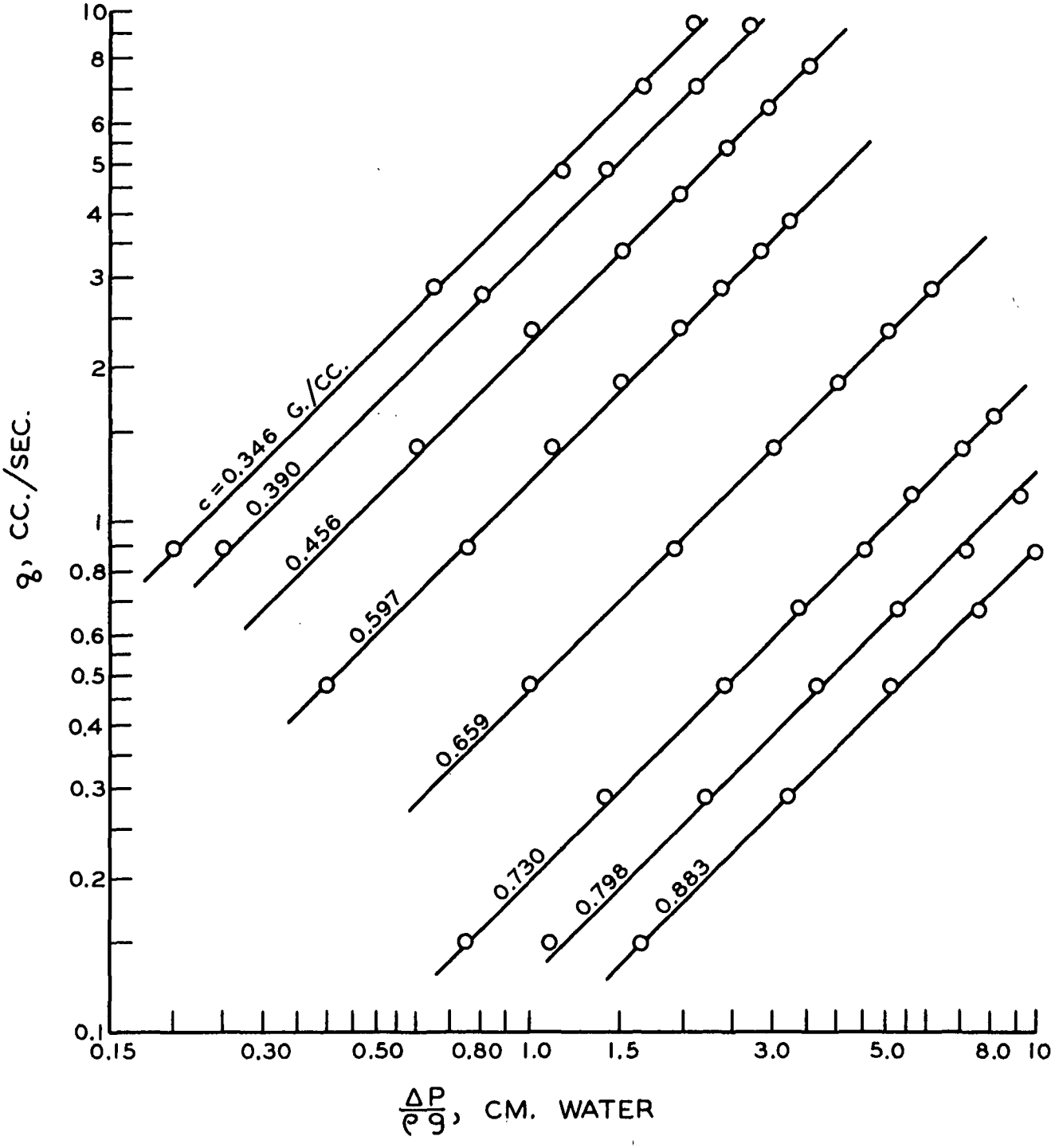

Figure 9. Transverse Permeability Data
(Sample 6)

that had passed through the pad and, therefore, at higher flow rates was observed at shorter time intervals.

On the basis of these considerations, the observed deviations of the data from linearity at the higher flow rates was believed caused by a decay in the pad permeability due in part to the total flow that had passed through the pad at preceding lower flow rates and in part to the more rapid incidence of decay at higher flow rates. Therefore, succeeding permeability determinations were limited to those lower flow rates where this deviation did not occur. Only data obtained at low flow rates where a good linear relationship existed between the flow rate and pressure drop were used in the calculation of the permeability constant.

To calculate the permeability coefficient from Equation (1), the ratio, $\Delta P/q$, for each value of pad thickness, L, was taken as the slope of the best straight line drawn through a linear plot of the pressure drop-flow rate data taken at the pad density corresponding to that value of pad thickness. A method of averages was used to determine the slope of this line (43). The viscosity of the water at the temperature of the run was obtained from the International Critical Tables. The test area of the pad, A, was an accurately known constant of the apparatus, being the pad area included within the guard rings. The pad thickness, L, was taken as the average of the two values determined from the indicator readings at the desired pad density and the respective zero readings.

The apparent pad density or pad concentration, c, at each thickness was evaluated from the oven-dry weight of the pad and the calculated

volume of the test zone at that pad thickness. Because the test zone was only a portion of the total pad weighed, the weight of the fibers in the test zone was obtained by multiplying the total pad weight by the ratio of the test area to the total area both of which were accurately known. An average deviation in oven-dry pad weight of less than 1% was observed between different pads from the same sample.

A sample calculation of the permeability coefficient of Sample 6 at several pad densities is given in Table III.

Although the manufacturing process was controlled as carefully as possible in the preparation of the felt samples, minor fluctuations in structure and basis weight within each sample were probable. Such fluctuations were expected because accurate control of the fulling operation in the felt manufacturing cycle was not possible. Therefore, to insure representative permeability data for each different felt structure, duplicate or triplicate density versus permeability measurements were made for each sample, using a new pad to obtain each set of data. The extent of the deviation of the individual data points from the sample average can be observed for Sample 6 in Fig. 10 where the permeability constant, K, is plotted as a function of the apparent pad density, c, for 3 different pads. The transverse permeability data for the other samples are plotted in Fig. 31 to 40 in the Appendix. The data for the first pad of each sample are also tabulated in Table XI in the Appendix. The average deviation of the permeability between different pads from the same sample varied from 3 to 7%. Some of this variation is due to experimental error, but the greatest source of the variation is probably due to unavoidable structural fluctuations within each sample.

TABLE III

TRANSVERSE PERMEABILITY CALCULATION

(Sample 6)

L, cm.	c, g./cu. cm.	$\Delta P/q$, c.g.s. units	μ, cp.	$10^9 K_2$, cm.^{2}	$10^4 (KL)^{1/3}$, cm.
0.228	0.346	211	0.889	210	36.4
0.202	0.390	274	0.888	143	30.7
0.173	0.456	431	0.892	78.2	23.9
0.147	0.537	811	0.890	35.3	17.3
0.121	0.653	2,065	0.890	11.4	11.1
0.108	0.730	4,920	0.890	4.27	7.74
0.099	0.798	7,850	0.890	2.45	6.24
0.089	0.883	11,500	0.890	1.52	5.15

Bed area, A = 45.6 sq. cm.

LATERAL PERMEABILITY DATA

The lateral permeability results have also been expressed in terms of the permeability constant defined by Equation (1). The lateral permeability coefficient has been designated as K_2 to differentiate it from the transverse permeability constant previously designated as K. In the transverse permeability calculations, the felt thickness and bed depth were equivalent and were designated as L. However, in the calculation of the lateral permeability constant, the felt thickness was not equivalent to the bed depth in the direction of flow. In this instance, the bed depth, L, was a constant of the apparatus and equal to 2.54 cm., but the cross-sectional area, A, of the pad normal to flow varied as the pad was compressed. Designating the pad thickness as L_2, the value

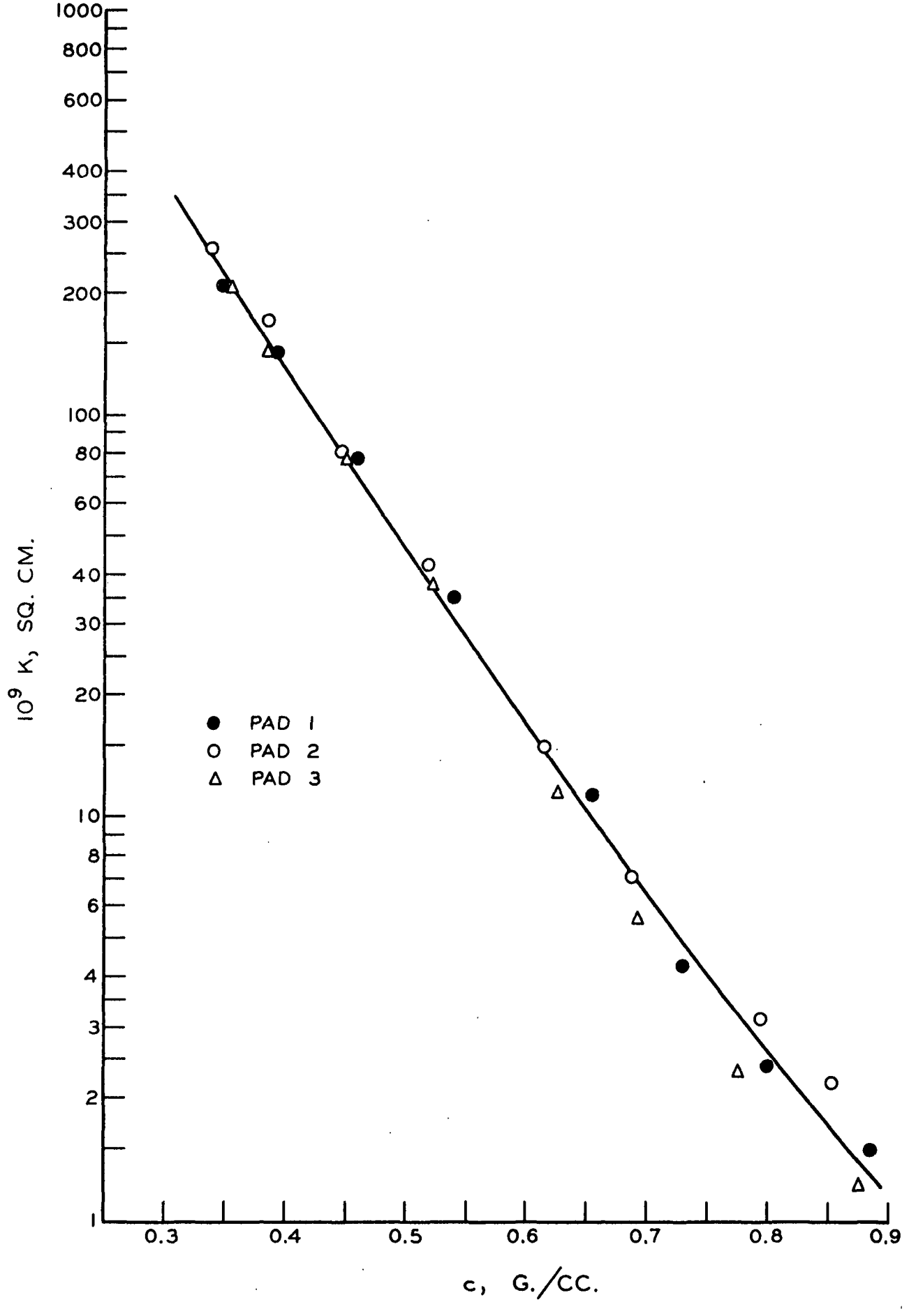

Figure 10. Transverse Permeability Data
(Sample 6)

of the area normal to the flow direction, A, was the product of L_2 and the constant length of the test zone of the apparatus, 7.72 cm.

The lateral permeability determination was made for the direction parallel to the warp yarn which would be the machine direction in the press section of a paper machine. Flow in this direction is of greater importance than flow in the direction of the fill yarns because the lateral fluid pressure differential in the felt in the nip of the press rolls is in the machine direction. The experimental felt pads were carefully cut so that the warp yarns would be in the flow direction in the permeability measurement.

To determine the permeability constant at a given pad density, pressure-drop measurements were obtained for 7 different flow rates. An average pressure drop at each flow rate was determined from measurements on 3 different pads compressed to the same density. Permeability constants were determined at 7 or 8 different pad densities for each sample. Figure 11 shows a plot of the pressure drop-flow rate data obtained at the different pad densities for Sample 6, which is representative of all samples for the deviation of the experimental points from a linear relationship. Maximum Reynolds numbers of 1.4 at the lowest pad densities and 0.02 at the highest pad densities were indicative of viscous flow conditions. A good linear relationship between the flow rate and pressure drop was observed at all times.

The ratio, $\Delta P/q$ at each value of pad thickness, L_2, was obtained as the slope of the best straight line drawn through a linear plot of the data for that pad thickness. The method of averages was used to

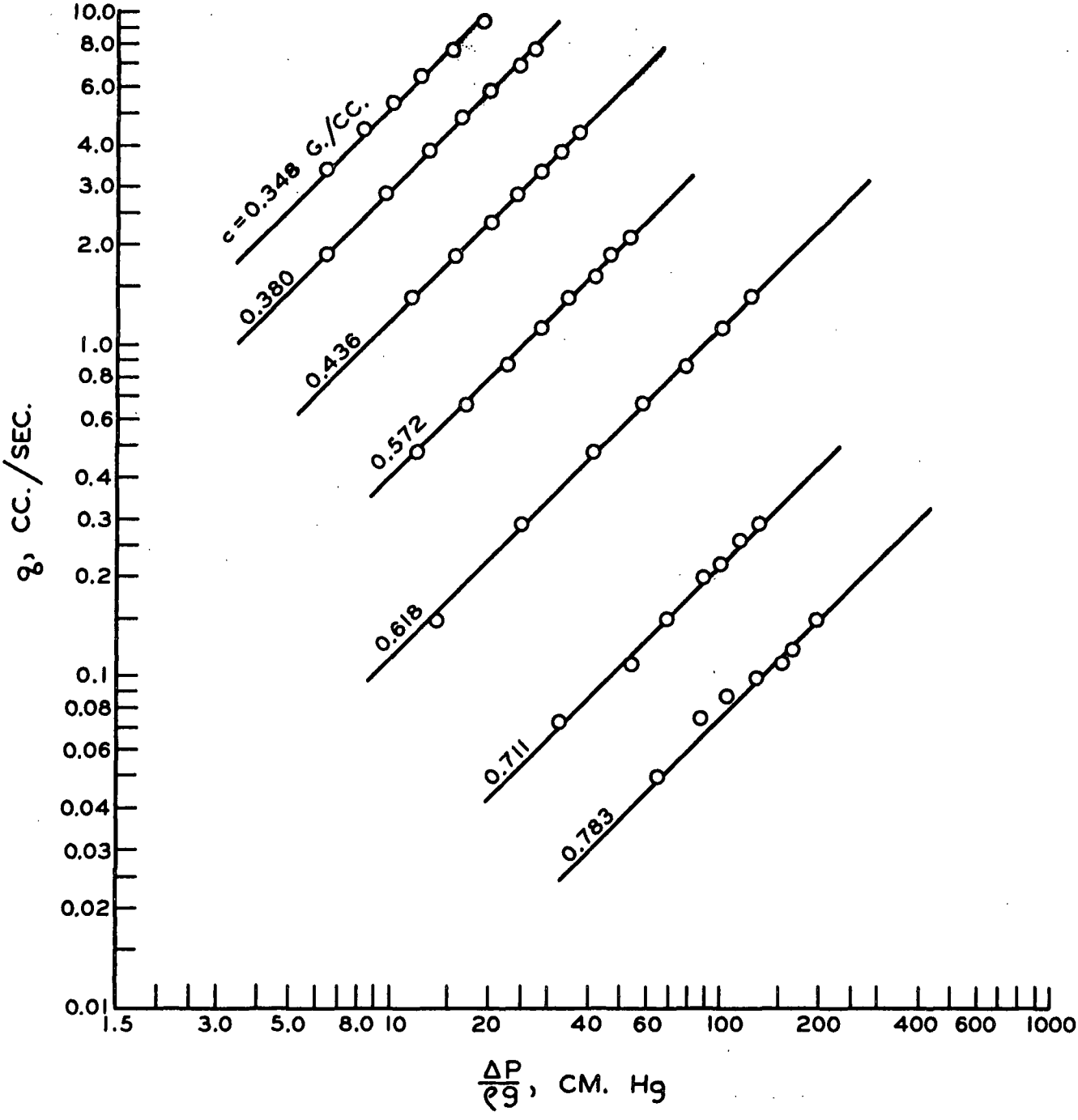

Figure 11. Lateral Permeability Data
(Sample 6)

calculate the slope of the line. The apparent pad density, c, at each pad thickness was evaluated from the oven-dry weight per unit area of the felt, the tested area of the felt, and the calculated volume of the test zone at that pad thickness.

Because the walls of the lateral permeability cell offered some resistance to flow, the experimental permeabilities were corrected for this wall effect. Carman (8, 12) has examined the wall effect in permeability studies and states that experimental permeabilities should be multiplied by the following factor to correct for the wall effect:

$$(1 + \frac{1}{2} S_c/S_o)^2 \qquad (20)$$

where S_c is the surface of the wall per unit volume of the bed and S_o is the surface of the particles per unit volume of the bed. Under the conditions of the lateral permeability determination, wall correction factors of 1.02-1.03 were calculated and used to correct the experimental permeabilities. A sample calculation of the wall correction factor for Sample 6 is given in Table XII in the Appendix.

A sample calculation of the lateral permeability constant, K_2, at several pad densities is given for Sample 6 in Table IV. A plot of the average lateral permeability constant, K_2, versus the apparent pad density, c, is given in Fig. 12 for Sample 6 and for the other samples in Fig. 41 to 50 in the Appendix. As was discussed previously, each permeability constant is a mean value based on data obtained from 3 different pads prepared from the same sample. Therefore, in Table XIII in the Appendix, the average deviation of the mean permeability constant for

TABLE IV

LATERAL PERMEABILITY CALCULATION

(Sample 6)

L_2, cm.	c, g./cc.	$10^{-4}\Delta P/g$, c.g.s.	μ, cp.	Wall Correction Factor	$10^9 K_2$, cm.^{2}	$10^4 (K_2 L_2)^{1/3}$, cm.
0.222	0.348	2.74	0.886	1.02	490	47.7
0.203	0.380	4.68	0.896	1.02	316	40.0
0.177	0.436	11.4	0.876	1.02	145	29.6
0.150	0.572	31.7	0.855	1.02	60.4	20.8
0.125	0.618	117.0	0.870	1.02	19.8	13.5
0.109	0.711	580.0	0.870	1.02	4.63	7.96
0.0987	0.783	1900.0	0.884	1.02	1.58	5.40

Depth of test zone: $L = 2.54$ cm.

Length of test zone: $L_3 = 7.72$ cm.

each sample is given. The magnitude of this deviation is about the same as was observed for the mean transverse permeability constant. The largest source of the variation is probably the structural fluctuations within the sample.

MICROSCOPIC FIBER DIAMETER DATA

Estimates of the swollen specific volume and specific surface of the wool fiber were obtained from the microscopic fiber diameter measurements. The data are given in Table V. The fiber diameter distributions for the different felt samples are similar and are typical of wool fiber distributions observed for commercial samples of medium wool grades (43). Both dry and water-swollen fiber diameter measurements are given for Sample 1. The fiber diameter distributions given for the other samples are for

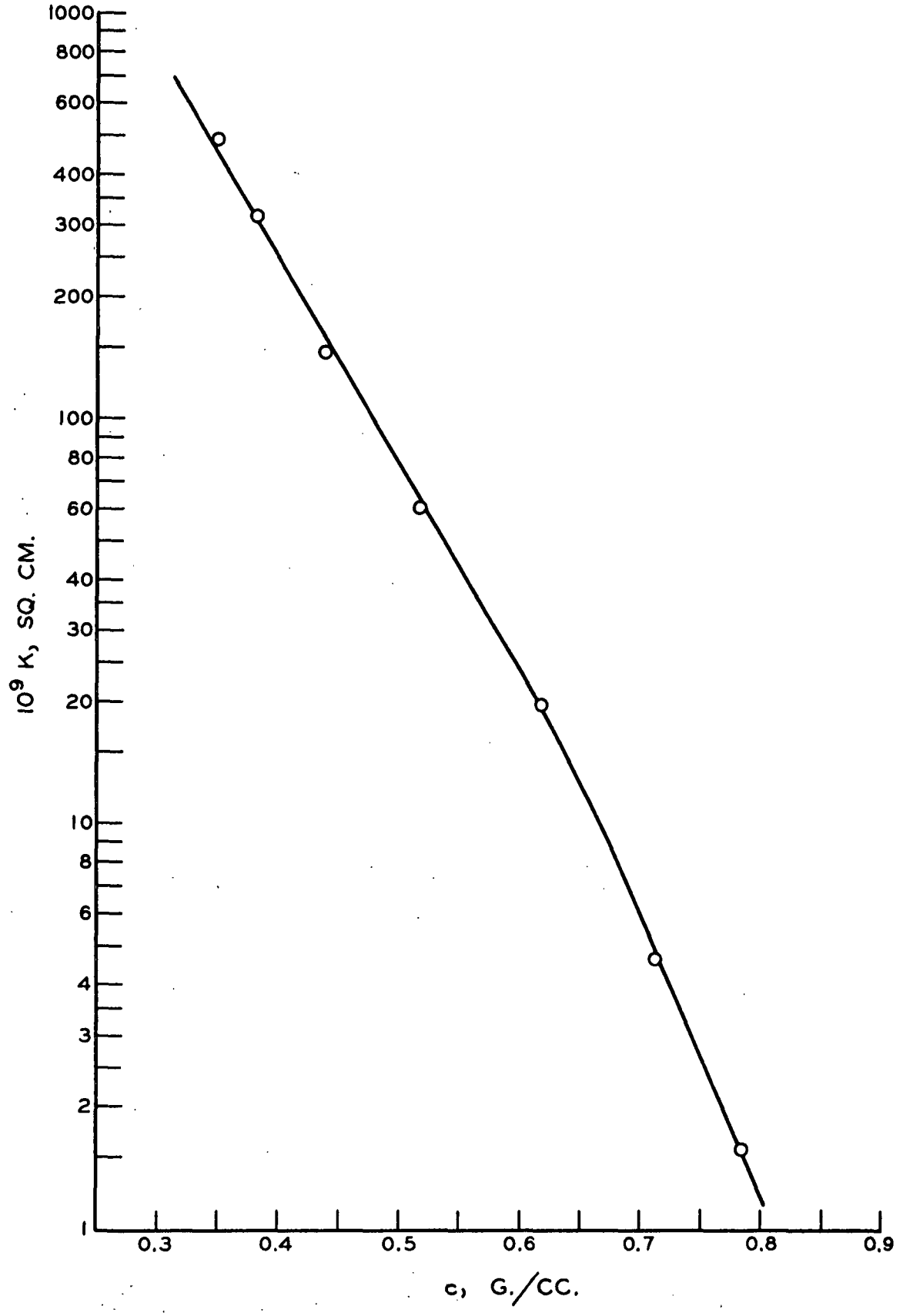

Figure 12. Lateral Permeability Data
(Sample 6)

TABLE V

FIBER DIAMETER DISTRIBUTION, %

Sample no.	1[a]	1	2	3	4	5	6	7	8	9	10	11
Range, microns												
10-14	0	0.4	0	0	0.9	0.4	0	0	0	0	0.5	0
15-22	32.5	14.8	7.5	13.2	31.4	22.7	12.3	32.9	22.1	19.5	19.1	13.2
23-30	50.8	48.7	35.5	40.7	30.8	48.9	28.1	46.4	38.5	35.9	39.7	40.6
31-38	15.2	29.0	36.4	32.4	23.8	20.1	38.9	18.5	32.3	24.6	32.0	29.7
39-46	1.5	6.2	14.0	12.8	8.4	6.6	14.8	2.2	4.3	13.3	6.7	13.2
47-54		0.9	5.6	0.9	4.7	1.3	5.9		2.8	6.7	2.0	3.3
55-62			1.0									
No. of fibers measured	203	224	214	219	214	229	203	222	208	240	209	212
Arithmetic average diameter[b], microns	24.9	29.0	32.6	30.4	28.0	27.7	32.7	26.2	28.9	30.6	29.6	31.0
Surface-weighted av. diameter[c], microns	26.5	30.8	33.3	31.2	31.0	29.2	34.5	26.5	30.6	32.8	31.2	31.3
Specific surface, sq. cm./cm.^{3}	1510	1300	1200	1280	1290	1370	1160	1510	1310	1220	1280	1275
Yarn size, cut	16	16	16	16	16	16	11	20	16	16	16	16

[a] Dry fiber; all other samples were water-swollen.

[b] Arithmetic average diameter = $\Sigma d/n$ where d = fiber diameter and n = total no. fibers measured.

[c] Surface-weighted average diameter = $\Sigma d^2/\Sigma d$.

water-swollen fibers. Both the arithmetic average fiber diameter and the surface-weighted average fiber diameter are given for each sample. These averages were calculated as indicated using the individual fiber diameter measurements. The distributions show only a small difference between the arithmetic and weighted average diameters. Because the data were used for surface area determinations, the surface-weighted average fiber diameter was used in the calculations.

The average fiber diameter does not vary too greatly between samples, particularly between those samples having the same yarn size. Sample 7, constructed with a lighter yarn, has the smallest average fiber diameter; Sample 6, constructed with a heavier yarn, has the largest average fiber diameter.

Specific surfaces were calculated for each sample using the individual fiber diameter measurements and Equation (18) assuming a circular cross section as has been discussed previously. The calculated specific surface values are given for each felt sample in Table V.

The diameter measurements for the dry and corresponding water-swollen fibers of Sample 1 were used to calculate the water-swollen specific volume, the volume denied to the flow of water per unit mass of dry fiber. The percentage increase of the fiber cross section in water was easily estimated from the weighted-average dry and water-swollen fiber diameters by assuming a circular cross section. By assuming a negligible increase in length during swelling (41), the water-swollen specific volume was calculated using King's (44) value for the specific volume of dry wool. King found that the density of wool, determined pycnometrically in benzene, is

substantially the same in all varieties of medulla-free wools. Von Bergen (43) quotes additional evidence for the constancy of the density of wool. The medium-grade wool used in the present study was found medulla-free by microscopic examination of fiber cross sections. A summary of the swollen specific volume calculation is given in Table VI.

TABLE VI

CALCULATION OF SWOLLEN SPECIFIC VOLUME

Weighted-Average Dry-Fiber Diameter, microns	Weighted-Average Wet-Fiber Diameter, microns	Increase in Cross Section, %	Dry Specific Volume (44), cc./g.	Water-Swollen Specific Volume, cc./g.
26.5	30.8	35.2	0.766	1.04

The 35.2% increase in the fiber volume in water due to swelling is in good agreement with the 36.3% calculated by King from regain and displacement measurements on wool. King measured the weight of water absorbed per gram by dry wool in a water-saturated atmosphere and the pycnometric density of dry wool in benzene and in water. When the density of dry wool was determined in water, a contraction in the total volume occurred and an apparent density of wool greater than the true value (determined in benzene) was obtained. The volume contraction per gram of fiber was the difference between the true specific volume of the fiber and the apparent specific volume of the dry fiber in water. The volume swelling of the fiber in water was then obtained as the volume of water absorbed per gram of fiber minus the volume contraction per gram of fiber.

APPLICATION OF THE KOZENY-CARMAN EQUATION TO THE DATA

To test the applicability of the Kozeny-Carman equation to the transverse and lateral permeability data, the following rectified form of the equation, discussed previously, was used.

$$(\underline{KL})^{1/3} = \left(\frac{1}{\underline{k}\underline{S}_v^{\,2}\,\underline{L}_o^{\,3}}\right)^{1/3} (\underline{L} - \underline{L}_o). \qquad (15)$$

A plot of the transverse permeability data in the form $(\underline{KL})^{1/3}$ against $\underline{L}$ and of the lateral permeability data in the form $(\underline{K}_2\underline{L}_2)^{1/3}$ against $\underline{L}_2$ would be linear where the quantity $(1/\underline{k}\underline{S}_v^{\,2}\,\underline{L}_o^{\,2})^{1/3}$ is constant. If the Kozeny-Carman equation applies, the slope of the line is equal to $(1/\underline{k}\underline{S}_v^{\,2}\,\underline{L}_o^{\,2})^{1/3}$ and the $\underline{L}$ intercept is the value $\underline{L}_o$, the pad thickness at zero porosity.

A plot of the transverse permeability data for each felt in the above form resulted in linear relationships over a wide porosity range. For all felts, a deviation from linearity was observed at very low porosities, and for a few felts a slight deviation from linearity was observed at the highest porosities studied. The first set of data for each sample is plotted in Fig. 13-17.

To indicate the agreement with the Kozeny theory, the lines drawn through the linear portion of the data have been calculated from Equation (15) using the specific surface calculated from microscopic fiber diameter measurements made for each sample. The water-swollen specific volume of the fiber determined from the microscopic fiber diameter measurements was used to evaluate $\underline{L}_o$, since by definition,

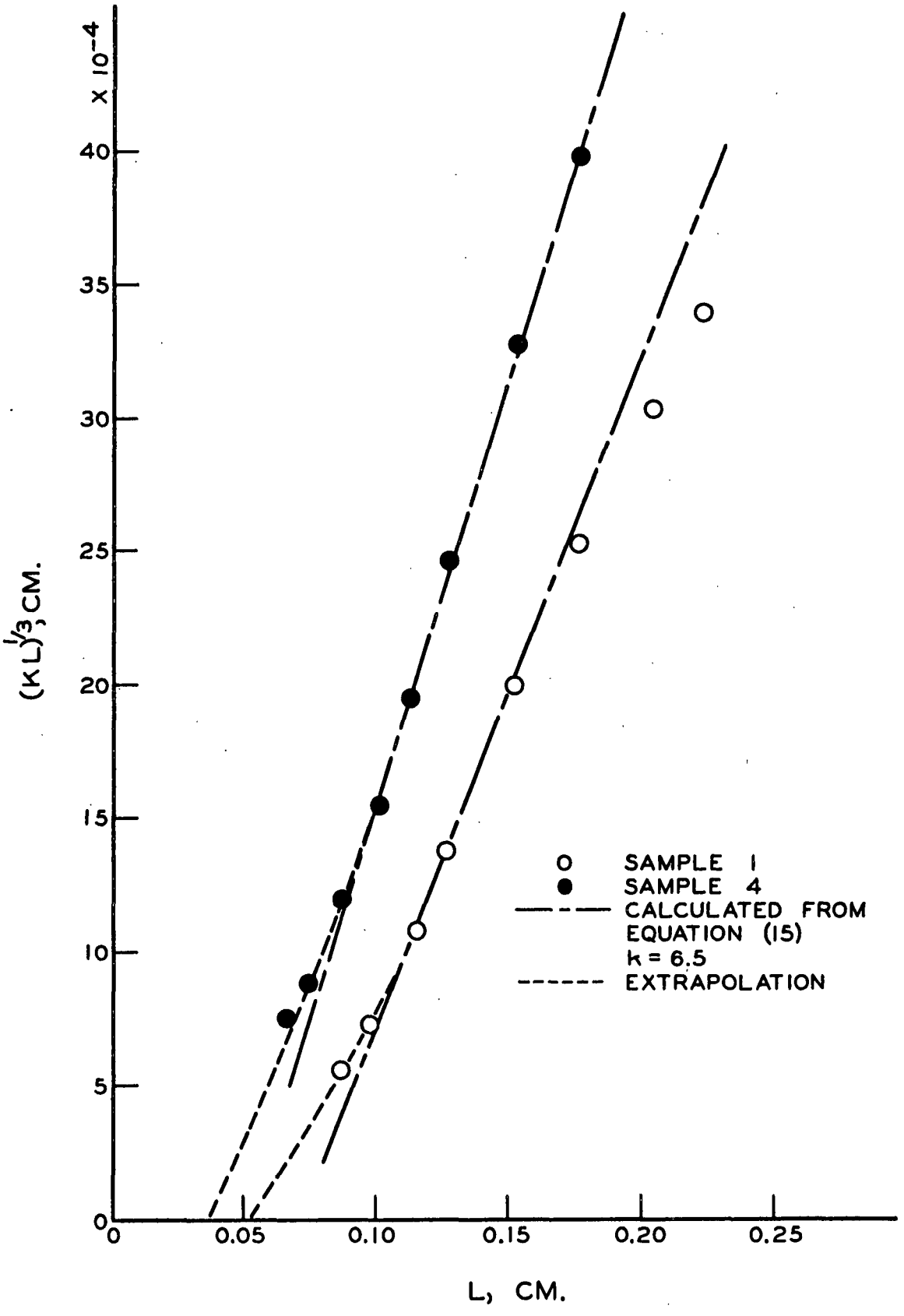

Figure 13. Transverse Permeability
(Samples 1 & 4)

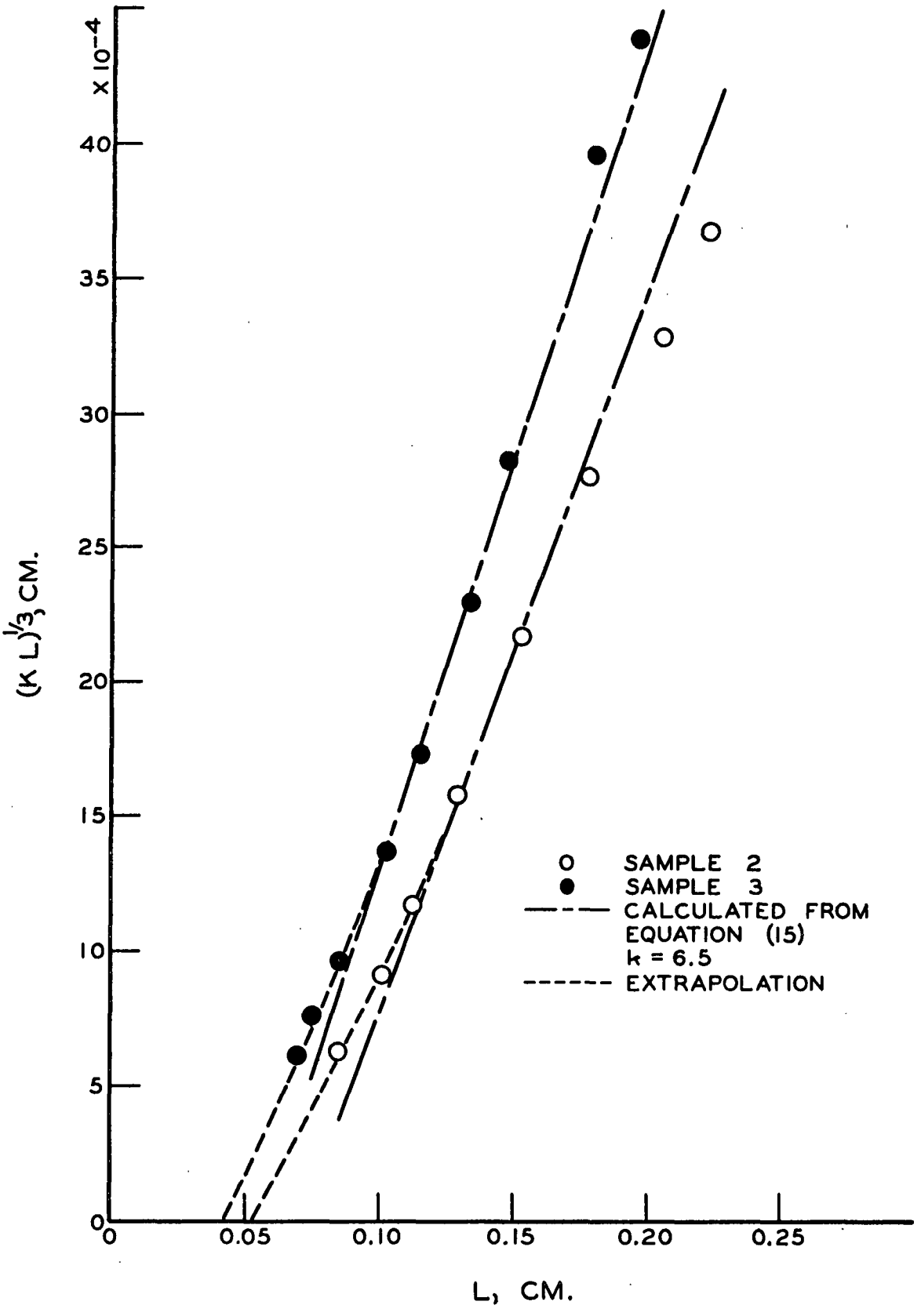

Figure 14. Transverse Permeability
(Samples 2 & 3)

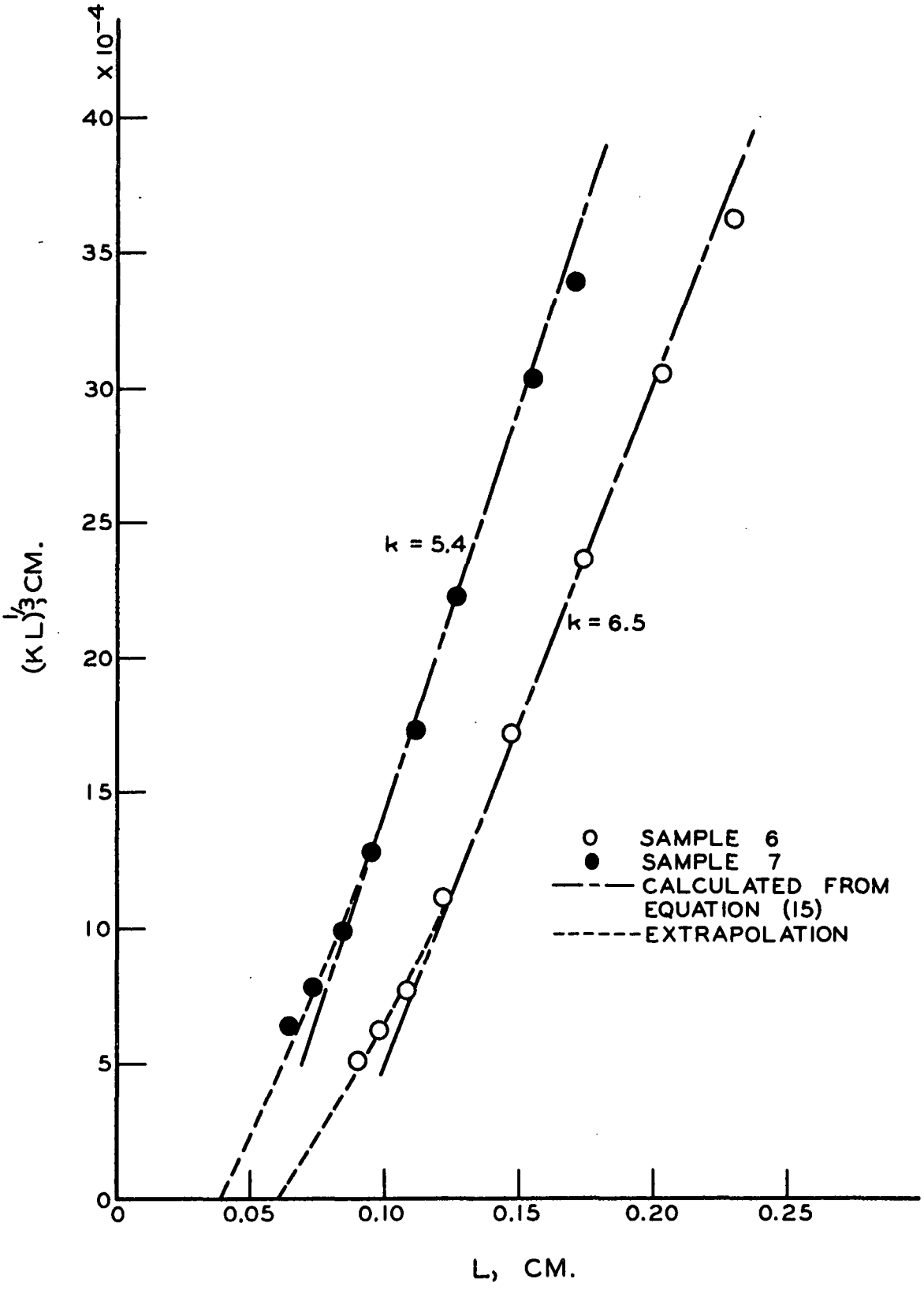

Figure 15. Transverse Permeability
(Samples 6 & 7)

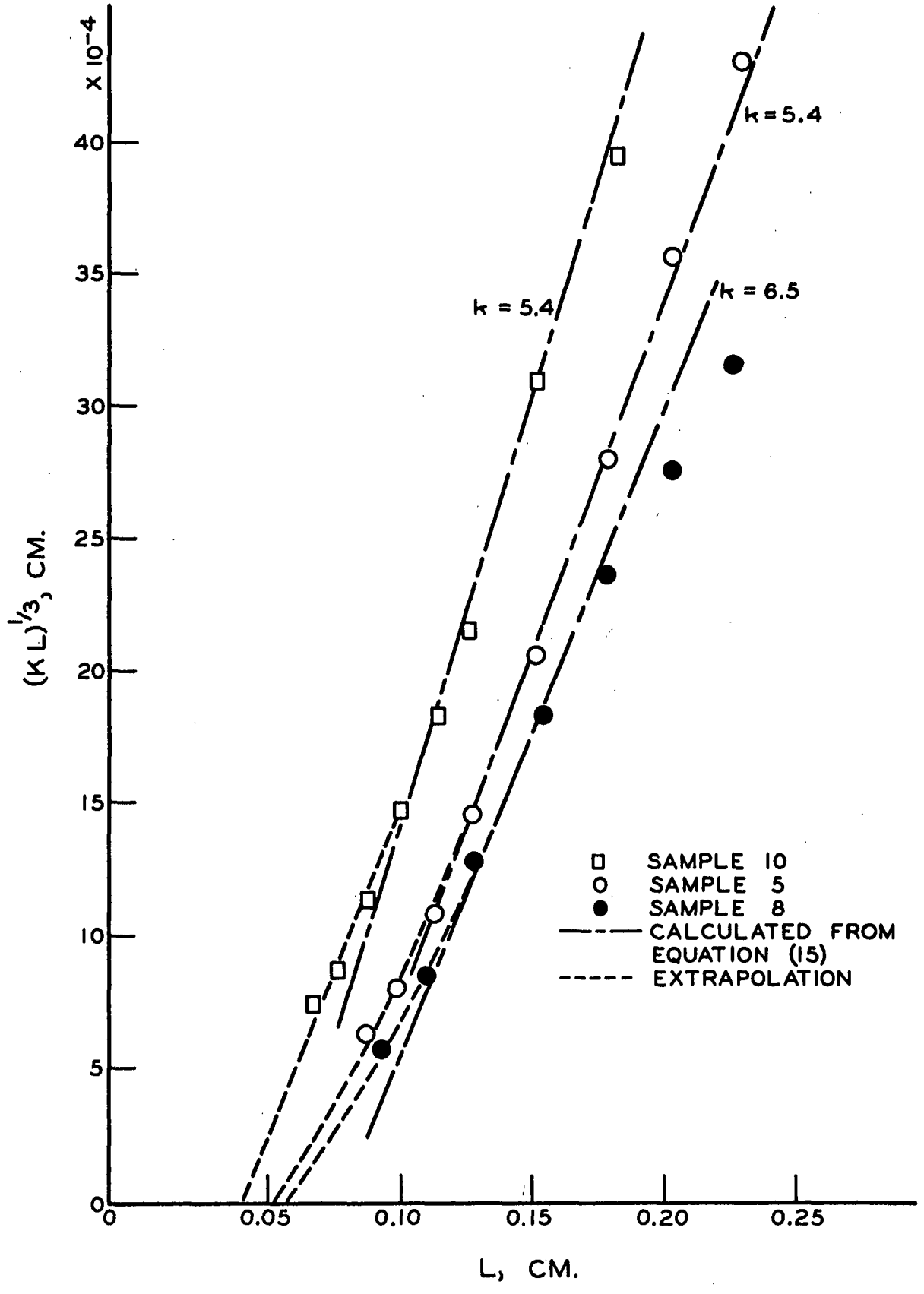

Figure 16. Transverse Permeability
(Samples 5, 8 & 10)

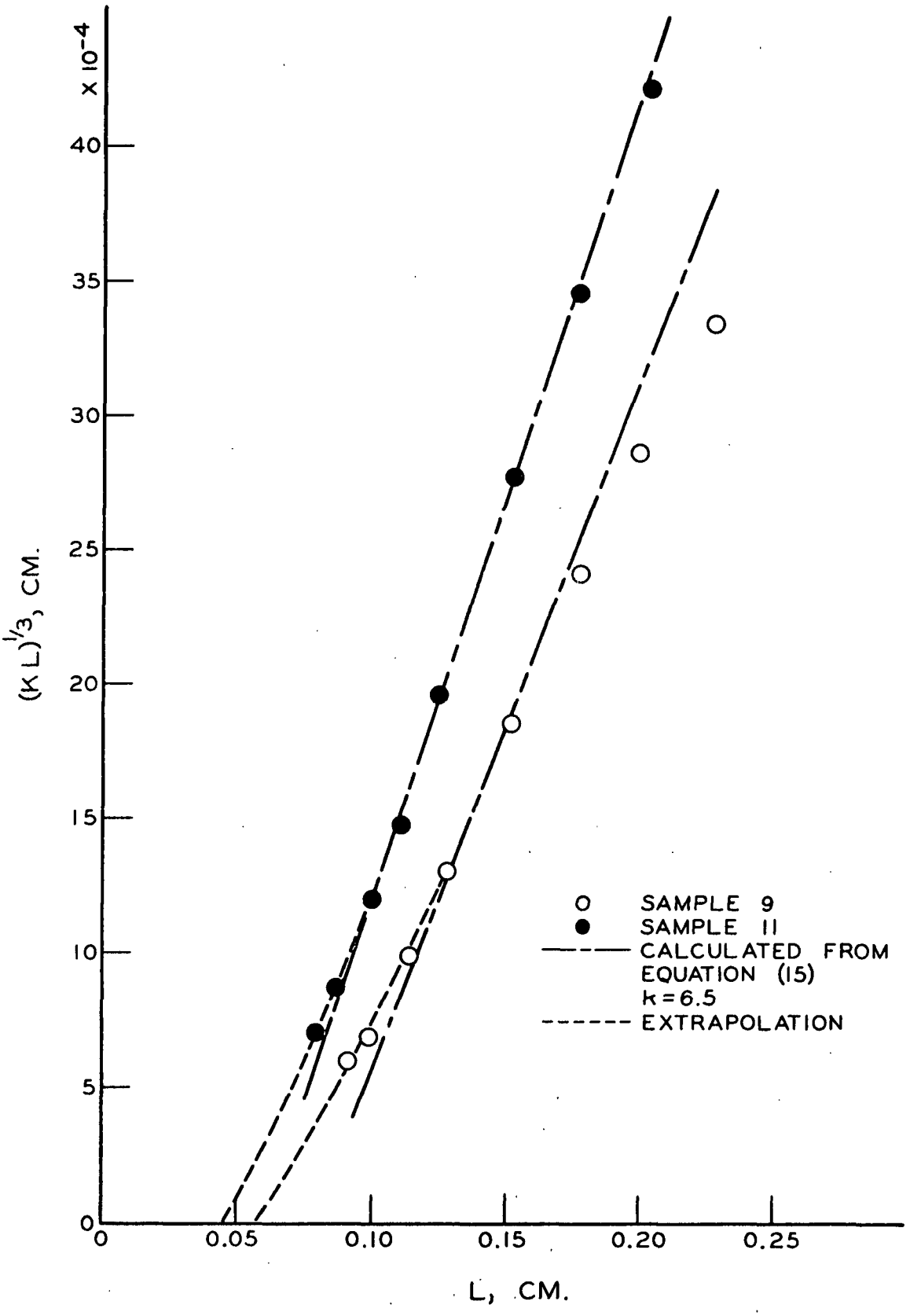

Figure 17. Transverse Permeability
(Samples 9 & 11)

$$L_o = (W/A)v. \qquad (21)$$

For reasons to be discussed later, the Kozeny constant was taken as 6.5 except for Samples 5, 7, and 10 where a k of 5.4 was used. Because the several felts differ from one another, particularly in weight per unit area, specific-surface and fiber-and-yarn-orientation (see Table I) data for the different samples fell on separate straight lines.

If the lower curved portion of the data for each sample is extrapolated to the L-axis, the value of L_o obtained corresponds closely to the value based on a bed density equivalent to the pycnometric density of dry wool--that is,

$$L_o = \left(\frac{W}{A}\right)\left(\frac{1}{1.304}\right)$$

where 1.304 g./cc. is the density of dry wool (44). In Fig. 13-14, a dotted line is drawn from the linear portion of the data to the above value of L_o for each sample. The data for all samples extrapolate to a value of L_o corresponding to a bed density equal to that of the dry fiber, but because the weight per unit area of the samples varies, this value of L_o is different for each felt.

It will be recalled that L_o is the bed thickness at zero porosity where the effective particle density and bed density are equal. Thus, the data indicate a change in the effective density of the fiber from that of the water-swollen fiber at medium bed porosities to that of the dry fiber at zero porosity. It is possible that as larger and larger compressive loads are applied to the felt, water is gradually

expressed from the swollen fibers at points where they contact other fibers. As compression proceeds, the number of points of contact between fibers would increase until in the limiting case at zero porosity, the bed becomes a mass of solid wool with a density equal to that of the dry fiber. If the swollen fibers are gradually deswelled in this manner, their effective specific volume (and thus L_o) would gradually decrease as larger and larger loads are applied to the felt, explaining the deviation of the data from the expected linear relationship at low porosities. Maximum compressive loads of 1000 p.s.i. were applied to the pad in these studies, but locally the loading at points of fiber contact would be much greater and might cause partial deswelling of the fiber. As mentioned previously, Brown (24) observed a similar deviation of his permeability data for dry pulp fibers at low porosities. An extrapolation of the data to zero porosity indicated that the pycnometric density of the fiber was approached. Carroll and Mason (20) ascribed a similar deviation of their water permeability data for pulp fibers to a decrease in specific volume.

A similar plot of the lateral permeability data for each felt also resulted in linear relationships over wide ranges of porosity. Slight deviations from linearity were observed for a few felts at very high porosities and at very low porosities, but the observed deviations, where they occurred, were of a different nature from those observed for transverse permeability. In contrast to the transverse permeability data, no general deviation from linearity at low porosities was observed for all the felts. Limitations in the experimental apparatus did not permit investigation of the lateral permeability at the lowest porosities

used in transverse permeability determinations. The data are plotted in Fig. 18-22. Because of the different structural characteristics, the data for the several felt samples fell on separate straight lines. To show agreement with the Kozeny theory, the lines drawn through the data points have been calculated from Equation (15) using the swollen specific surface determined from microscopic fiber diameter measurements. The water-swollen specific volume of the fiber determined from microscopic fiber diameter measurements was used to evaluate L_o. For reasons to be discussed later, the Kozeny constant was taken as 6.5 for Samples 1, 2, 5, 7, 8, 9, and 10, and as 3.8 for Samples 3, 4, 6, and 11.

Comparison of the results of this investigation with those of Ginn (37), described previously, is difficult because tabular data were not given and the calculated Kozeny porosity values for the water-permeability data were not corrected for the change in fiber volume caused by swelling. The rather large differences reported between the air-permeability and water-permeability characteristics of the same felts are also difficult to understand. For these reasons, a detailed comparison between Ginn's results and those of this investigation would not be too useful.

EFFECT OF THE FELT STRUCTURE ON PERMEABILITY

Since the fit of the permeability data to the Kozeny-Carman equation is very good, the deviations of the felt structure and flow mechanism from the assumed bed structure and flow mechanism upon which the Kozeny theory is based apparently are not serious enough to invalidate

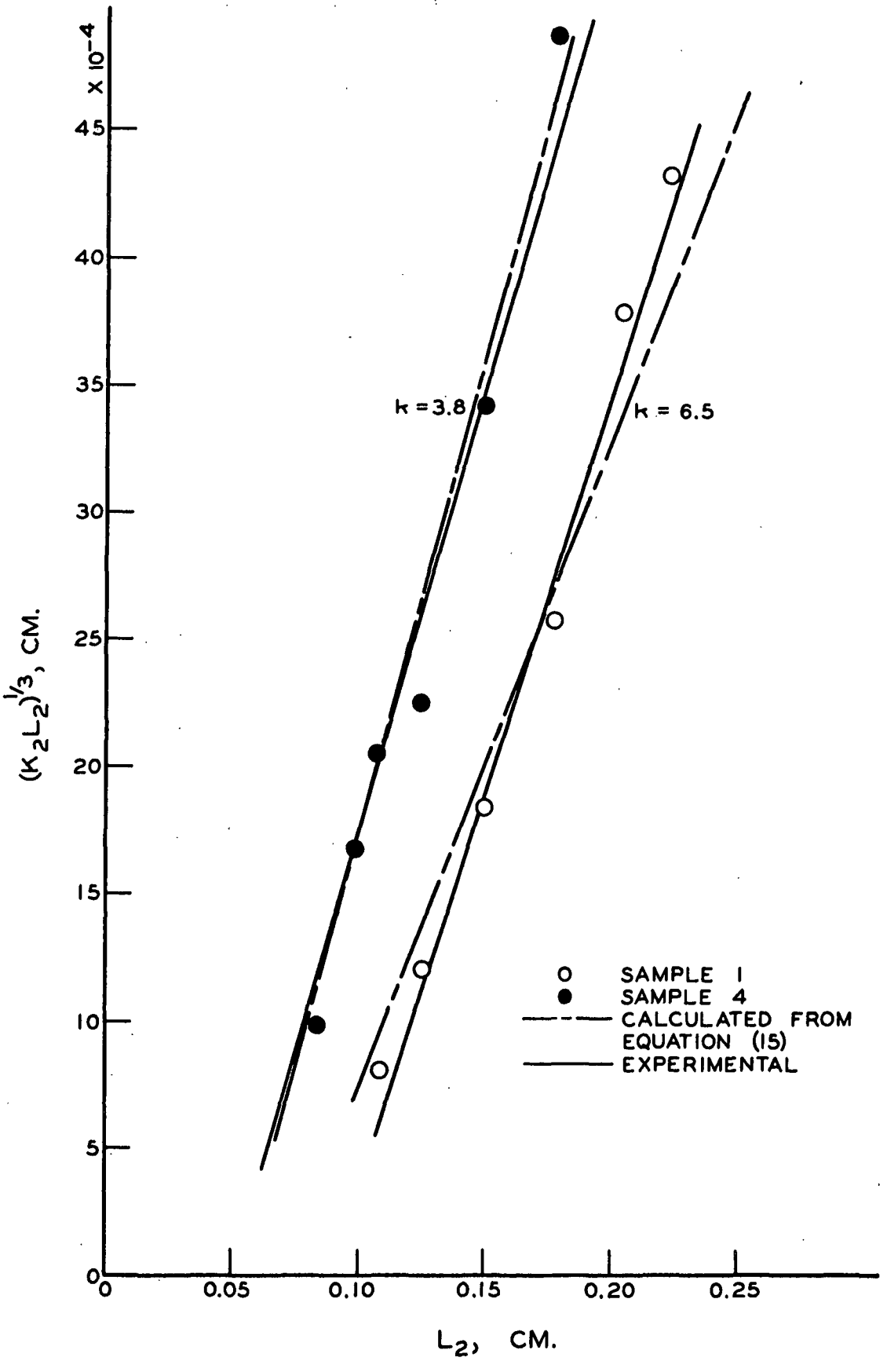

Figure 18. Lateral Permeability
(Samples 1 & 4)

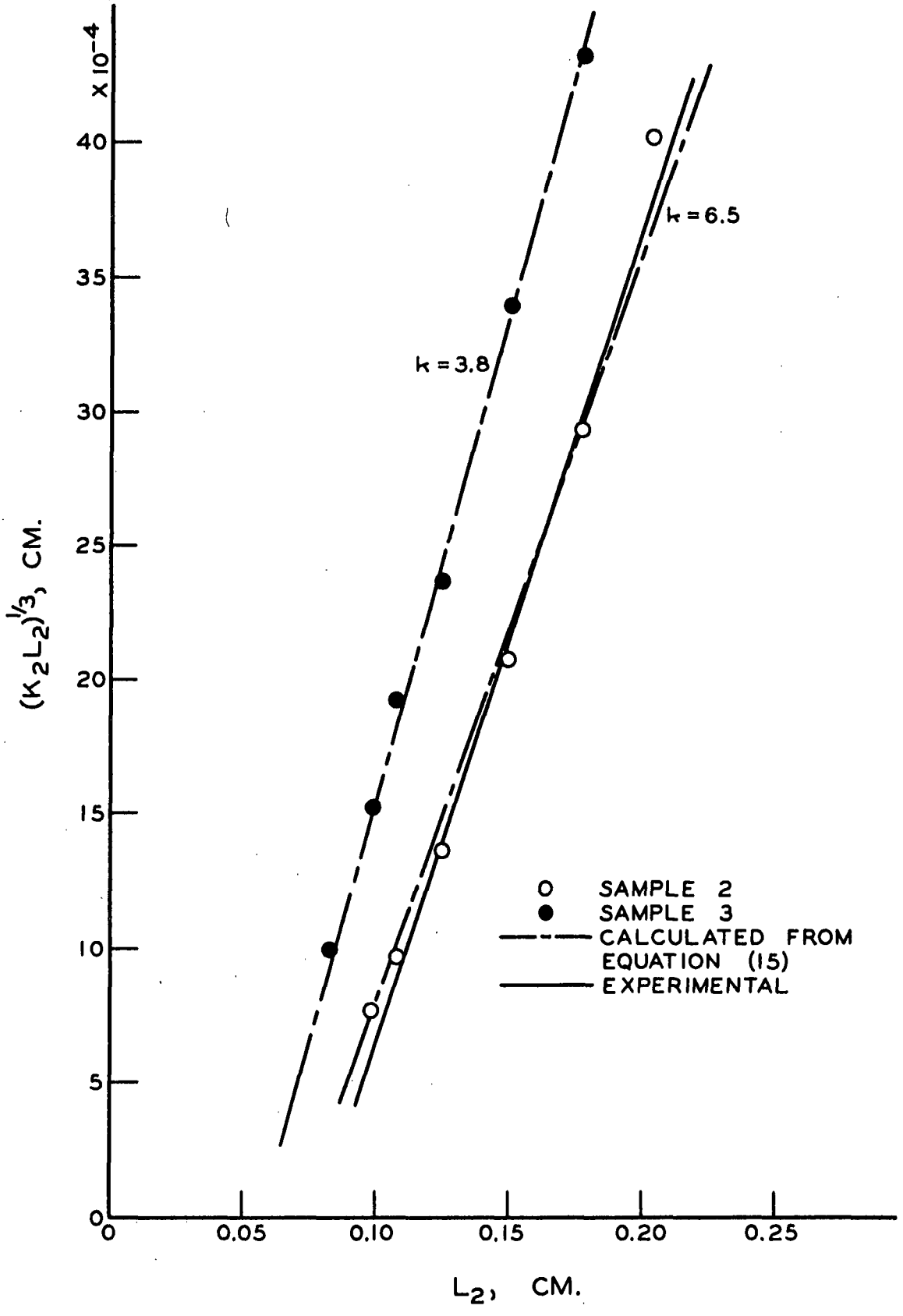

Figure 19. Lateral Permeability
(Samples 2 & 3)

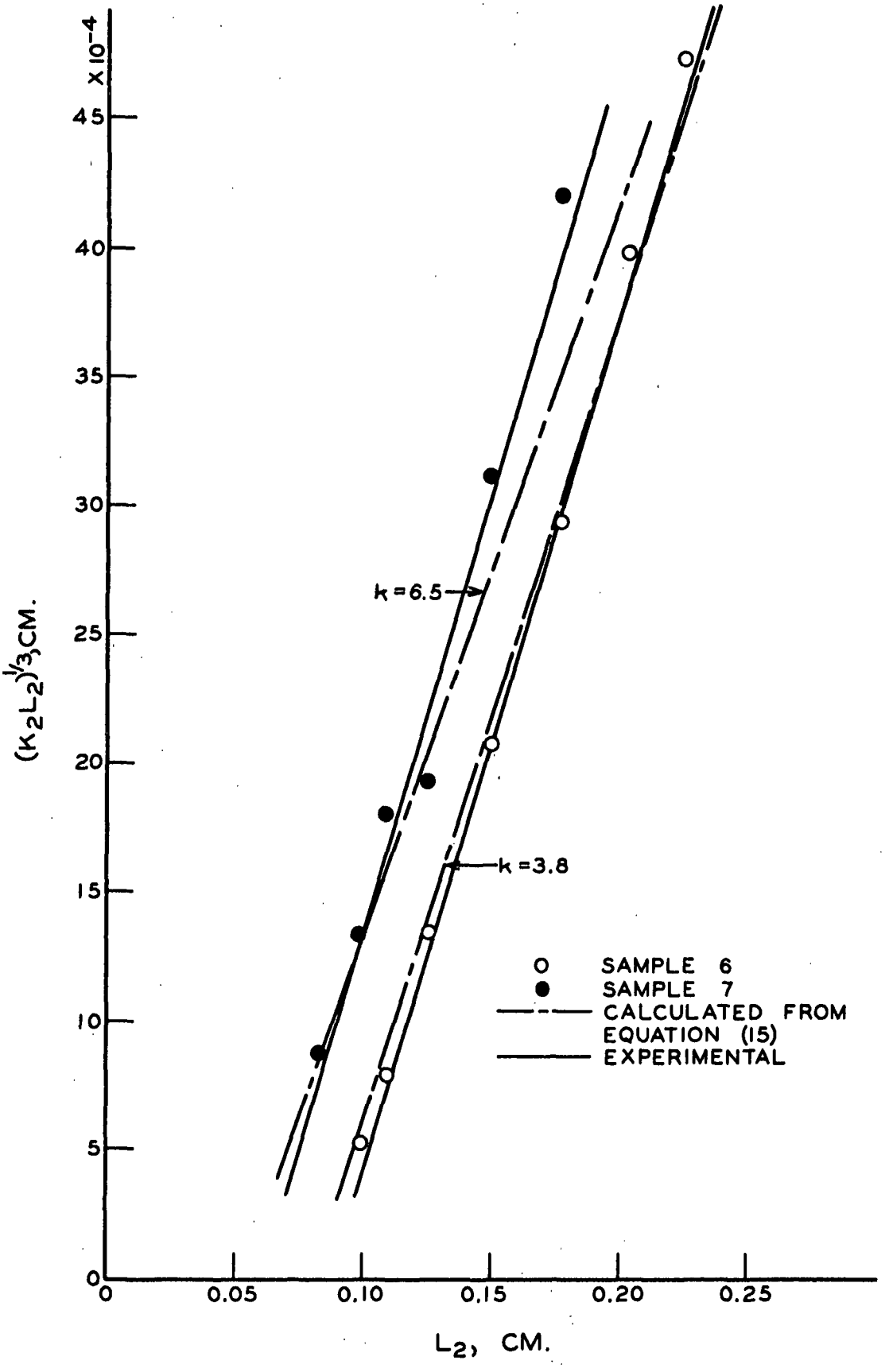

Figure 20. Lateral Permeability
(Samples 6 & 7)

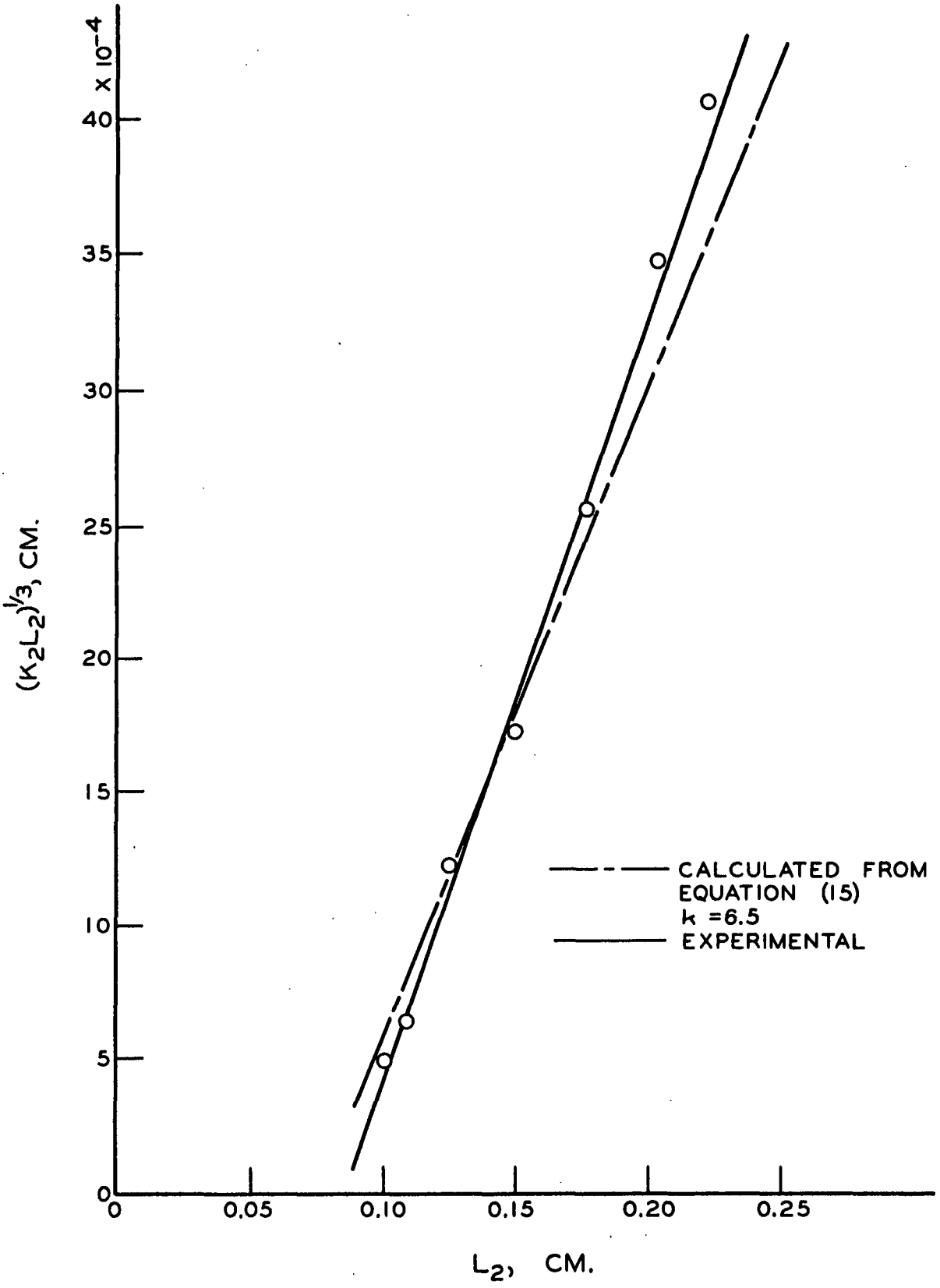

Figure 20a. Lateral Permeability
(Sample 8)

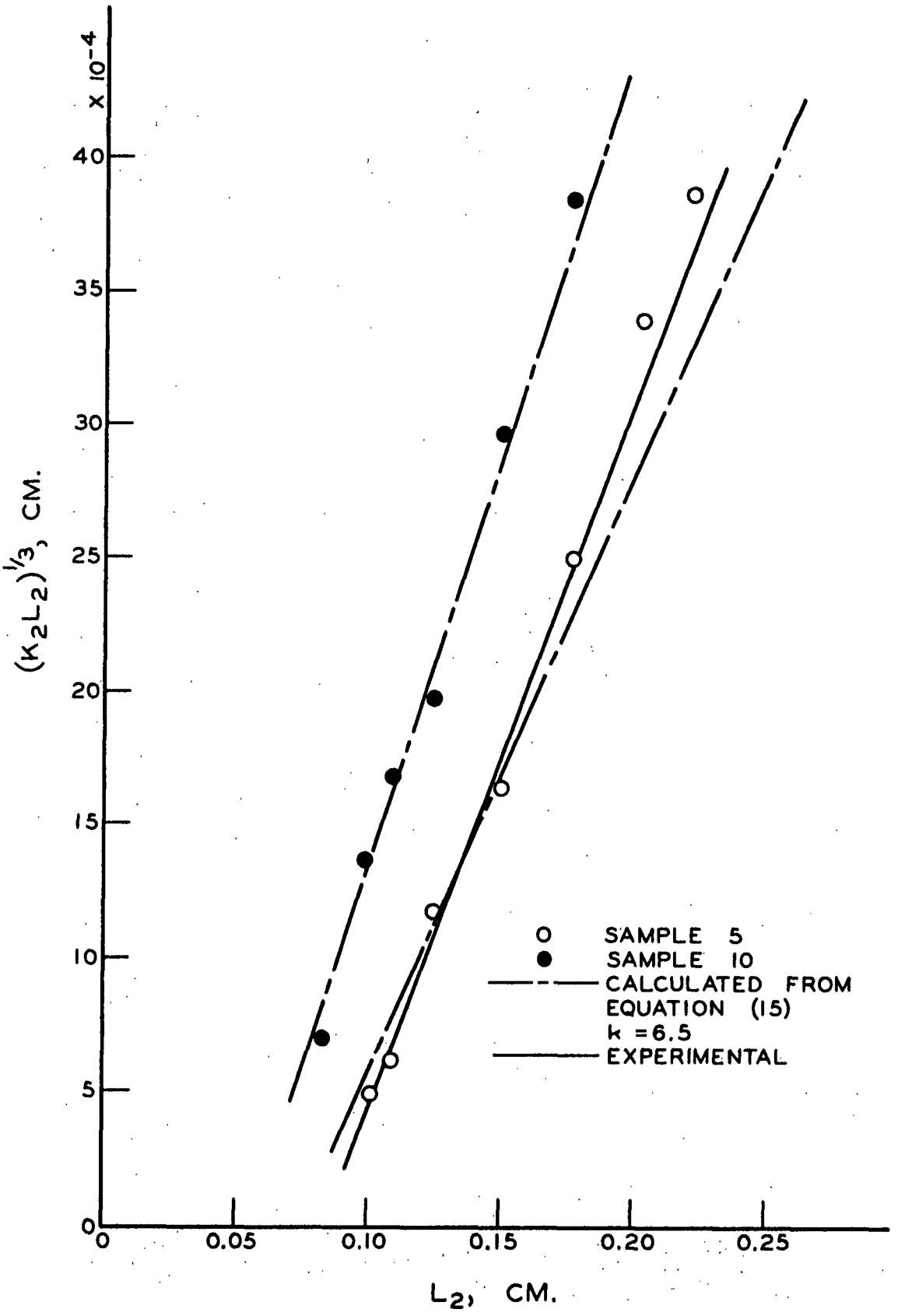

Figure 21. Lateral Permeability
(Samples 5 & 10)

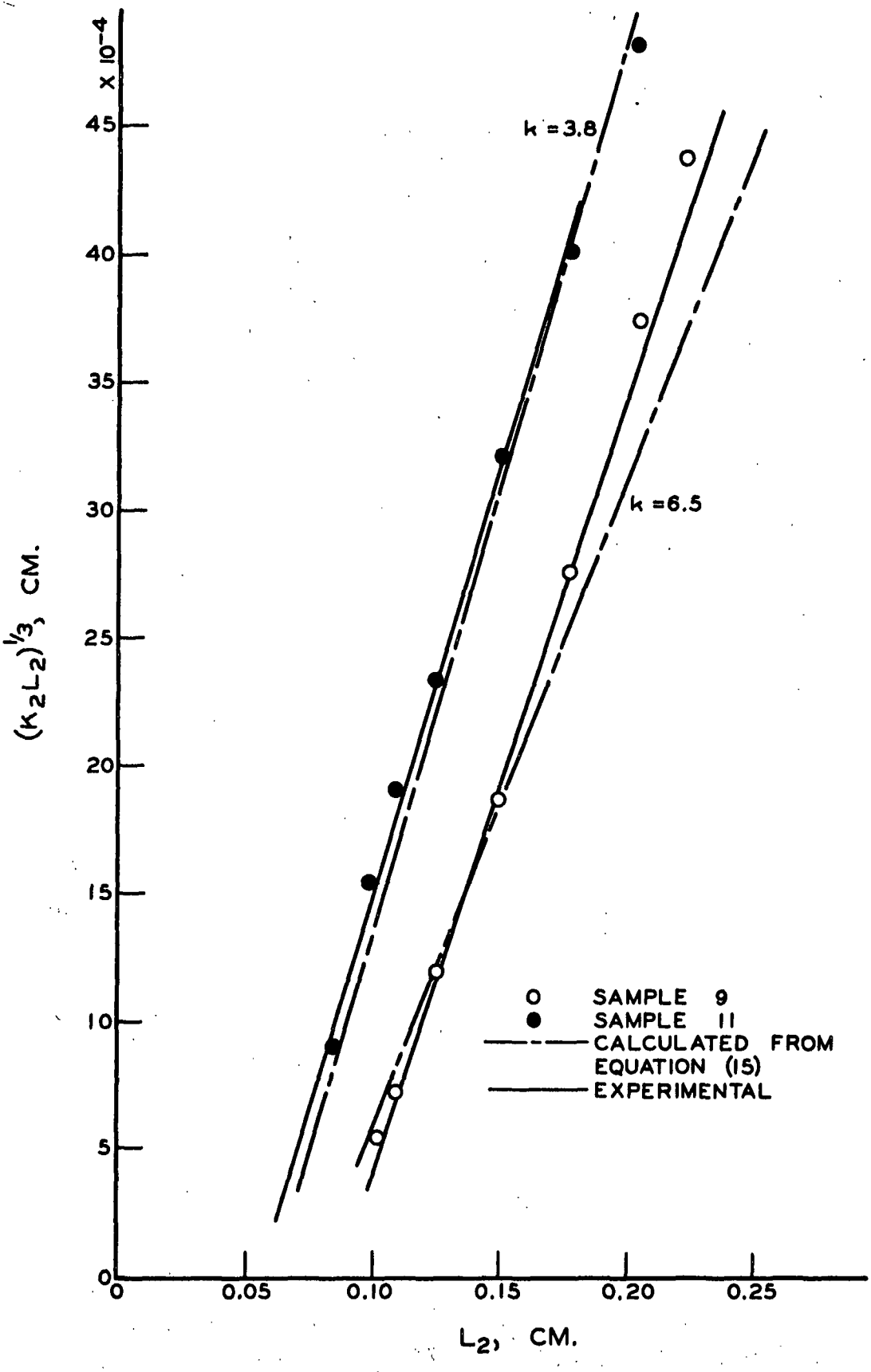

Figure 22. Lateral Permeability
(Samples 9 & 11)

the theory for the analysis of viscous flow through woven wool felts. Under the experimental conditions used here, the Kozeny-Carman equation appears valid over a wide porosity range for the felts tested. To evaluate the effect of the felt structure upon the permeability, the orientation-dependent Kozeny constant, $\underline{k}$, has been calculated and compared with values reported by others for fibrous beds of known orientation. Because the permeability of the felts in the lateral direction was quite different from their permeability in the transverse direction, the following discussion will consider each direction separately.

TRANSVERSE DIRECTION

The Kozeny constant, $\underline{k}$, was evaluated for each felt sample at several pad densities from Equation (9).

$$\underline{k} = \frac{\epsilon^3}{(1 - \epsilon)^2 \underline{KS}_v^2} \qquad (9)$$

The porosity of the water-swollen felt was evaluated from Equation (12):

$$\epsilon = 1 - \underline{vc} \qquad (12)$$

using the swollen specific volume, $\underline{v}$, determined microscopically, and the apparent pad density, $\underline{c}$, determined from the bed dimensions and oven-dry weight of the pad. The swollen specific surface of the fiber was evaluated from the microscopic fiber diameter measurements, and the transverse permeability constant, $\underline{K}$, was calculated as described previously.

In Table VII are given the corresponding values of porosity and Kozeny constant calculated from the transverse permeability data, assuming the swollen specific volume and specific surface invariant over the

TABLE VII

TRANSVERSE PERMEABILITY

POROSITY VERSUS KOZENY CONSTANT

($\underline{v}$ = 1.04 cc./g., assumed constant)

ϵ	$\underline{k}$	ϵ	$\underline{k}$	ϵ	$\underline{k}$	ϵ	$\underline{k}$
Sample 1		Sample 2		Sample 3		Sample 4	
0.671	9.2	0.672	8.6	0.708	5.8	0.698	6.3
0.639	8.5	0.645	8.5	0.681	5.5	0.652	6.0
0.587	7.5	0.591	7.2	0.613	6.1	0.581	5.8
0.520	6.8	0.525	6.6	0.572	6.8	0.530	6.3
0.421	6.3	0.434	5.7	0.500	6.8	0.474	6.3
0.365	6.3	0.350	5.0	0.442	6.7	0.394	5.2
0.255	4.4	0.280	3.5	0.325	4.3	0.286	3.0
0.164	1.8	0.149	1.1	0.230	2.1	0.204	1.3
				0.174	1.4		
Sample 5		Sample 6		Sample 7		Sample 8	
0.684	4.9	0.640	7.1	0.684	6.0	0.654	9.7
0.644	5.0	0.595	6.7	0.654	5.6	0.614	8.8
0.595	5.4	0.526	6.2	0.578	5.4	0.562	7.2
0.524	5.7	0.463	7.2	0.520	5.5	0.494	6.7
0.433	5.6	0.324	4.9	0.435	4.5	0.390	5.6
0.364	5.6	0.243	4.3	0.366	4.2	0.292	5.1
0.271	3.9	0.172	2.3	0.269	2.3	0.160	1.6
0.178	1.6	0.082	0.2	0.165	0.7		
Sample 9		Sample 10		Sample 11			
0.658	10.2	0.688	6.0	0.696	6.1		
0.610	8.8	0.628	5.5	0.651	5.9		
0.562	8.0	0.550	6.2	0.606	6.4		
0.486	7.1	0.504	5.8	0.505	5.4		
0.390	6.3	0.431	4.7	0.444	5.5		
0.315	5.4	0.354	3.8	0.383	5.2		
0.210	3.1	0.255	2.1	0.285	3.6		
0.140	1.1	0.150	0.2	0.215	2.3		

entire porosity range. At low porosities, an apparent abrupt decrease in the calculated Kozeny constant occurred, and calculated porosities of 0.1 and less were obtained. Since, from geometrical considerations, the lowest possible porosity obtainable with equal circular cylinders in parallel alignment is 0.093, and the diameters and alignment of the fibers in the felts do not approximate this ideal condition, such very small porosities are not realistic. Iberall (45) computed a minimum porosity of 0.41 for a closely packed array of fibers perpendicular to each other in three dimensions, and believed that lower porosities were obtained by compression of the material rather than fiber bending.

Since the fiber orientation in the felt does not closely approximate Iberall's model, a somewhat lower porosity would be expected, but certainly not the low porosities calculated on the basis of an invariant specific volume. These considerations lend support to the idea of a gradual decrease in the effective specific volume of the fiber under high compressive loads.

For most of the samples at calculated porosities greater than 0.35, the variation in the Kozeny constant was not great. From the work of others, a very gradual decline in the value of k with a decrease in porosity is to be expected in the porosity range of interest here (0.7 and less). The precision of these data, however, is not good enough to show such a gradual variation, and it seems better to assume an average constant value of the Kozeny constant over the porosity range of interest. From Table VII it may be observed that an average value of k of 6.5 is applicable for most samples over the porosity range, 0.40 to 0.70. For Samples 5, 7, and 10, an average value of k of 5.4 seems more probable.

On the basis of the previously quoted work of others relative to the dependence of k on fiber orientation, the fiber orientation for most of the samples appears to be predominantly perpendicular to flow. The fiber orientation in Samples 5, 7, and 10, however, tends toward a more random arrangement as indicated by the lower value of k. The more complex weave pattern of Samples 5 and 10 probably presents a more randomized fiber orientation than the regular pattern of the other weaves. Because Sample 7 is characterized by a smaller yarn size and smaller average fiber diameter, it probably is deformed more easily under load and assumes a more randomized fiber orientation than the other samples having the same weave but larger fiber and yarn sizes. When the felt samples are compressed to porosities lower than 0.40, their fiber and yarn orientation would not be expected to change much, and the Kozeny constant probably remains relatively constant.

The effective specific surface of the fibers probably does not vary significantly at these lower porosities. The increase in specific surface due to the deswelling of the fiber would be offset by the simultaneous increase in fiber-to-fiber contact.

Therefore, in the lower porosity region, a logical assumption is that the effective specific surface and the effective fiber orientation (and thus the Kozeny constant) do not change too much with compression, but the effective specific volume varies significantly. Assuming S_v and k constant, the effective specific volume, v, may be calculated from Equations (9) and (12). This calculation was made for each felt sample at several pad densities, and the results are presented

in Table VIII. The effective specific volume is actually a function of the compacting load applied to the sample. For convenience in this discussion and in the plotting of the specific volume data, effective specific volume, $\underline{v}$, is given as a function of the porosity and the apparent pad density in Table VIII, and the effective specific volume is plotted as a function of the apparent pad density, $\underline{c}$, in Fig. 23-25. Conversion of the values of pad density to the corresponding values of compressive load, $\underline{P}$, can easily be made, if desired, with the compressibility data to be presented in the following section because it will be shown that the apparent pad density is a logarithmic function of the compressive pressure applied to the pad.

Referring to Table VIII and Fig. 23-25, the effective specific volume for all the samples remains relatively constant at 1.04 cc./g. down to a pad density around 0.6 g./cc. (ϵ of about 0.4). As the pad density is increased above 0.6 g./cc., the effective specific volume decreases. As discussed previously, extrapolations of the data in Fig. 13-17 to $\underline{L}_o$ indicated that the pycnometric density of the fiber was closely approached at zero porosity. At zero porosity the bed density, $\underline{c}$, and effective fiber density, $1/\underline{v}$, would be the same, and from the extrapolation were shown to be equal to the density of the dry wool fiber, 1.304 g./cc. Therefore, on the plot of $\underline{c}$ versus $\underline{v}$ when the bed density reaches that of the dry fiber, 1.304 g./cc., the effective specific volume of the fiber would be the reciprocal, 0.766 cc./g. The curves of Fig. 23-25 are drawn to this point. Compressive loads greater than 1000 p.s.i. could not be applied to the pad with the apparatus as designed, and thus no data are available for pad densities larger than 0.8 to 0.9 g./cc.

TABLE VIII

VARIATION IN SPECIFIC VOLUME WITH POROSITY

(k, S_v assumed constant)

ϵ	c, g./cc.	v, cc./g.	ϵ	c, g./cc.	v, cc./g.	ϵ	c, g./cc.	v, cc./g.
	Sample 1			Sample 2			Sample 3	
0.671	0.317	1.15	0.672	0.316	1.12	0.708	0.282	1.0
0.639	0.348	1.11	0.645	0.342	1.12	0.681	0.307	0.99
0.587	0.400	1.07	0.591	0.394	1.06	0.613	0.373	1.02
0.520	0.463	1.04	0.525	0.460	1.04	0.572	0.412	1.05
0.421	0.558	1.04	0.434	0.546	1.02	0.50	0.481	1.05
0.365	0.612	1.04	0.375	0.626	1.0	0.442	0.537	1.05
0.280	0.718	1.00	0.318	0.694	0.985	0.359	0.650	0.99
0.235	0.806	0.95	0.250	0.820	0.915	0.307	0.743	0.935
						0.268	0.796	0.92
	Sample 4			Sample 5			Sample 6	
0.698	0.291	1.03	0.684	0.304	1.01	0.640	0.346	1.07
0.652	0.336	1.02	0.644	0.343	1.02	0.595	0.390	1.05
0.581	0.404	1.01	0.595	0.390	1.05	0.526	0.456	1.03
0.530	0.453	1.03	0.524	0.459	1.05	0.463	0.537	1.02
0.474	0.507	1.03	0.433	0.546	1.04	0.345	0.653	1.0
0.415	0.585	1.00	0.364	0.613	1.04	0.270	0.730	1.0
0.349	0.688	0.945	0.296	0.702	1.0	0.232	0.798	0.963
0.315	0.768	0.890	0.273	0.792	0.92	0.203	0.883	0.905
	Sample 7			Sample 8			Sample 9	
0.684	0.304	1.07	0.654	0.334	1.15	0.658	0.330	1.17
0.654	0.334	1.05	0.614	0.372	1.12	0.610	0.376	1.12
0.578	0.407	1.04	0.562	0.422	1.07	0.562	0.422	1.09
0.520	0.463	1.04	0.494	0.488	1.04	0.486	0.495	1.06
0.435	0.545	1.02	0.402	0.587	1.02	0.390	0.587	1.04
0.380	0.610	1.02	0.311	0.682	1.01	0.330	0.660	1.02
0.334	0.705	0.945	0.238	0.810	0.94	0.259	0.761	0.975
0.294	0.805	0.88				0.233	0.829	0.928

TABLE VIII (Cont'd.)

ϵ	c, g./cc.	v, cc./g.	ϵ	c, g./cc.	v, cc./g.
	Sample 10			Sample 11	
0.688	0.301	1.07	0.696	0.293	1.01
0.628	0.359	1.04	0.651	0.336	1.02
0.550	0.433	1.07	0.606	0.379	1.03
0.504	0.478	1.04	0.505	0.476	1.0
0.431	0.549	1.02	0.444	0.536	1.01
0.383	0.623	0.995	0.402	0.595	1.0
0.325	0.717	0.94	0.330	0.689	0.975
0.296	0.816	0.86	0.286	0.756	0.944

At low pad densities (high porosities), an apparent increase in the effective specific volume above the water-swollen value of 1.04 cc./g. is observed for 4 samples. These points correspond to the deviations from linearity observed for Samples 1, 2, 8, and 9 at large values of L in Fig. 13-17. The accuracy of these high-porosity data is probably not as good as the medium and low-porosity data, because the measured pressure drops were small and had to be corrected for the resistance of the septum and piston. Nevertheless, the deviation in the effective specific volume from the average of 1.04 cc./g. is greater for these samples than for the others, and these samples are similar in having the same yarn size, same number of picks per inch, and either a plate or sateen weave. Thus, their structure rather than experimental error may be responsible for the observed deviation.

Because an increase in specific volume larger than that determined for the swollen fiber is not realistic, the Kozeny constant must increase

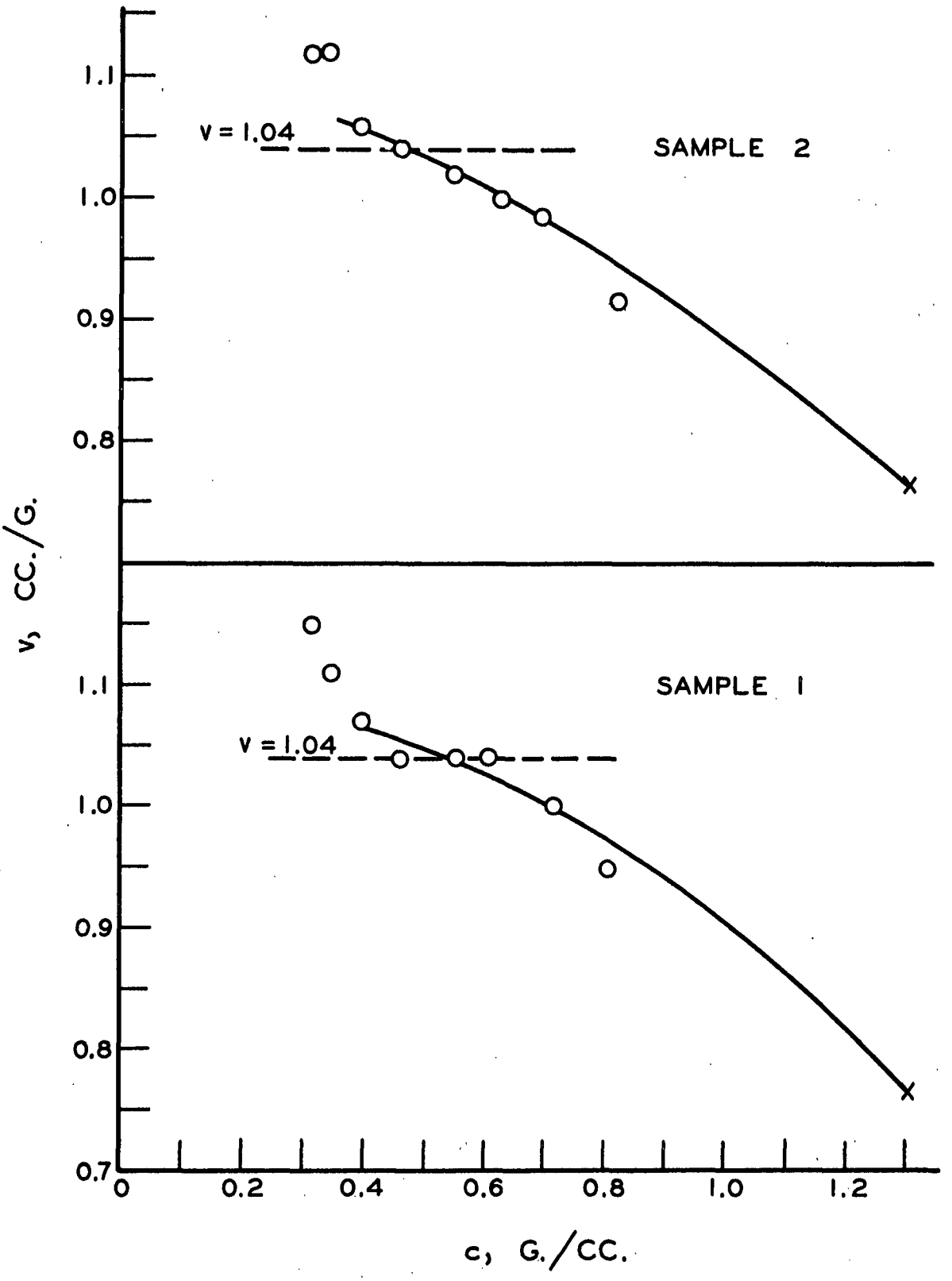

Figure 23. Transverse Permeability Variation v With c

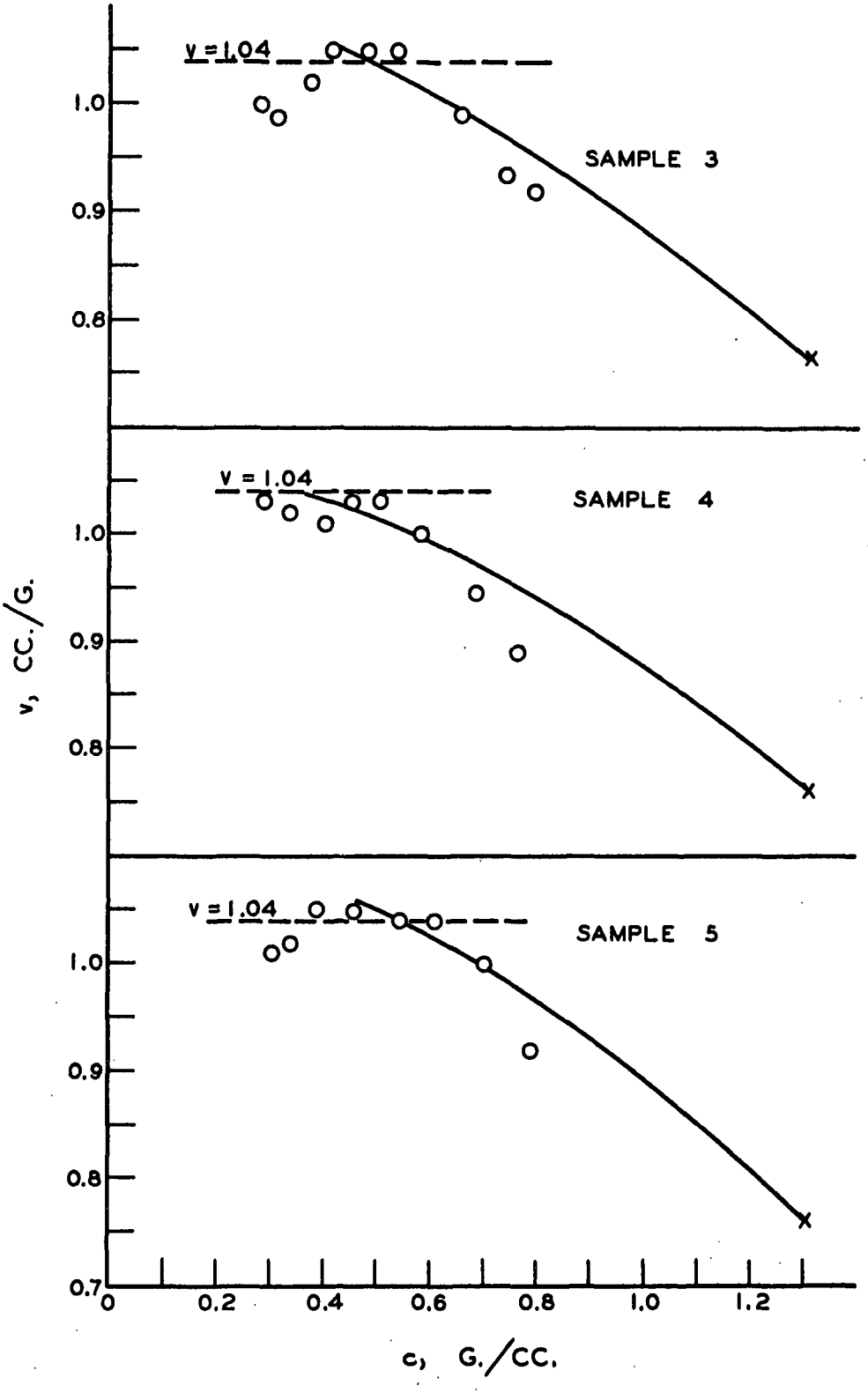

Figure 23a. Transverse Permeability Variation v With c

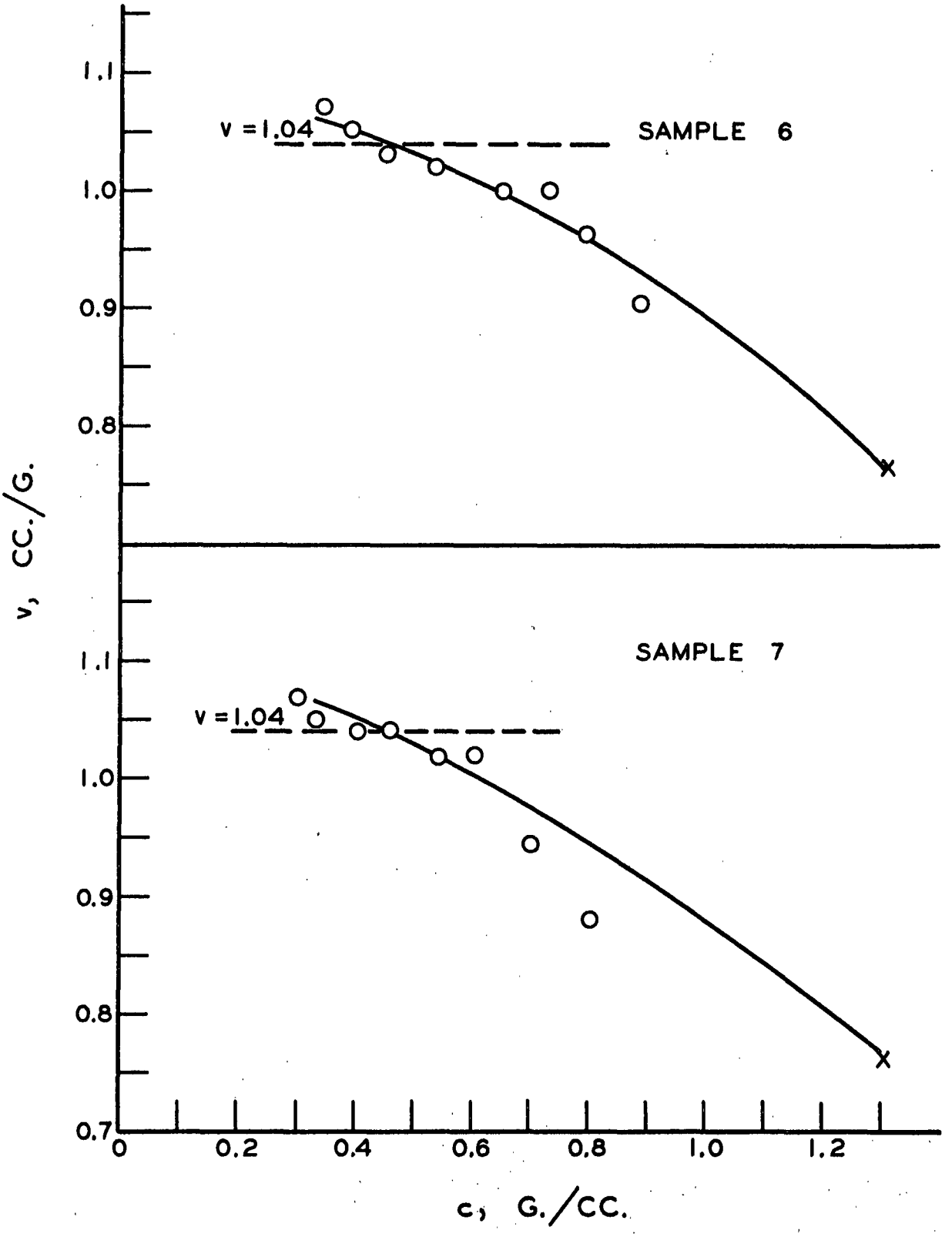

Figure 24. Transverse Permeability Variation v With c

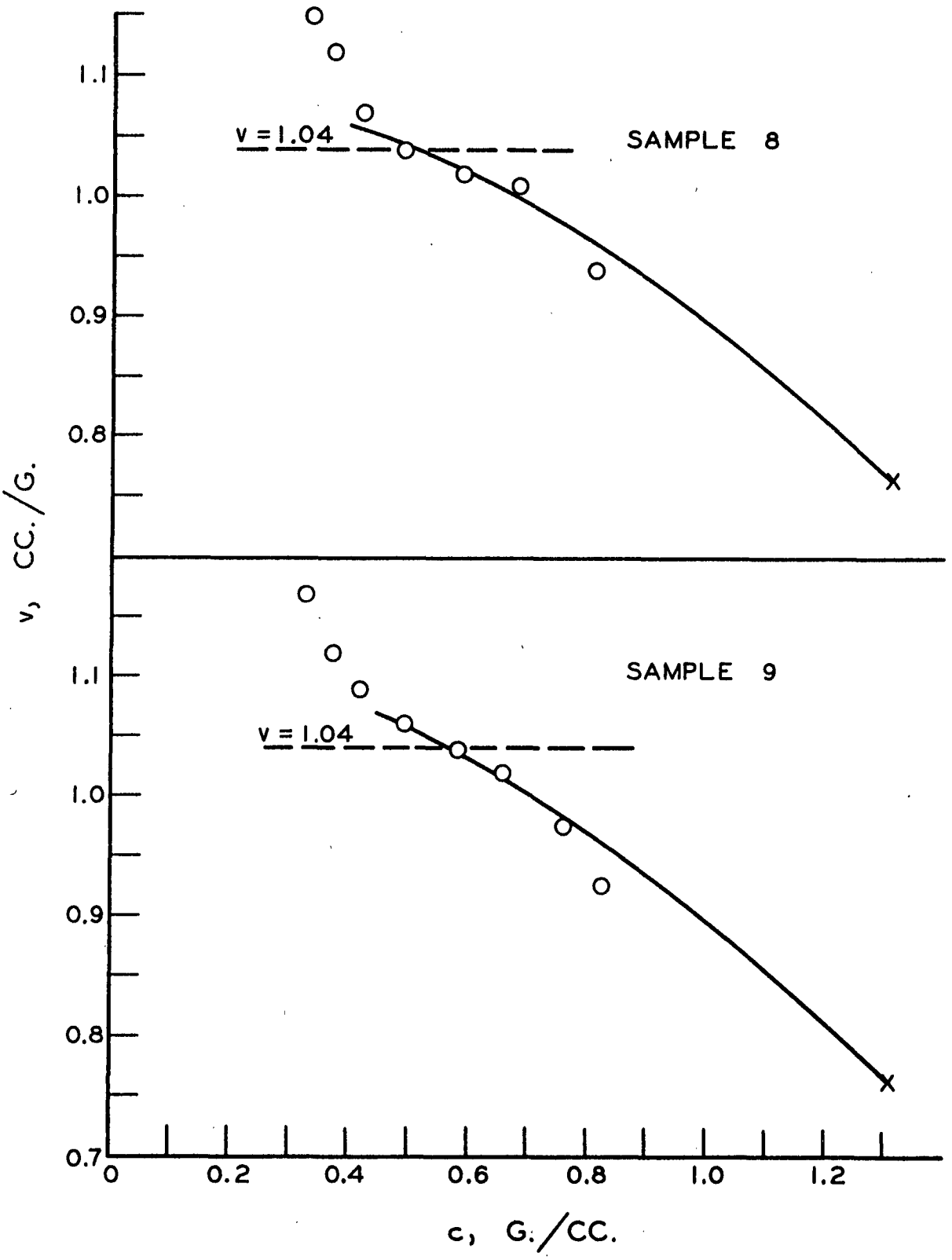

Figure 24a. Transverse Permeability Variation v With c

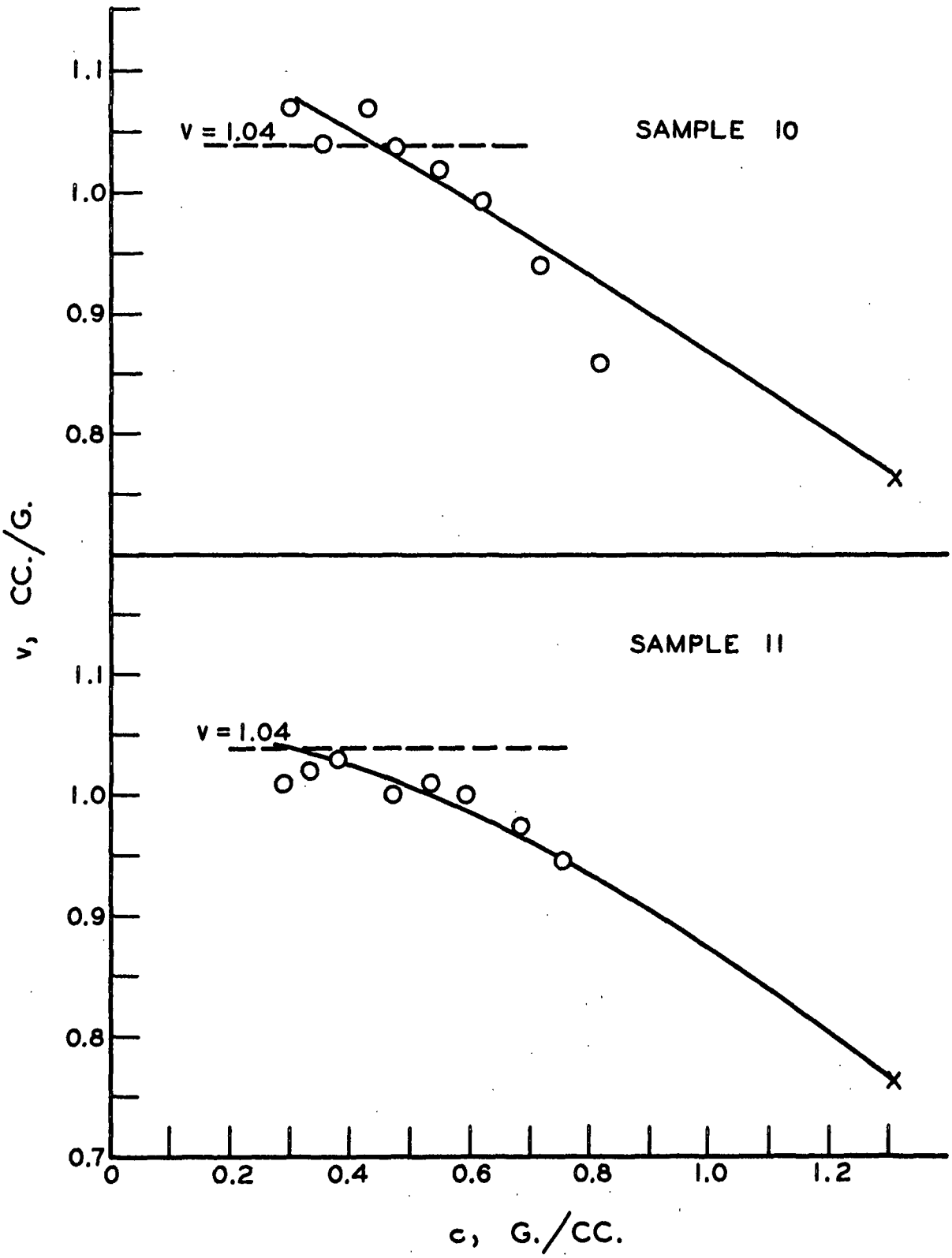

Figure 25. Transverse Permeability Variation v With c

at high porosities for these samples. The two weaves possessed by these samples, in contrast to the duplex weave, are somewhat stratified with respect to warp and fill yarns. Thus, in the uncompressed state, flow would proceed through a series of two or three layers of fibers, one-yarn-diameter thick, oriented parallel to each other and normal to flow. The fiber and yarn orientation in alternate layers would be at right angles to those preceding or following. The shape of the flow channels in each layer would be similar to parallel slits, for which Carman (12) has determined a shape factor, k_o, of 3.0. As the sample is compressed, the yarns flatten out and the layers of fibers merge to form square- or rectangular-shaped flow channels, for which Carman gives a shape factor of 1.94. Therefore, a larger shape factor (and thus Kozeny constant) would be expected for the uncompressed felt than for the compressed felt, and a gradual transition from the larger shape factor to the smaller with increasing compressive loads would be expected. This behavior is not observed in other samples with the same weave but fewer picks per inch or a smaller yarn size, probably because the yarns are less crowded and flatten out under compressive loads smaller than the initial loading used.

Brief mention has already been made of the more randomized fiber orientation observed for Sample 7 as indicated by the smaller average value of k. The small yarns and small fibers of Sample 7 are probably more easily deformed under load than are the heavier yarns and larger fibers of Sample 2, which is otherwise of the same construction. No important difference in transverse flow characteristics is observed between Samples 6 and 3, which also are of similar construction except

for yarn size. The average fiber diameters given in Table V indicate a difference of 20% in the fiber diameters of Samples 2 and 7 but only a difference of about 10% in the fiber diameters of Samples 3 and 6. Therefore, the more randomized fiber orientation of Sample 7 is more likely caused by the difference in average fiber size rather than yarn size. Yarn size, therefore, does not significantly affect the transverse permeability, at least for the samples considered here.

The effect of napping upon transverse permeability may be observed by consideration of the data for sample pairs 1 and 8, 2 and 9, and 3 and 11. The sample appearing first in each pair was not napped; the other sample was of the same construction but napped. The specific surface, determined from microscopic fiber diameter measurements, was closely the same for both samples of each pair. These specific surface values were used in conjunction with the appropriate permeability data to calculate the Kozeny constant for each sample at several pad densities. Any significant variation noted in $\underline{k}$ between the samples of each pair could be the result of an erroneous value of the specific surface as well as a difference in the fiber orientation. Therefore, if napping increased the specific surface in some manner such as fibrillation, a much larger value of $\underline{k}$ would be obtained for the napped sample than for the sample with no nap. If the specific surface remained unchanged after napping but the fiber orientation changed, the value of $\underline{k}$ for the napped felt would be significantly different from the $\underline{k}$ of the felt with no nap. Examination of the transverse-permeability data in Table VII shows no significant difference in the average value of $\underline{k}$ between the napped and

unnapped felts. Napping, therefore, does not appear to significantly change the specific surface of the fibers or the fiber orientation affecting transverse permeability. As discussed before, the napping operation merely teases out fiber ends from the fill yarns. It seems reasonable then that the specific surface of the fibers is not changed. The fiber orientation may be disturbed somewhat by napping, but evidently the loose ends of the fibers resume an orientation normal to flow when a compressive load is applied or flow is initiated. Also, the number of fibers affected in napping is so small in comparison with the total number of fibers in the pad that the measurable effect upon permeability is negligible.

From the preceding discussion it may be concluded that the effect of the different structural variables upon transverse permeability is minor. In general, the fiber and yarn orientation is normal to flow. A more randomized fiber orientation is observed for an irregular-weave pattern where the fill and warp yarns are entwined to a greater extent than in the more regular-weave patterns. Combinations of the regular-weave patterns and a high number of picks per inch were observed to cause a slight variation in the shape factor at very high porosities. Yarn size in itself did not affect permeability, but finer, smaller diameter fibers appeared to assume a more randomized orientation under compression than coarser, larger diameter fibers. The major effect observed, which was largely independent of the structural characteristics of the felt, was the deswelling of the water-swollen wool fiber as larger and larger compressive loads were applied to the pad.

LATERAL DIRECTION

In the calculation of the Kozeny constant for the lateral permeability of the various samples, the effective specific volume of the fiber was corrected for the deswelling observed under large compressive loads. The Kozeny constant was calculated for each sample at several pad densities from Equation (9) using the specific surface determined from microscopic fiber diameter measurements and the effective porosity at each pad density calculated from Equation (12). The water-swollen specific volume of the fiber, determined microscopically, was used in the porosity calculation except at pad densities greater than 0.6 g./cc. where the decrease in specific volume of the fiber became significant. At the larger pad densities, the correct value of the specific volume was obtained from Fig. 23-25.

The calculated value of the Kozeny constant at several porosities is given for each sample in Table IX. Comparison of these data with the structural properties of the various felt samples given in Table I indicates a strong dependence of the Kozeny constant upon the number of picks per inch and the weave pattern. As will be recalled, the number of warp yarns per inch (i.e., 48) is the same for all samples and thus is not a consideration.

The variation in Kozeny constant with porosity was similar for all samples having 70 picks per inch and also for Sample 10, which has 48 picks per inch but a duplex-weave pattern. The data for these samples are plotted in Fig. 26. The variation in Kozeny constant with porosity

TABLE IX

LATERAL PERMEABILITY
POROSITY VERSUS KOZENY CONSTANT

ϵ	k	ϵ	k	ϵ	k	ϵ	k
Sample 1		Sample 2		Sample 3		Sample 4	
0.678	3.9	0.644	4.2	0.674	3.8	0.693	3.2
0.652	4.9	0.591	5.8	0.614	3.6	0.638	4.4
0.595	7.5	0.516	6.6	0.538	4.1	0.567	6.2
0.510	7.6	0.419	7.2	0.469	3.2	0.500	3.7
0.415	8.4	0.350	8.2	0.419	3.6	0.449	3.7
0.345	11.1	0.311	9.2	0.336	4.3	0.370	6.6
Sample 5		Sample 6		Sample 7		Sample 8	
0.662	5.1	0.639	3.0	0.692	3.6	0.650	3.6
0.630	4.9	0.606	3.3	0.638	4.2	0.618	4.3
0.575	6.2	0.547	4.1	0.565	6.9	0.561	5.6
0.499	8.6	0.468	4.3	0.500	3.9	0.486	7.1
0.399	7.0	0.375	5.1	0.449	5.2	0.390	6.2
0.336	20.6	0.306	9.6	0.366	7.6	0.322	16.7
0.304	26.3	0.269	18.4			0.291	24.4
Sample 9		Sample 10		Sample 11			
0.646	3.8	0.678	5.5	0.694	3.8		
0.613	4.0	0.620	5.6	0.649	3.6		
0.555	5.0	0.545	7.5	0.586	3.8		
0.477	6.2	0.476	5.4	0.504	3.0		
0.386	7.5	0.426	5.4	0.432	2.3		
0.317	12.8	0.350	13.8	0.385	2.8		
0.284	17.9			0.310	4.1		

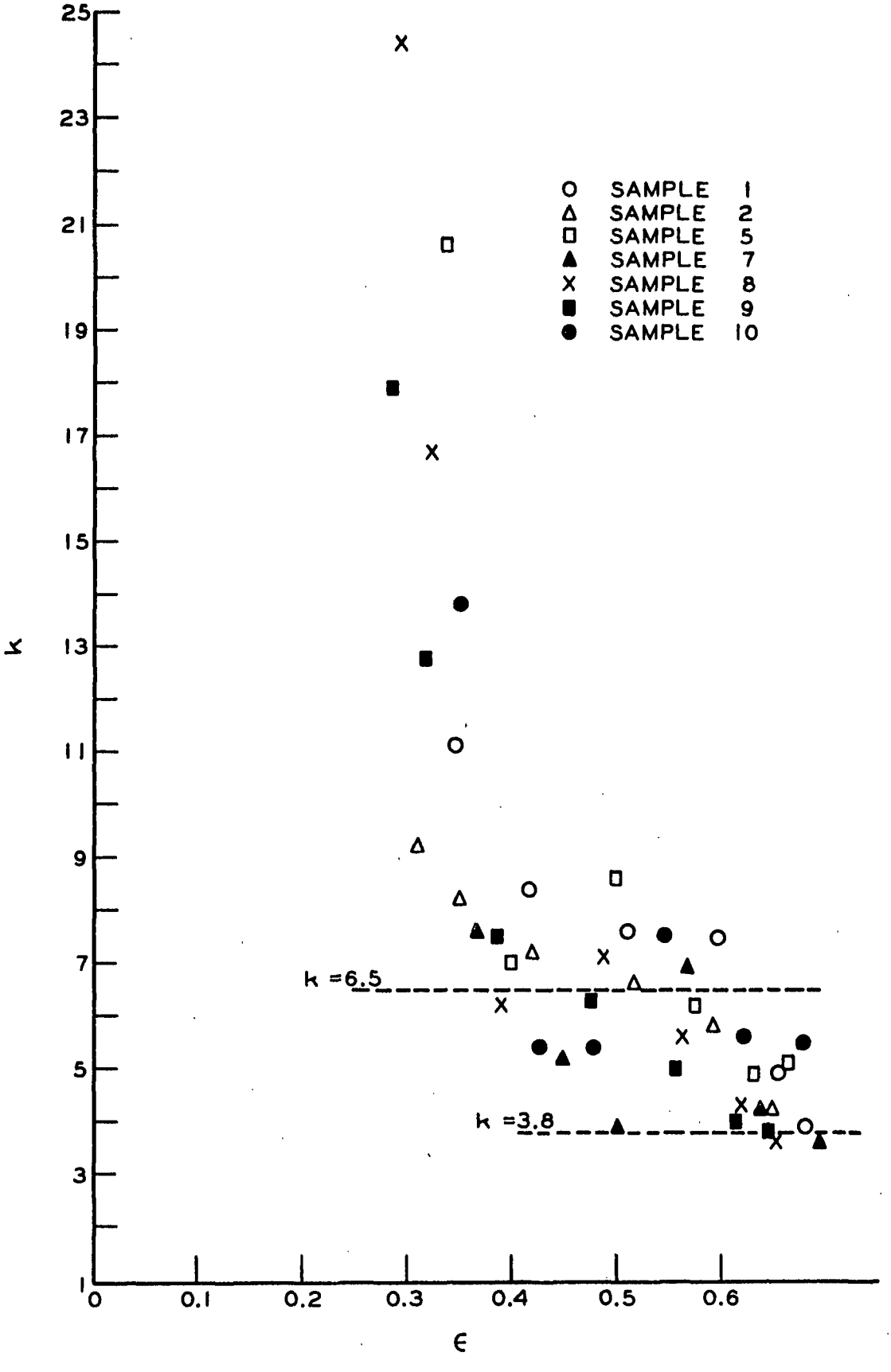

Figure 26. Lateral Flow Variation k With ϵ

for all samples having 48 picks per inch and either a plate or sateen weave was similar, but differed from the variation noted for the other samples. The data for the latter group are plotted in Fig. 27.

For all samples, the warp yarns are oriented parallel to the flow direction. Therefore, a certain proportion of the total flow would be expected to proceed parallel to these yarns and to the fibers in them. The calculated values of the Kozeny constant presented are average values based on the proportions of the total flow proceeding parallel to and perpendicular to the fiber axes. The major portion of the flow parallel to the fiber axes would occur in the warp yarns, and the major portion of the flow perpendicular to the fiber axes would occur in the fill yarns (picks). However, the weave pattern and applied compressive load will each modify this basic flow orientation, particularly the parallel fiber alignment in the warp yarns. The sensitivity of the value of the Kozeny constant to the degree of parallelism of the fibers and to the porosity for flow parallel to the fiber axes will be recalled from the research of others discussed previously. For example, research (25, 27) on flow parallel to carefully aligned circular fibers has shown a decline in the Kozeny constant from a value of 3.0 at a porosity of 0.8 to 1.0 at a porosity of 0.35. Other work (28) concerned with different bundles of wool fibers aligned parallel to flow indicated that k was reasonably independent of porosity in the porosity range 0.45 to 0.7, having values ranging from 1.6 for coarse fibers to 2.5 for fine fibers. This range of values no doubt reflects the degree of parallelism of the fibers, because the coarser fibers, more easily straightened than the fine fibers, would tend to be more closely parallel and would

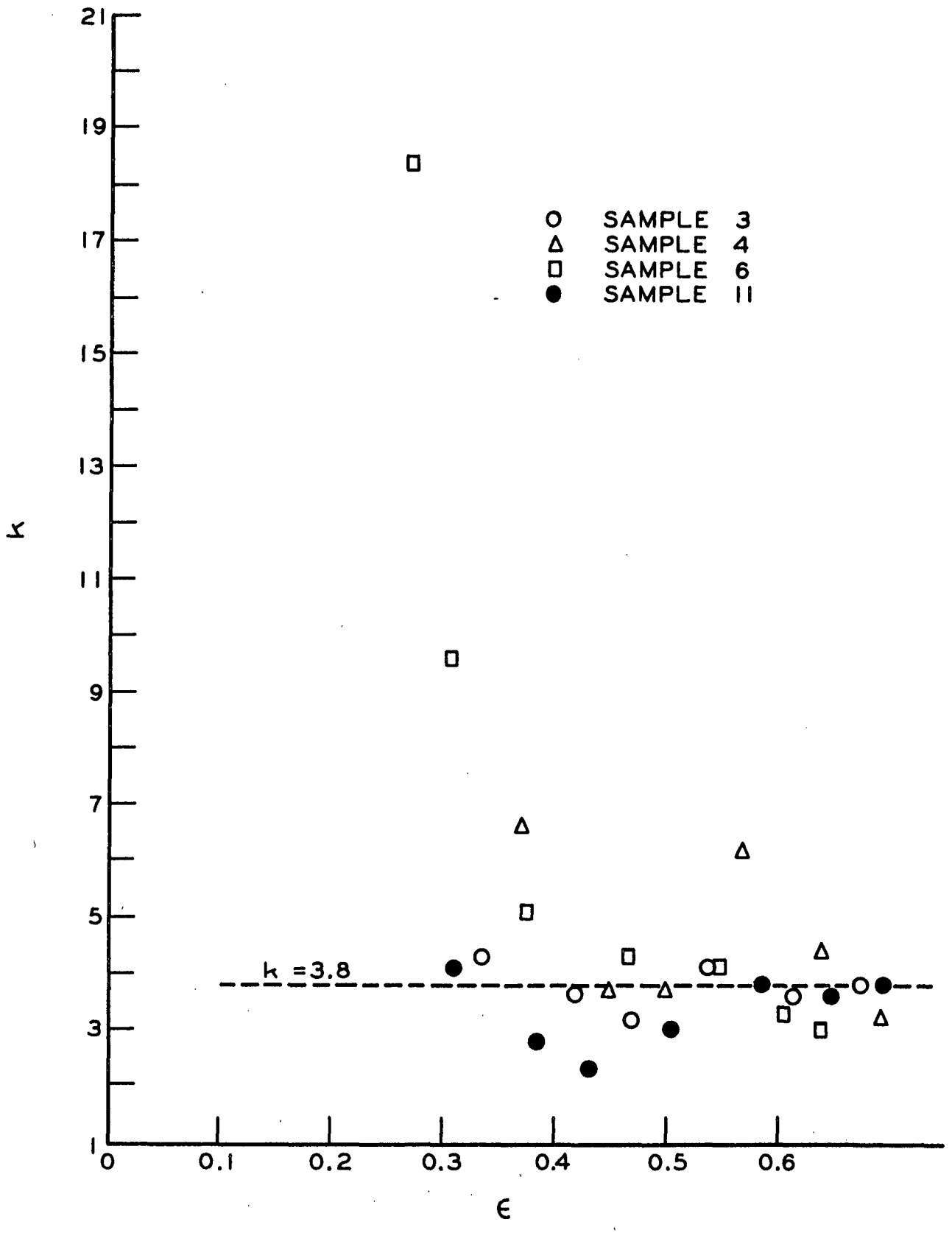

Figure 27. Lateral Flow Variation k With ϵ

present a less tortuous flow path. When these same fibers were rearranged into random beds of 0.7 porosity, an average value of $\underline{k}$ of 6.1 was observed for all fiber bundles with very little variation of the individual values from the average. Using the above considerations and observations as a basis, the importance of the felt structure to the lateral permeability of the various samples may be better understood from Fig. 26 and 27.

Referring to Fig. 27, those samples having 48 picks per inch (and 48 warp yarns per inch) and either the sateen or plate weave are characterized by an average Kozeny constant of 3.8 over the porosity range 0.3 to 0.7. This small, relatively constant value of $\underline{k}$ indicates that a considerable portion of the flow must proceed through the warp yarns parallel to the fiber axes. Because perfect parallel fiber alignment is not possible in these felts, the decrease in $\underline{k}$ with porosity observed by others would not be expected. The relatively constant value of $\underline{k}$ probably indicates a gradual alteration in the parallel fiber alignment with the compression of the samples.

Referring to Fig. 26, those samples (1, 2, 7, 8, 9) having the plate or sateen weave and 70 picks per inch are characterized by a relatively constant value of $\underline{k}$ of 6.5 over the porosity range 0.3-0.6 and a relatively constant average value of $\underline{k}$ of 3.8 at higher porosities. A Kozeny constant of 6.5 was also observed for transverse permeability and from the research of others, discussed previously, is characteristic of flow perpendicular to the fiber axes. The average value of $\underline{k}$ of 3.8, also observed for lateral flow for those samples having an equal number of picks and warp yarns per inch, is indicative of a large proportion

of flow parallel to the fiber axes. Evidently, the greater number of picks per inch in these samples not only constitutes the larger proportion of the total pad volume, but upon compression, they must twist and distort the initially parallel warp yarns and thereby produce an effective fiber orientation primarily perpendicular to flow. At high porosities, parallel flow through the warp yarns is not interrupted greatly by the fill yarns, and in spite of the greater number of fill yarns per unit volume, the warp yarns still carry a large proportion of the flow.

Samples 5 and 10 (Fig. 26), having the duplex weave, are characterized by an average Kozeny constant of 6.5, and thus flow primarily perpendicular to the fiber axes, in the porosity range 0.3-0.7. The small value of $\underline{k}$ at high porosities observed for all other samples is not characteristic of these samples. Evidently, the more irregular duplex weave, in contrast to the more regular sateen and plate weaves, results in more distortion of the parallel warp yarns by the fill yarns. As discussed previously, the plate weave is characterized by predominantly fill yarns on both surfaces which envelop the warp yarns in the center; the sateen weave is characterized by predominantly fill yarns on one surface and warp yarns on the other; but the duplex weave is formed in such a manner that both felt surfaces have a mixed amount of warp and fill yarns.

All of the samples were characterized by an apparent increase in the Kozeny constant at porosities of 0.3 and less. Calculated values of $\underline{k}$ as large as 26.3 were observed. If an average value of 2.5 is assumed for the shape factor, $\underline{k}_o$, a tortuosity, $(\underline{L}_e/\underline{L})^2$, of about 10 would be indicated.

Carman (12) has argued that the value of L_e/L should be about 1.5 for unconsolidated porous beds. A tortuous path around 50% longer than the bed depth seems logical, but a tortuous flow path more than three times as long as the bed depth ($L_e/L = \sqrt{10}$) does not seem realistic.

In the calculation of the Kozeny constant, the porosity was evaluated from Equation (12). Therefore, the assumption was made that all of the pore space in the highly compressed felt was equally available for lateral flow. However, it seems probable that under high compression, the distortion of the yarns and the orientation of the areas of fiber-to-fiber contact must produce a pore network of such a nature that the fractional void area at some sections is much less than at others. If so, some of the pore space may become sealed off and would not take an effective part in the permeation. If such were the case, the effective porosity would be less than the value used here, and the calculated value of the Kozeny constant is thus too high. Therefore, the high calculated values of the Kozeny constant observed at porosities less than 0.3 probably result primarily from the use of a value of ϵ that includes pore space unavailable for lateral flow. Some changes in the tortuous flow path and the shape factor probably occur also under the high compressive loads used because of the twisting and distortion of the warp yarns by the fill yarns, but probably contribute less to the observed increase in k than the changes in the effective porosity.

The reason that some of the pore space can be unavailable to lateral flow under high compression, but can still be available to transverse flow under the same compression is probably related to the differences in the

effective fiber and yarn orientation in the two directions. As large compressive loads are applied to the felt, the fibers must tend to move in a direction normal to the applied load into the larger adjacent inter-yarn pore spaces. When these spaces are occupied, increasing consolidation of the individual yarns occurs by slippage of the fibers into inter-fiber pore spaces below. This slippage can occur because the fibers in each yarn are generally parallel to one another. Where the fibers cannot slip between other fibers, they are deformed and deswelled as other fibers are contacted. Because the fill and warp yarns are perpendicular to each other, compression would cause a gridlike orientation of the fibers for transverse flow. Thus, the average pore size could be reduced with compression without greatly affecting the availability of the pore space.

Viewing the felt from the lateral direction, the fibers in the fill yarns, which are normal to flow, can slip behind one another under compression, making a considerable amount of the included pore space unavailable to lateral flow and forcing most of the flow through the available pore space in the warp yarns. This pore space may become somewhat more tortuous as the compressive load is increased because of distortion of these yarns by the fill yarns.

From the preceding discussion, it may be seen that lateral flow is influenced more by the availability of the pore space in the warp yarns, whereas the pore spaces in both warp and fill yarns are equally available for transverse flow.

In the above discussion, the influence of the weave pattern and the number of picks per inch upon the lateral permeability has been considered. The influence of the yarn size and napping upon lateral permeability can be observed by referring to the data for the appropriate samples in Fig. 26 and 27.

Samples 7 and 2, which are similar in structure except for yarn size, show the same variation in Kozeny constant with porosity. Samples 6 and 3, which also are similar in structure except for yarn size, also show similar variations in Kozeny constant with porosity. Data were obtained at lower porosities for Sample 6 than Sample 3, and thus the increase in $\underline{k}$ at low porosities is more apparent for the former. Sample 7 shows slightly more scatter in the data than Sample 2, but small disturbances in the fiber alignment in the warp yarn would be more probable for the finer fibers of Sample 7 and could be responsible for the larger scatter.

The larger yarn size in Sample 6 gives it a weight per unit area about the same as that of most samples having 70 picks per inch. Its lateral permeability characteristics, however, are the same as those of samples having a smaller weight per unit area but an equal number of picks per inch. In like manner, Sample 7, because of its small yarn size, has a smaller weight per unit area than the other samples with 70 picks per inch, but its lateral permeability characteristics are the same. Therefore, basis weight as well as yarn size apparently is unimportant to the lateral permeability of the samples studied here. As already noted, basis weight was not important to the transverse permeability either.

Napping also did not significantly affect the lateral permeability. Comparison of the data for sample pairs 1 and 8, 2 and 9, and 3 and 11 (the second-named sample being napped) indicate only a very slightly smaller value of the Kozeny constant at any given porosity for the napped felt. Because the lateral permeability has been found to be sensitive to slight changes in fiber alignment, the disturbance of the fiber orientation in the fill yarns during napping may either tend to randomize the structure or may cause a different distribution of the compressive load upon the fibers and thereby cause less distortion of the parallel warp yarns by the fill yarns. Since the difference in the value of k between napped and unnapped felts is so small, however, not much significance should be attached to it.

COMPRESSIBILITY OF THE FELT SAMPLES

Since it was desirable to establish which range of pad densities was likely to be encountered in actual practice on the paper machine, load-compression data were obtained for all of the felt samples. The data in each case could be represented by the empirical relationship,

$$c = MP^N, \qquad (22)$$

where c is the apparent pad density, P is the applied load, and M and N are experimentally determined constants. This relationship has also been found to apply to the compression of fibrous mats of other types (9, 22, 46).

The constants, M and N, were evaluated for each felt sample. Equation (22) may be rearranged as follows:

$$\log c = N \log P + \log M \qquad (23)$$

and a plot of the compressibility data on double logarithmic paper will yield a straight line. Such a plot for Sample 1 is given in Fig. 28. Similar plots were obtained for the other samples. In Table X are given values for the empirical constants, M and N, calculated from the compressibility data for each sample by the method of averages.

TABLE X

COMPRESSIBILITY CONSTANTS FOR THE EQUATION, $c = MP^N$

(c, g./cc.; P, kg./sq. cm.)

Sample Number	M	N
1	0.365	0.194
2	0.351	0.205
3	0.342	0.214
4	0.372	0.208
5	0.375	0.221
6	0.364	0.200
7	0.340	0.201
8	0.386	0.196
9	0.360	0.205
10	0.358	0.218
11	0.343	0.216

Van Wyk (47), and more lately Wilder (46), making certain assumptions regarding the structure and compression mechanism of a fibrous network, have been able to relate the dependence of the constants, M and N, upon certain properties of the mat and fiber. The analytical

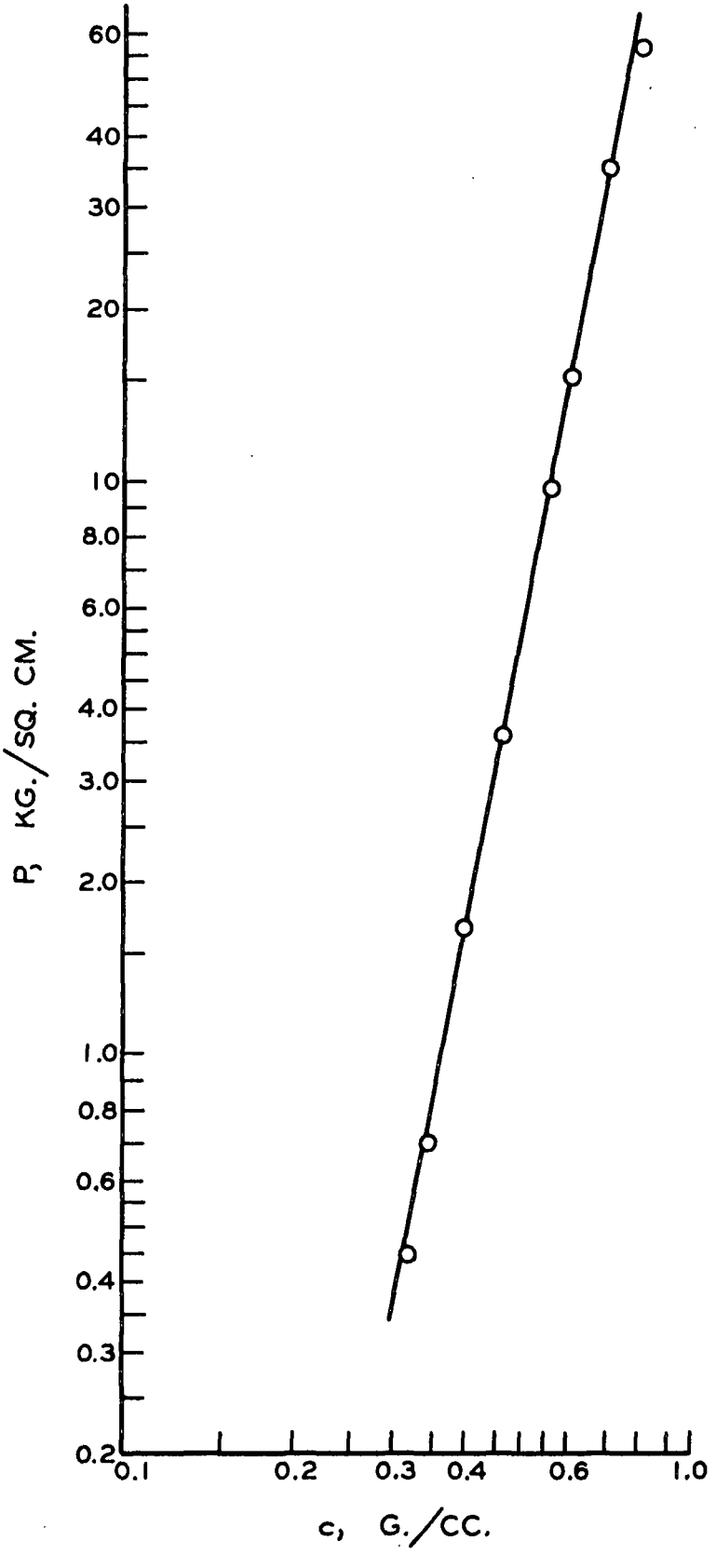

Figure 28. Compressibility of
(Sample 1)

treatment imposes some severe restrictions on the type of fibrous network for which the relationship will apply. Some of the most important of these, as given by Wilder, are: (1) The deformation is the result of fiber bending, fiber slippage being negligible; (2) the fibers can be treated as beams, and the ordinary beam equations can be applied; (3) the fibers are oriented so as to be at random in a plane perpendicular to the direction of the applied force; and (4) the unsupported fiber length, $\underline{\ell}$, may be related to the pad density, $\underline{c}$, by

$$\underline{\ell} = \frac{\underline{K'}}{\underline{c}^{\alpha}} \qquad (24)$$

where $\underline{K'}$ and α are constants. He then shows that $\underline{N}$ is a function only of α, and the constant multiplier $\underline{M}$ is a function of the mechanical properties of the material making up the fiber, the fiber size and geometry, and the specific volume of the fiber.

It may be observed from Table X that the values of $\underline{M}$ and $\underline{N}$ differ slightly from sample to sample. The importance of the fiber and yarn orientation to the value of the constant $\underline{N}$ seems indicated when the data for sample pairs 1 and 8, 2 and 9, and 3 and 11 are considered. It will be recalled that the samples in each pair have the same basic structure and differ from each other only in the presence or absence of a raised nap. From Table X, it is seen that the two samples of each pair have closely the same value of $\underline{N}$. As mentioned previously, Wilder has shown that $\underline{N}$ depends only on the relationship between the pad density and unsupported fiber length. This relationship would probably be the same for both samples in each of the above pairs because the flow measurements have shown that napping apparently does not greatly alter the fiber

orientation. The differences noted in N between most of the samples would be expected because the yarn and fiber orientation differ from sample to sample. When samples having the same value of N are compared with respect to the value of constant M, deviations from Wilder's theory are observed. For example, Samples 6 and 7 have equal values of N, but the M for Sample 7 is less than M for Sample 6. According to Wilder's theory, M is inversely proportional to the elastic modulus of the material of which the fiber is made, and the specific volume, radius, and length of the fiber. For the above two samples, these quantities would all be reasonably constant, except the fiber radius, which is less for Sample 7. Therefore, a larger, rather than a smaller, value of M would be predicted for Sample 7. Samples 10 and 11 have nearly equal values of N but different values of M although their fiber properties are the same. The same argument applies to Samples 2 and 9 and 1 and 8. Only Samples 3 and 11 appear to agree with the predictions of Wilder's theory. The possibility of a change in the fiber properties great enough to affect the value of M during napping is unlikely. If napping did affect M, its value for Sample 11 should be different from that for Sample 3, which is not the case.

Although the value of N seems to be related to the fiber and yarn orientation for these samples, the basis for the relationship is not necessarily in accordance with Wilder's theory. Generally, the theory does not apply for the compression of these samples because the value of M in most cases is not properly predicted. The probable reasons for nonagreement are to be found in the deviations of the felt samples from the assumed structure and assumed compression mechanism. The following are important reasons for this nonagreement: (1) Fibers in the felts

possess a very definite special orientation instead of the random orientation assumed by Wilder. (2) Fiber slippage, as already discussed, is probably an important mechanism in felt compression because of the parallel fiber orientation in the yarn. Wilder's treatment does not consider this mechanism. (3) Under large compressive loads, compression of the swollen fiber occurs, a mechanism not included in Wilder's theory.

To establish which range of felt porosities might be encountered in the nip of the press rolls, the nip width and loading must be known. These would vary considerably with different paper machines, but two analyses reported in the literature will serve to give the approximate range of felt porosities of importance in the nip. Fahlin (48) in an investigation of the deformation in the nip of rubber-covered press rolls, found that the nip width was an exponential function of the machine speed and of the linear pressure in the press. In addition, the nip width was dependent on the felt used. The press roll diameter and thickness and hardness of the rubber cover, which also affect the nip width, were held constant at 45 cm. and 2 cm., respectively, in his study. At the maximum machine speed and loading studied by Fahlin, 250 meters per min. (800 f.p.m.) and 35 kg./cm. (195 lb. per inch), respectively, a nip width of 27 mm. was observed. Thus, a nip pressure of about 185 p.s.i. is indicated. Gavelin (49), studying a suction press on a machine running 300 m. per min. (1000 f.p.m.), estimated a nip width of 3 cm. and a corresponding nip pressure of 86×10^5 dynes per sq. cm. (125 p.s.i.). In the present study under compressive loads of 125 to 185 p.s.i., felt porosities ranging from 0.45 to 0.38 were observed.

SUMMARY AND CONCLUSIONS

Apparatus and techniques have been developed to measure the lateral and transverse water permeabilities of woven wool felts under static compressive loads ranging up to 1000 p.s.i. The annular guard ring principle which had previously been designed and used only for air-permeability studies on paper was adapted for water-permeability measurements on felts under compression. By this procedure, flow along the felt toward the edges of the precut pad was avoided and an accurate permeability measurement was obtained. The contribution of the woven structure of the felt to its lateral and transverse permeabilities was a point of particular interest in this investigation. For that reason, permeability data were obtained on eleven samples which were carefully designed and constructed to permit a separation of the contribution of different structural variables to the permeability. The variables of particular interest were the basic weave pattern, the number of fill yarns per inch, the yarn size, and the presence or absence of a napped surface. Considerable difficulty was experienced in attaining perfect uniformity of felt structure in the test sample, and a variation of about 5 to 7% was observed in the permeability data between different pads from the same felt sample. The manufacturing process, particularly the fulling operation, could not be controlled to give a smaller variation than this.

Lateral and transverse permeability constants defined by Darcy's law were evaluated for each of the 11 samples at several different pad densities. The lateral and transverse permeability data for all eleven samples were correlated over a wide porosity range by the Kozeny-Carman

equation. The good correlation obtained was unexpected because the woven structure of the felt had seemed to place it outside of the types of porous beds for which the validity of the equation had been established. The Kozeny-Carman equation previously had been verified only for randomly packed, unconsolidated media having a uniform pore structure and with modification for a few consolidated media. Its applicability to flow through woven wool felts as demonstrated here will not only be of great use in the analysis of the flow of water in the nip of the press rolls in the paper machine, but it may also promote a more extensive investigation of the applicability of this equation to the permeability of other types of textiles, particularly textile filter media. Much of the thought and research work in the permeability of textiles has been based on the ideas of interyarn versus interfiber flow, and a consideration of the major flow mechanism as an orifice type through interyarn pores. Although such a mechanism may be important for high-velocity flow through very open-weave fabrics, some consideration might be given to interfiber flow and the possible extension of the Kozeny-Carman theory to the permeability of other types of textiles. The good fit of this permeability data to the Kozeny-Carman equation indicates that for woven felts under compression, the concept of capillary flow through interfiber pores is basically correct, and considerations of interyarn versus interfiber flow in woven felts is not necessary. The relative unimportance of such structural variables as yarn size and napping to the permeability, as observed in this study, emphasize the importance of the interfiber flow concept. Certainly, if interyarn flow were of greater importance, these two factors would have

an important influence on the permeability. The importance of interfiber pore spaces is further demonstrated by the relatively minor effects of the felt structure upon the transverse permeability where the basic fiber orientation is predominantly perpendicular to flow. Varying such factors as the number of yarns per inch, which control the size of interyarn pore spaces, had no effect on the transverse permeability at any given porosity.

The main effect of the structural felt variables is their influence on the fiber orientation affecting flow. This effective fiber orientation may be further modified by the applied compressive load. The evaluation of this contribution of the felt structure to the effective fiber orientation was accomplished by calculations of the Kozeny constant for each sample at several pad densities. A great deal of research has been carried out in the past relating this factor to the fiber orientation for fibrous beds of known structure. These past studies served as an excellent basis for the evaluation of the importance of the felt structure to the effective fiber orientation.

The evaluation of the Kozeny constant required an independent measurement of the water-swollen specific volume and specific surface of the fiber. Microscopic fiber diameter measurements of water-swollen fibers were used to make these evaluations.

In general, the permeability measurements indicated that the effective fiber orientation for transverse flow is predominantly perpendicular to flow, and that variations in the felt structure and the compressive load applied to the pad have little effect on this basic fiber orientation. The application of large compressive loads to the pad did change

the effective specific volume of the fiber, however. Extrapolation of the permeability data to zero porosity indicated that the effective fiber density approached the pycnometric density of dry wool. This observed decrease in the effective specific volume of the fiber was attributed to a partial deswelling of the fiber as larger compressive loads were applied. Because the compressibility characteristics of the different samples were not identical, the decrease in the specific volume with applied load was slightly different for each sample, but for most samples occurred where pad densities of about 0.6 g./cc. and greater (porosities of 0.4-0.3) were reached.

In contrast to the rather minor effects of structure on transverse permeability, the effects on lateral permeability were found to be very significant. Particularly important was the availability of the pore spaces in the warp yarns, which in these studies were aligned parallel to flow. Any disturbances in the parallel orientation of the fibers in these yarns, whether caused by variations in the compressive load, the type of weave pattern used, or the number of fill yarns per inch, significantly altered the lateral permeability. For example, an increase of about 50% in the number of fill yarns (picks) per inch over the number of warp yarns per inch altered the fiber orientation to such an extent that the predominantly parallel flow pattern was broken up and the effective fiber orientation became more nearly perpendicular to flow. The use of a weave pattern characterized by much entwinement of the warp yarns about the fill yarns resulted in a more randomized effective orientation than a weave pattern characterized by a minimum of interference of the warp yarns by the fill yarns. Where the number of fill yarns per inch

were more numerous than the warp yarns but the weave pattern caused a minimum interference of the warp yarns by the fill yarns, a change from a predominantly parallel flow pattern at high porosities to a predominantly perpendicular fiber orientation was observed with compression.

When the samples were compressed to porosities of 0.3-0.35, a deswelling of the water-swollen wool fiber occurred, and the lateral permeability decreased more than that predicted from the Kozeny-Carman theory. A similar decrease in the transverse permeability was not observed. Because this decrease in lateral permeability was too large to be caused by an increase in the tortuosity and/or the pore shape factor alone, it appeared that a portion of the pore volume must be unavailable to lateral flow. If a slippage of the fibers into pore spaces between other fibers during compression is assumed, a gridlike fiber orientation would be formed for transverse flow. Viewing the felt from the lateral direction, as the individual yarns are flattened out, the fill yarns would become thin, and the individual fibers would tend to slip behind one another. Therefore, the pore spaces between the fibers would become partially unavailable to lateral flow. The parallel fiber alignment in the yarns makes such a mechanism possible. Also, as compression proceeds, the areas of fiber-to-fiber contact increase, causing a partial deswelling of the fiber, and perhaps blocking of the lateral flow channels.

The compressibility data indicated that the compression characteristics of the felt are related to the felt structure but probably not in the manner described by compressibility theory based only on fiber

bending. On the basis of these observations and the analysis of the permeability data, it was concluded that fiber slippage is an important mechanism in the compression of felts.

In spite of the complex fiber orientation of the felts, the data showed that an average value of the Kozeny constant was applicable over a sufficiently wide porosity range to permit estimation of the flow through woven wool felts if their structural properties and fiber properties are known. With these data for a basis, the Kozeny-Carman equation can be used to predict the flow properties of the felt in the nip of the press rolls. The extension of these findings to commercial felts should be viewed with some caution. The number of picks per inch has been found to have an important effect on lateral permeability, and the specific effect of pick counts greatly different from those used here is not known. For the large group of press felts similar in design to these samples, however, the findings of this study will be of use in the flow calculations.

Other findings of the present study of interest in the use and manufacture of press felts follow. Very large press loadings may compress the felt to such an extent that lateral flow through it is greatly impeded. Because the lateral permeability is of great importance in the nip, felts should be designed to provide as little interference as possible with the important parallel flow channels in the warp yarns. In the present study, felts with a plate weave and an equal number of fill and warp yarns per inch provided the least resistance to lateral flow.

Existing felt permeability tests based on the transverse permeability may not always be a good indication of the effectiveness of the felt in water removal, because, in many cases, the transverse and lateral permeabilities may be quite different. An evaluation of the lateral permeability of the felt would seem to be of as great and probably of more importance as an estimate of the felt's water removal ability.

NOMENCLATURE

A = cross-sectional area of a porous bed normal to flow, sq. cm. (area of the test zone in this study)

A_e = cross-sectional area of a circular channel, sq. cm.

c = mass of fibers per unit volume of bed, g. per cc.

d = fiber diameter, cm.

g = acceleration due to gravity, 980 cm. per sec.^{2}

K = transverse permeability coefficient defined by Darcy's law, sq. cm.

K_2 = lateral permeability coefficient, sq. cm.

k = Kozeny constant, $k = k_o(L_e/L)^2$, dimensionless

L = depth of a porous bed in the flow direction, cm.

L_2 = width of felt sample in lateral permeability determination, cm.

L_e = length of equivalent channels in a porous bed, cm.

L_o = depth of bed at zero porosity, cm.

ℓ = distance between fiber supports in Wilder's equation (46), cm.

M,N = empirical constants in compressibility equation, $c = MP^N$

m = mean hydraulic radius, cm.

ΔP = frictional pressure drop across a porous bed, dynes per sq. cm.

P = compacting load on the pad, kg. per sq. cm.

q = volumetric rate of flow, cc. per sec.

r_e = radius of a circular tube, cm.

S_o = external surface area of fibers per unit volume of bed, sq. cm. per cm.^{3}

S_v = specific surface of fibers, surface area per unit volume of fibers, sq. cm. per cm.^{3}

S_w = specific surface of fibers, surface area per unit mass of fibers, sq. cm. per g.

T = tortuosity factor, $T = L_e/L$

$\underline{u}$ = superficial velocity of the fluid through the porous bed, cm. per sec.

$\underline{u_e}$ = superficial velocity of the fluid through a circular channel, cm. per sec.

$\underline{v}$ = effective specific volume of the fibers, $cm.^3$ per g.

$\underline{W}$ = total mass of fibers in the bed, g.

α = constant in Wilder's equation relating $\underline{c}$ and frequency of fiber-fiber contacts (46)

ϵ = fractional void volume of the porous bed, dimensionless

μ = viscosity of the fluid, poises

ρ = density of the fluid, g. per $cm.^3$

ACKNOWLEDGMENTS

The writer would like to express his appreciation for the help and advice given him by Dr. William L. Ingmanson and the other members of the thesis advisory committee.

Also, the assistance of the following is appreciated:

Mr. Donald J. Wulgart and Mr. Harwood Orbison of the Appleton Woolen Mills who furnished the experimental felt samples and assisted in their design.

Mr. Henry W. Marx and Mr. M. C. Filz of The Institute of Paper Chemistry for their assistance in the design and construction of the apparatus.

Mr. John D. Hankey of the Fiber Microscopy Group of The Institute of Paper Chemistry for assistance in the preparation of fiber cross sections.

Mr. Donald Sternhagen of the Container Section of The Institute of Paper Chemistry for assistance in the compressibility measurements.

LITERATURE CITED

1. Robertson, A. F., Textile Research J. 20, no. 12:838(Dec., 1950).

2. Backer, S., Textile Research J. 21, no. 10:703(Oct., 1951).

3. Penner, S. E., and Robertson, A. F., Textile Research J. 21, no. 11:775(Nov., 1951).

4. Goglio, M. J., La Vier, A. W. S., and Brown, C. D., Textile Research J. 25, no. 4:296(April, 1955).

5. Cunningham, G. E., Broughton, G., and Kraybill, R. R., Ind. Eng. Chem. 46, no. 6:1196(June, 1954).

6. Brownell, L. E., Dumbrowski, H. S., and Dickey, C. A., Chem. Eng. Progr. 46:415(1950).

7. Kozeny, J., Sitzber. Akad. Wiss. Wien., Math. Naturw. Klasse 136 (Abt. IIa):271(1927).

8. Carman, P. C., Trans. Inst. Chem. Engrs. (London) 15:150(1937).

9. Ingmanson, W. L. An investigation of the mechanism of water removal from pulp slurries. Doctoral Dissertation. Appleton, Wis., The Institute of Paper Chemistry, 1951. 119 p.

10. Scheidegger, A. E. The physics of flow through porous media. New York, Macmillan, 1957.

11. Whitney, R. P., Ingmanson, W. L., and Han, S. T., Tappi 38, no. 3: 157(1955).

12. Carman, P. C. Flow of gases through porous media. New York, Academic Press, 1956.

13. Ingmanson, W. L., and Whitney, R. P., Tappi 37 no. 11:523(Nov., 1954).

14. Miller, S. A., Ind. Eng. Chem. 49, no. 3:486(March, 1957).

15. Wyllie, M. R. J., and Ross, W. D., Nature 165:972(1950).

16. Wyllie, M. R. J., and Spangler, M. B., Bull. Am. Assoc. Petrol. Geol. 36:359(1952).

17. Wyllie, M. R. J., and Gregory, A. R., Ind. Eng. Chem. 47, no. 7: 1379(July, 1955).

18. Cornell, D., and Katz, D. L., Ind. Eng. Chem. 45, no. 10:2145(1953).

19. Robertson, A. A., and Mason, S. G., Pulp Paper Mag. Can. 50, no. 13: 103(Dec., 1949).

20. Carroll, M., and Mason, S. G., Can. J. Technol. 30, no. 12:321(1952).

21. Mason, S. G., Tappi 33, no. 8:403(1950).

22. Ingmanson, W. L., Andrews, B. D., and Johnson, R. C., Tappi 42, no. 10:840(1959).

23. Fowler, J. L., and Hertel, K. L., J. Appl. Phys. 11:496(1940).

24. Brown, Joseph C., Jr. Determination of the exposed surface area of pulp fibers from air permeability measurements, using a modified Kozeny equation. Doctoral Dissertation. Appleton, Wis., The Institute of Paper Chemistry, 1949. 146 p.

25. Sullivan, R. R., and Hertel, K. L., J. Appl. Phys. 11:761(1940).

26. Emersleben, O., Physik Z. 26:601(1925).

27. Sullivan, R. R., J. Appl. Phys. 13:725(1942).

28. Anderson, S. L., and Warburton, F. L., J. Textile Inst. 40:749T(1949).

29. Roy, M. M., Mukherjee, R. R., and Sen, M. K., J. Textile Inst. 41: 249T(1950).

30. Lord, E., J. Textile Inst. 46:191T(1955).

31. Sullivan, R. R., J. Appl. Phys. 12:503(1941).

32. Davies, C. N., Proc. Inst. Mech. Engrs. (London) 1B:185(1952).

33. Happel, J., A.I.Ch.E. Journal 5, no. 2:174(June, 1959).

34. Shearer, J. L., Textile Research J. 29:467(June, 1959).

35. Carman, P. C. Flow of gases through porous media. p. 25-6. New York, Academic Press, 1956.

36. Grace, H. P., A.I.Ch.E. Journal 2, no. 3:307(Sept., 1956).

37. Ginn, R. F., Proc. Tech. Sect., Brit. Paper and Board Makers' Assoc. 40:241(1959).

38. Carson, F. T., J. Research Natl. Bur. Standards 12:567, 587(1934).

39. Bublitz, W. J., Dappen, J. W., and Van den Akker, J. A., Tech. Assoc. Papers 31:305(1948).

40. Lane, W. H. A study of the relationship between air permeability and oil permeability of paper. Doctoral Dissertation. Appleton, Wis., The Institute of Paper Chemistry, 1942. 124 p.

41. Speakman, J. B., Nature 126:565(1930).

42. Davis, Dale S. Empirical equations. In Empirical equations and nomography. p. 3-37. New York, McGraw-Hill, 1943.

43. Von Bergen, Werner. In Mauersberger's Textile fibers. 5th ed. p. 507-560. New York, John Wiley & Sons, Inc., 1947.

44. King, A. T., J. Textile Inst. 17:53T(1926).

45. Iberall, A. S., J. Research Natl. Bur. Standards 45:398(1950).

46. Wilder, H. D. The compression creep properties of wet pulp mats. Doctoral Dissertation. Appleton, Wis., The Institute of Paper Chemistry, 1960. 184 p.

47. Van Wyk, C. M., J. Textile Inst. 37:285T(1946).

48. Fahlin, B., Svensk Papperstidn. 60, no. 12:460(June, 1957).

49. Gavelin, G., Svensk Papperstidn. 61, no. 11:345(June, 1958).

APPENDIX I

CALIBRATION OF THE FLOWMETERS

After installation, the flowmeters were calibrated at several tube readings by measuring the time required for the collection of a measured volume of water. The permeability tube and auxiliary piping were filled with water at 25°C. Provision was made to collect the water flowing from the test zone at the point where it normally would re-enter the storage bottle. The guard zone pump and piping system were not used during the calibration. Water from the storage bottle was allowed to flow into the permeability tube, the flow rate being controlled by adjustment of the pinch clamp on the rubber inlet hose. The needle valves in the pump discharge and by-pass lines were adjusted until a constant tube reading of the desired magnitude was observed on the rotameter. Then, using a stop watch reading to 0.1 sec., measurement was made of the time required to collect an appropriate volume of water in a graduated cylinder. The calibration was repeated for several tube readings for both rotameters. The calibration curves obtained are given in Fig. 29 and 30. The average value of several determinations of the flow rate at each tube reading was used in the construction of the calibration curve. An average deviation of 1% was observed between successive flow measurements at a given tube reading.

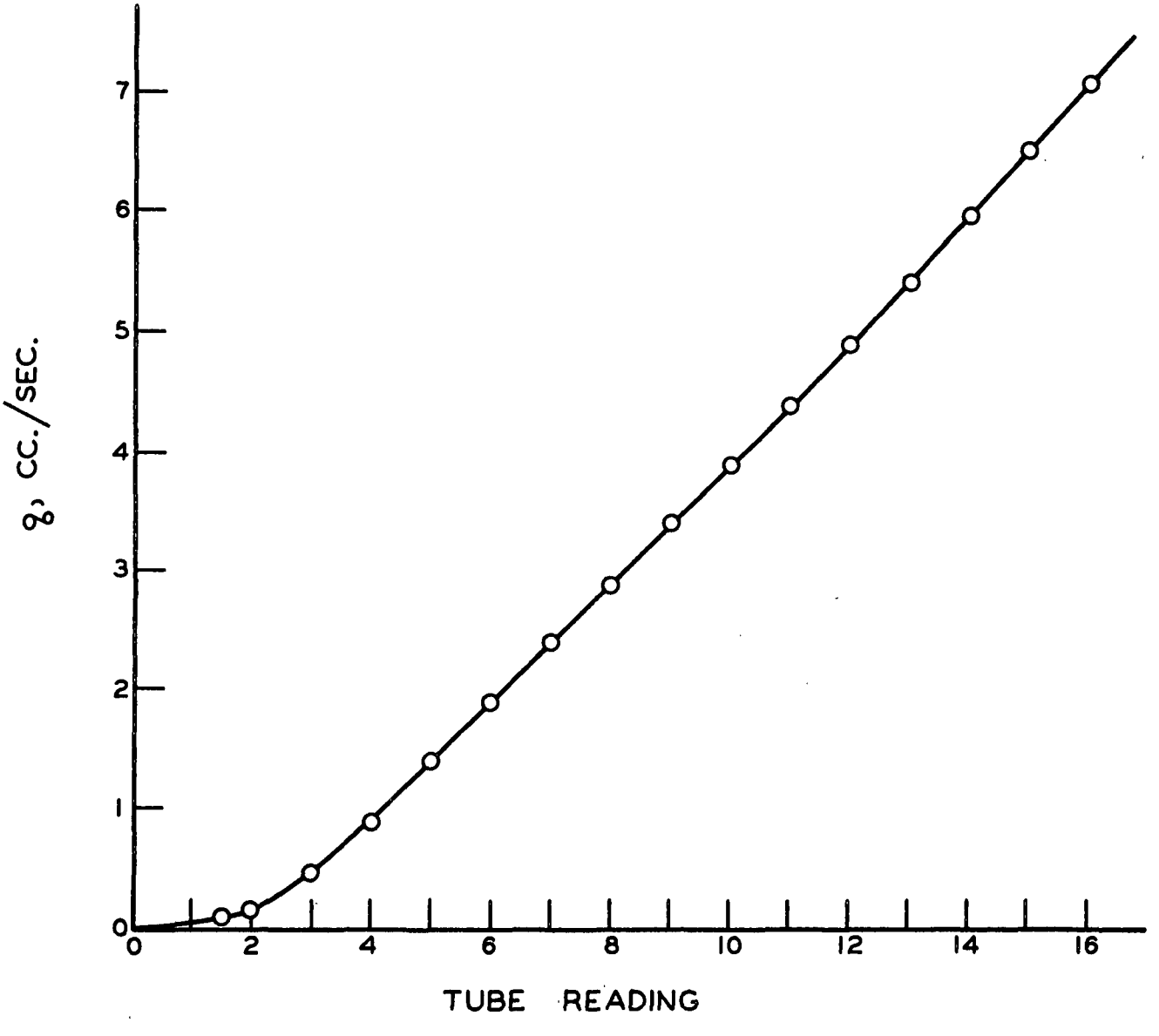

Figure 29. Calibration Curve For Small Flowmeter at 25°C.

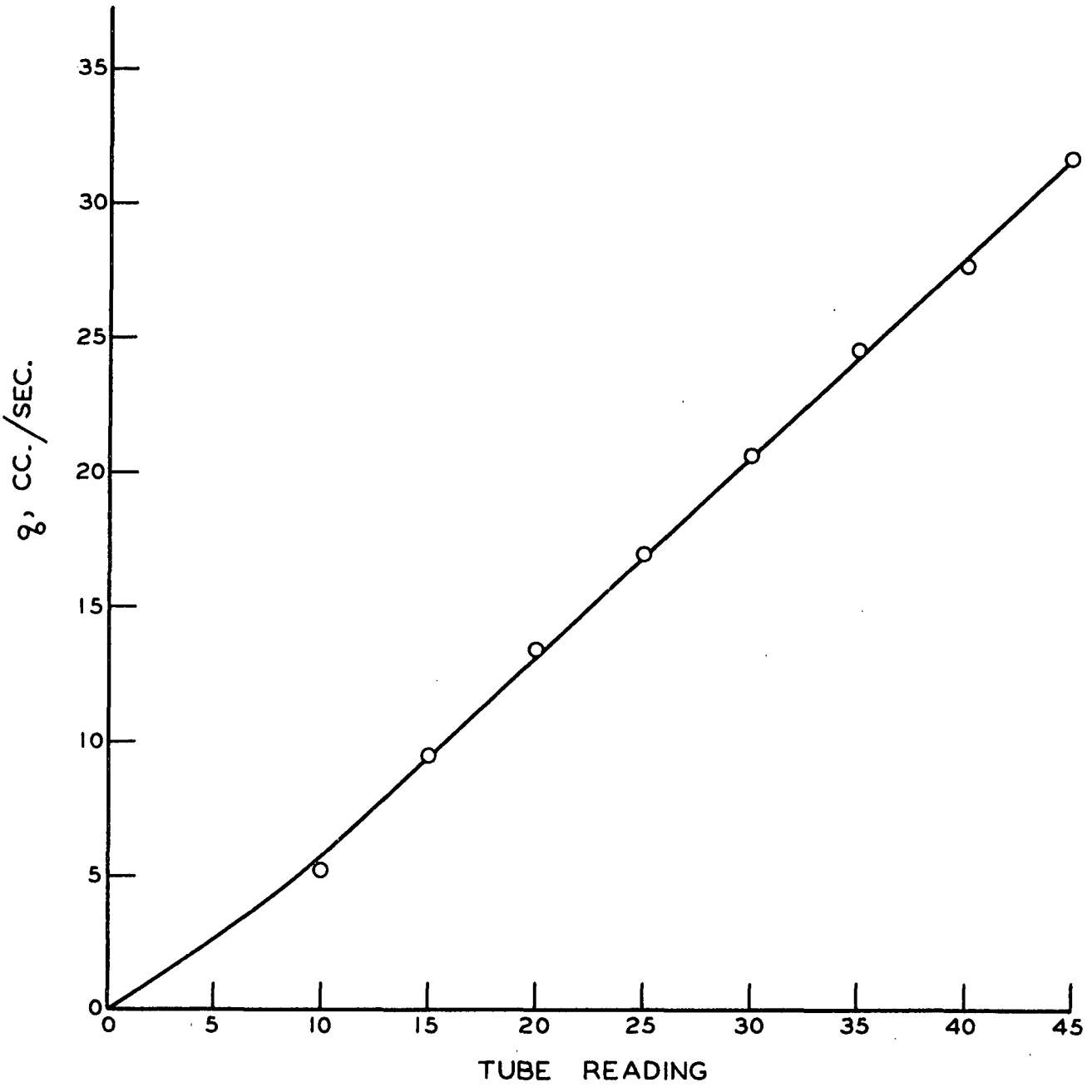

Figure 30. Calibration Curve For Large Flowmeter at 25°C.

APPENDIX II

TABLE XI

TRANSVERSE PERMEABILITY DATA

L, cm.	c, g./cc.	$10^9 K_2$, cm.^{2}	L, cm.	c, g./cc.	$10^9 K_2$, cm.^{2}	L, cm.	c, g./cc.	$10^9 K_2$, cm.^{2}
Sample 1			Sample 2			Sample 3		
0.222	0.317	176	0.222	0.316	226	0.196	0.282	435
0.203	0.348	138	0.205	0.342	173	0.180	0.307	346
0.177	0.400	91.9	0.178	0.394	119	0.148	0.373	153
0.152	0.463	52.6	0.153	0.460	66.4	0.134	0.412	91.9
0.126	0.558	20.7	0.129	0.546	30.5	0.115	0.481	44.8
0.115	0.612	10.8	0.112	0.626	14.3	0.103	0.537	25.0
0.098	0.718	4.0	0.101	0.694	7.31	0.085	0.650	10.6
0.087	0.806	2.0	0.085	0.820	2.95	0.075	0.743	5.88
						0.069	0.796	3.31
Sample 4			Sample 5			Sample 7		
0.176	0.291	362	0.228	0.304	348	0.169	0.304	231
0.153	0.336	234	0.202	0.343	224	0.154	0.334	182
0.127	0.404	118	0.178	0.390	123	0.126	0.407	88
0.113	0.453	66.3	0.151	0.459	58	0.111	0.463	48
0.101	0.507	36.9	0.127	0.546	23.8	0.094	0.545	22.7
0.088	0.585	19.7	0.113	0.613	11.3	0.084	0.610	11.7
0.075	0.688	9.45	0.099	0.702	5.16	0.073	0.705	6.80
0.067	0.768	6.35	0.088	0.792	2.79	0.064	0.805	4.15
Sample 8			Sample 9			Sample 10		
0.225	0.334	139	0.228	0.330	165	0.181	0.301	340
0.202	0.372	102	0.200	0.376	117	0.152	0.359	196
0.178	0.422	73.8	0.178	0.422	79	0.126	0.433	80.5
0.154	0.488	40.4	0.152	0.495	42.4	0.114	0.478	54.3
0.128	0.587	16.4	0.128	0.587	17.4	0.099	0.549	32
0.110	0.682	5.7	0.114	0.660	8.58	0.088	0.623	16.8
0.093	0.810	2.07	0.099	0.761	3.35	0.076	0.717	8.54
			0.091	0.829	2.31	0.067	0.816	5.97
			Sample 11					
			0.203	0.293	373			
			0.177	0.336	234			
			0.153	0.379	139			
			0.125	0.476	60			
			0.111	0.536	31.2			
			0.100	0.595	17.4			
			0.086	0.689	7.67			
			0.079	0.756	4.32			

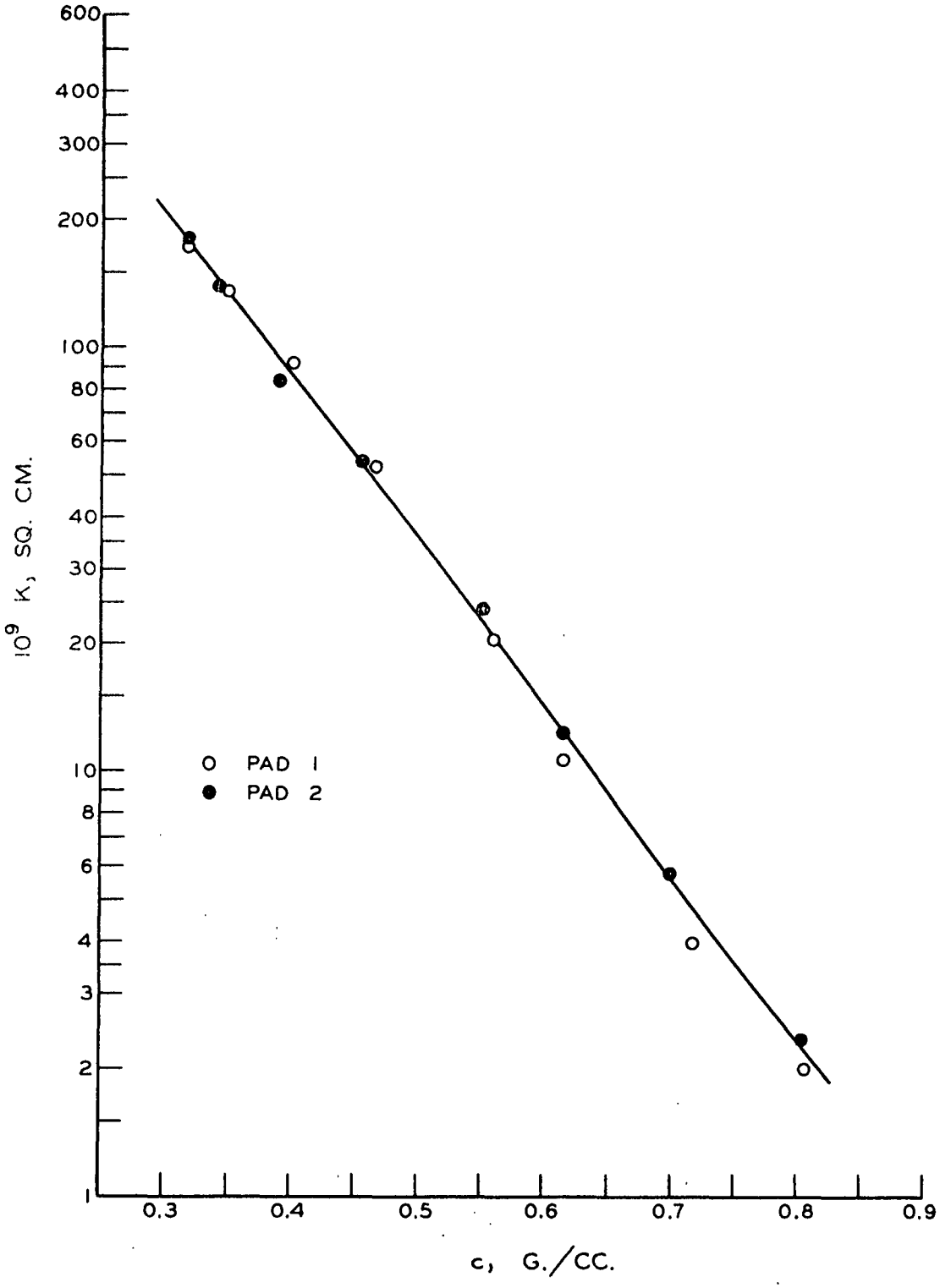

Figure 31. Transverse Permeability
(Sample 1)

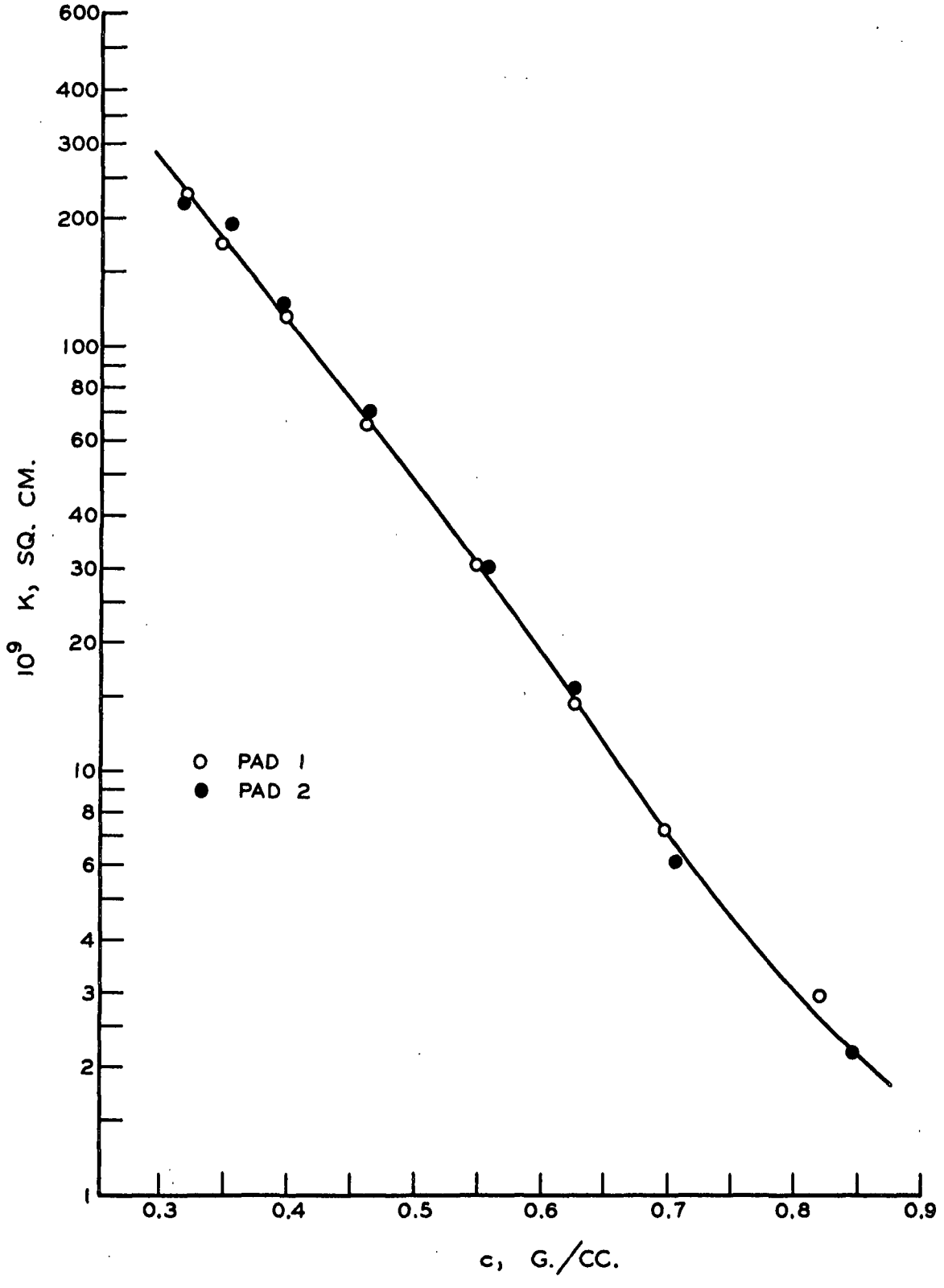

Figure 32. Transverse Permeability
(Sample 2)

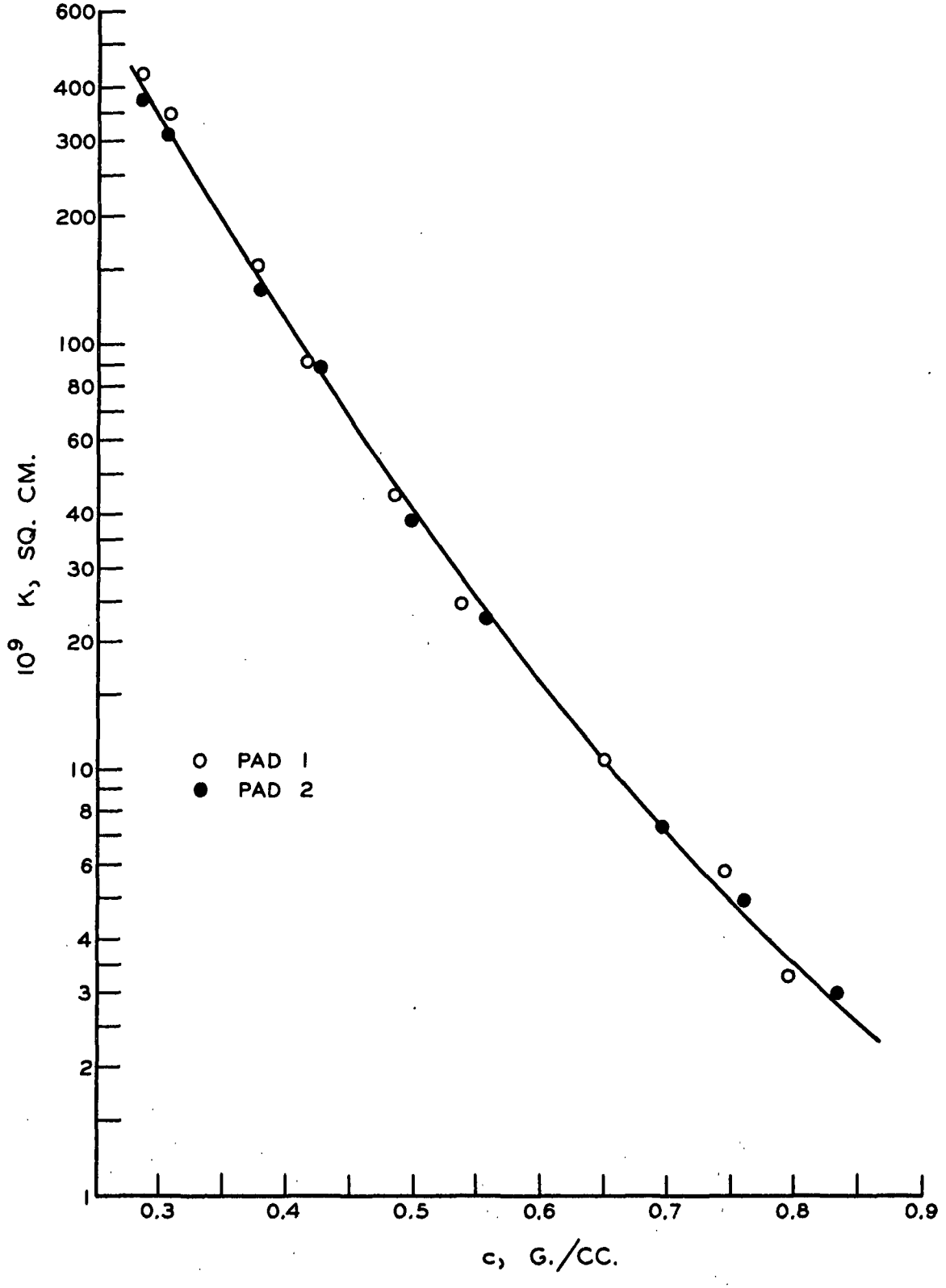

Figure 33. Transverse Permeability
(Sample 3)

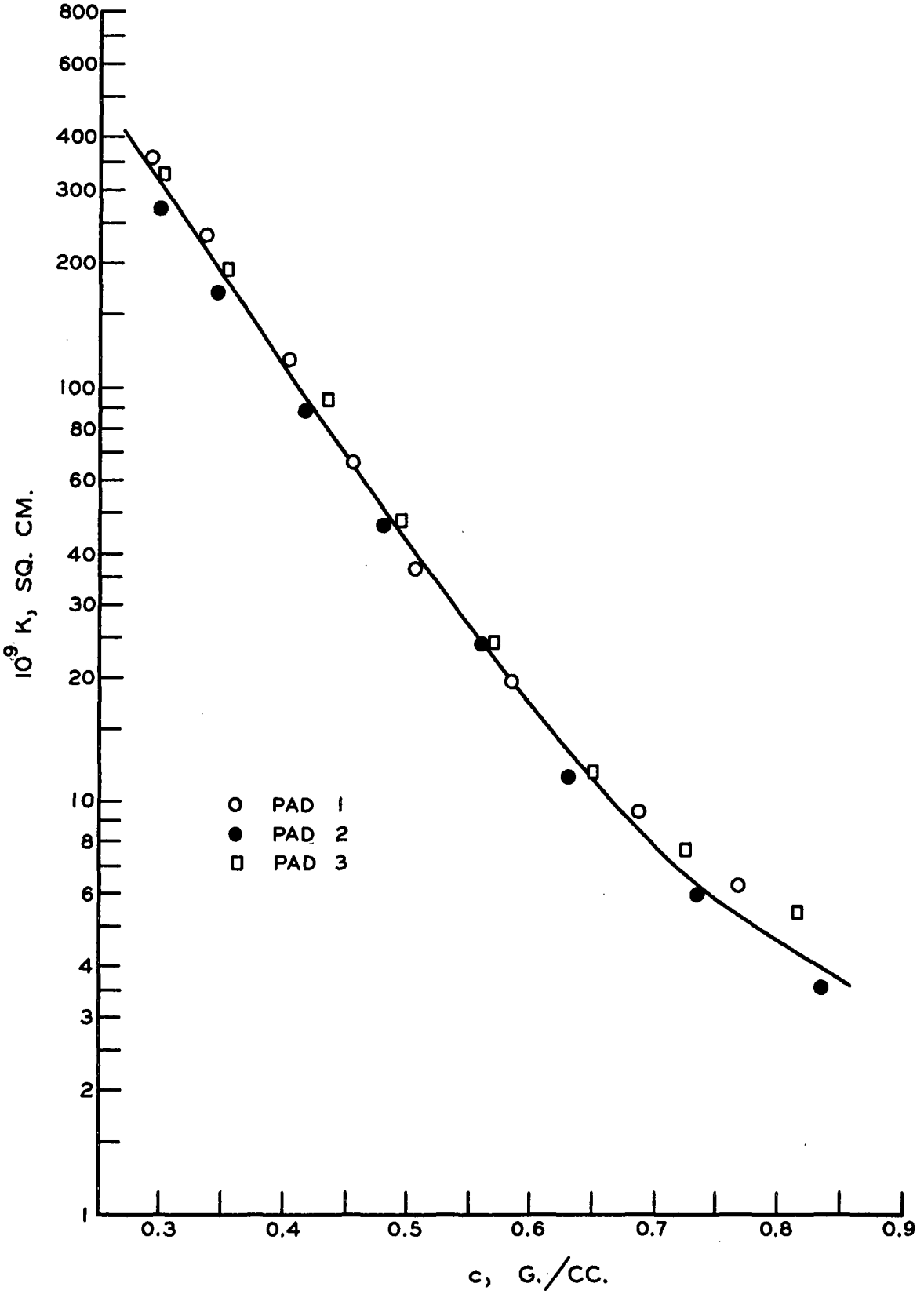

Figure 34. Transverse Permeability
(Sample 4)

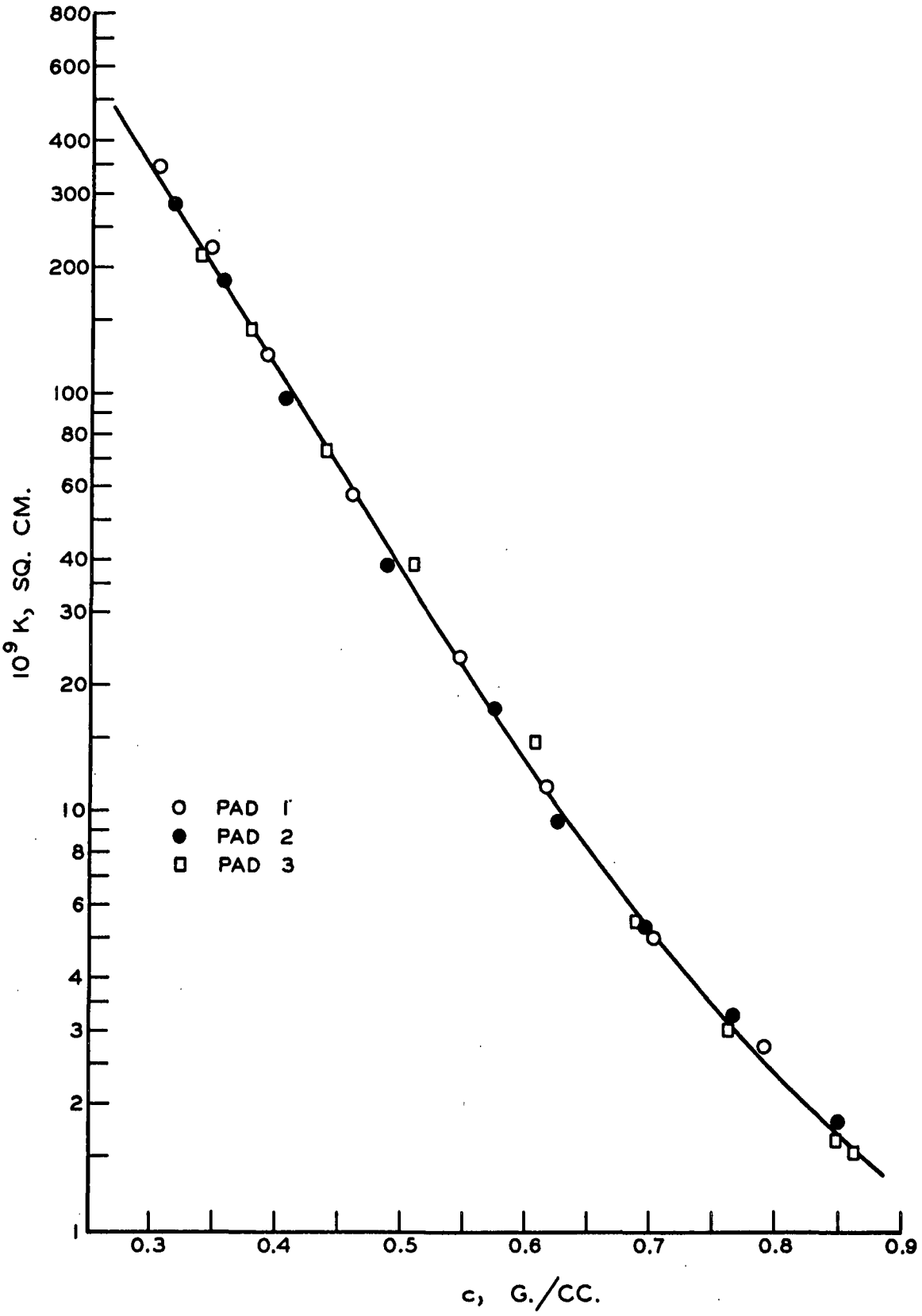

Figure 35. Transverse Permeability
(Sample 5)

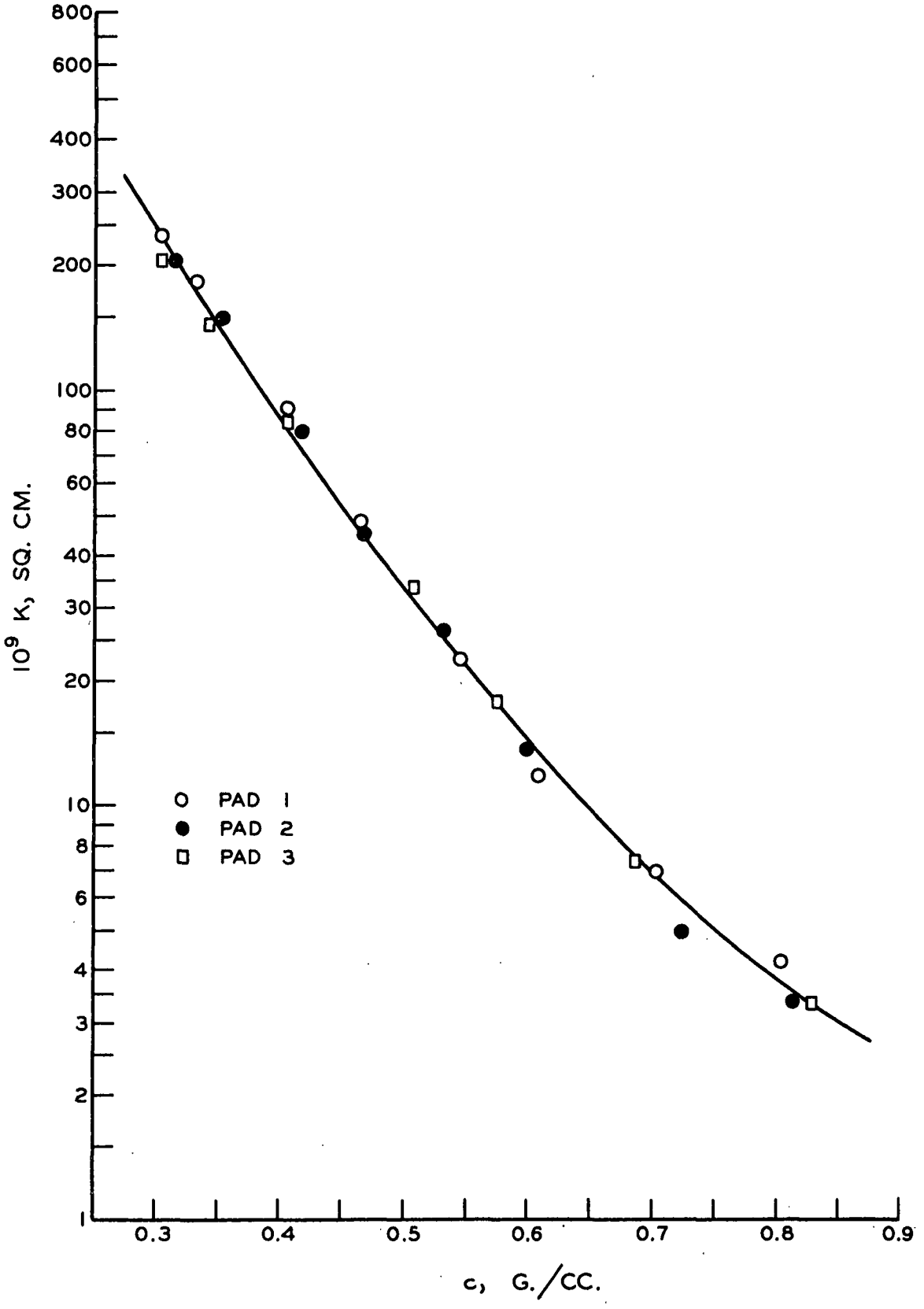

Figure 36. Transverse Permeability
(Sample 7)

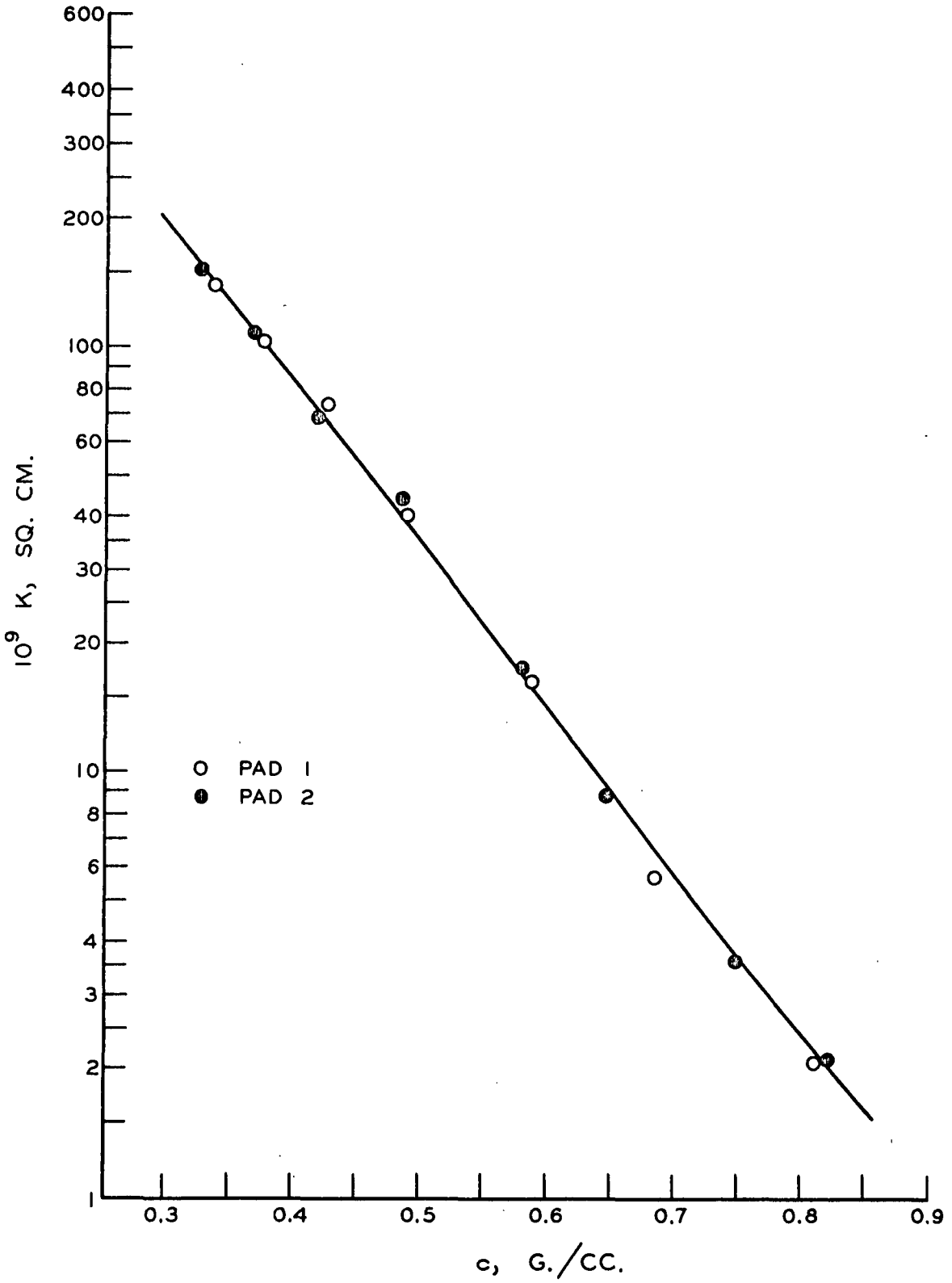

Figure 37. Transverse Permeability
(Sample 8)

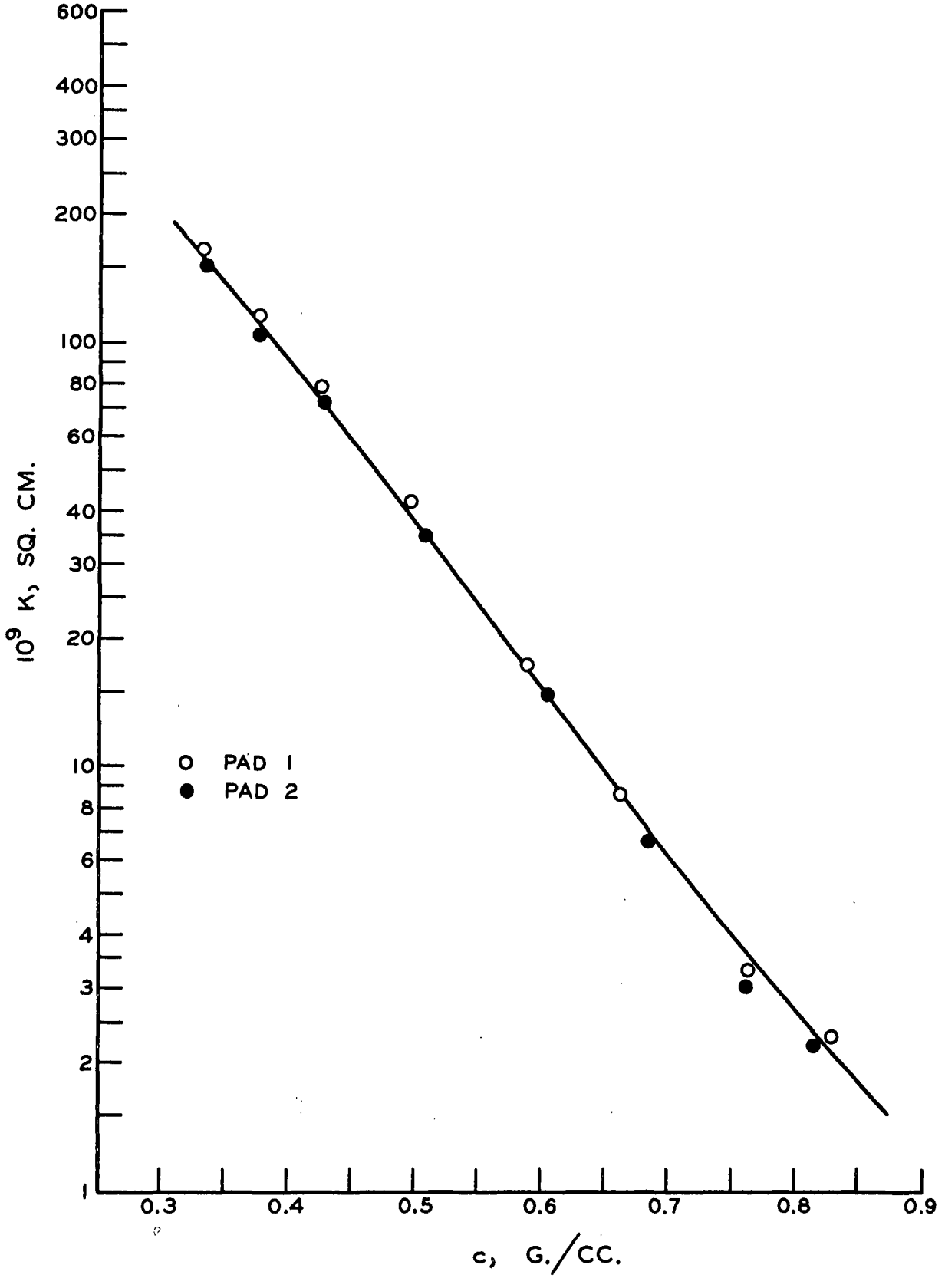

Figure 38. Transverse Permeability
(Sample 9)

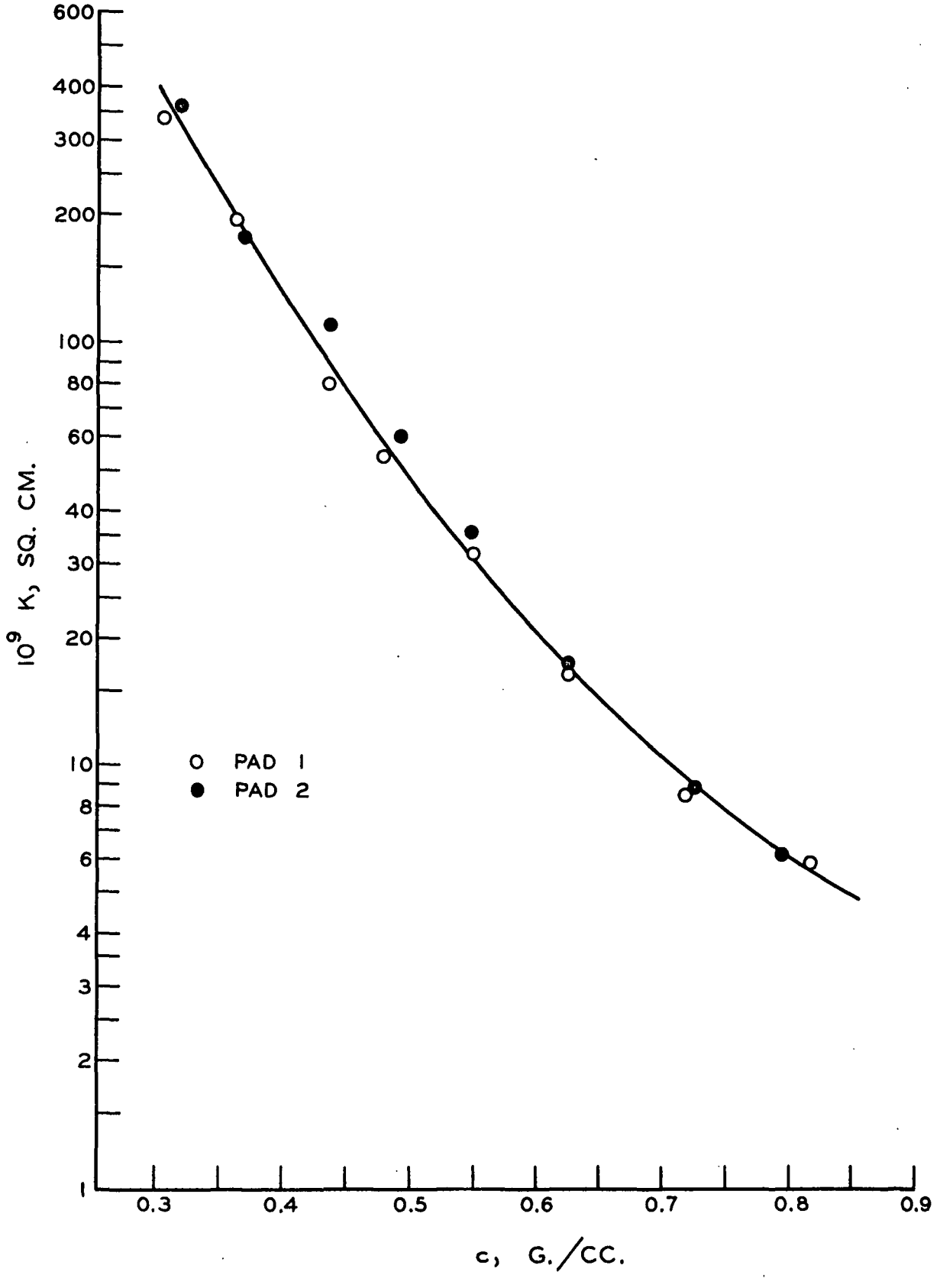

Figure 39. Transverse Permeability
(Sample 10)

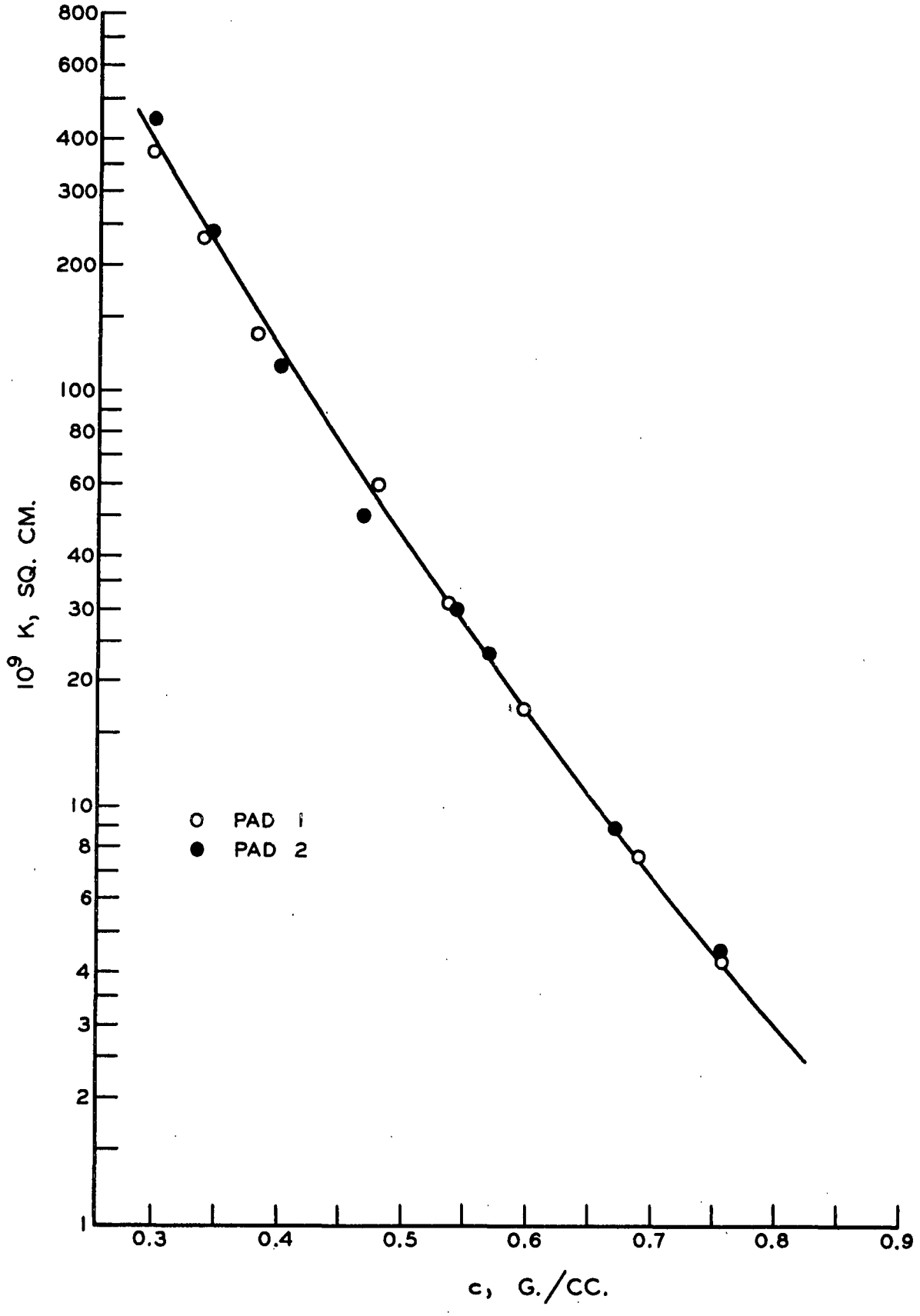

Figure 40. Transverse Permeability
(Sample 11)

APPENDIX III

TABLE XII

WALL CORRECTION FACTOR CALCULATION
(Sample 6)

L_2 cm.	ϵ	$S_o = S_v(1 - \epsilon)$, $cm.^2/cm.^3$	S_c, $cm.^2/cm.^3$	S_c/S_o	$[1 + \frac{1}{2}(S_c/S_o)]^2$
0.222	0.639	418	9.0	0.0215	1.02
0.203	0.606	456	9.84	0.0216	1.02
0.177	0.547	525	11.3	0.0215	1.02
0.150	0.468	616	13.3	0.0216	1.02
0.125	0.375	724	15.9	0.0220	1.02
0.109	0.306	804	18.3	0.0228	1.02
0.099	0.269	847	20.2	0.0238	1.02

S_v = 1158 $cm.^2/cm.^3$.

Cell wall area = 39.2 sq. cm.

TABLE XIII

LATERAL PERMEABILITY DATA

L_2, cm.	c, g./cc.	$10^9 K_{2av}$, $cm.^2$	Av. Dev., %	L_2, cm.	c, g./cc.	$10^9 K_{2av}$, $cm.^2$	Av. Dev., %
	Sample 1				Sample 2		
0.222	0.311	443	3.0	0.203	0.345	328	8.6
0.203	0.336	274	3.9	0.177	0.394	146	9.7
0.177	0.391	99.5	4.3	0.150	0.466	61.9	6.3
0.150	0.472	42.5	6.7	0.125	0.560	20.8	1.7
0.125	0.565	14.4	6.3	0.108	0.650	8.55	7.1
0.108	0.658	4.97	9.4	0.0987	0.706	4.78	8.1
		Av.	5.6			Av.	6.9
	Sample 3				Sample 4		
0.177	0.314	471	3.7	0.177	0.296	674	1.1
0.150	0.371	265	10.1	0.150	0.349	278	5.8
0.125	0.445	110	7.4	0.125	0.418	95.0	3.4
0.108	0.512	68.1	2.9	0.108	0.481	84.0	4.9
0.0987	0.564	37.3	0.7	0.0987	0.530	49.3	5.1
0.0835	0.666	12.3	3.4	0.0835	0.627	11.9	2.1
		Ave.	4.7			Av.	3.7
	Sample 5				Sample 6		
0.222	0.326	279	1.0	0.222	0.348	490	9.1
0.203	0.357	198	6.6	0.203	0.380	316	2.2
0.177	0.410	90.9	6.7	0.177	0.436	145.5	5.5
0.150	0.483	30.0	6.6	0.150	0.514	60.4	2.9
0.125	0.580	13.3	7.9	0.125	0.618	19.8	3.0
0.108	0.667	2.21	3.8	0.108	0.711	4.63	5.0
0.101	0.715	1.17	8.0	0.0987	0.783	1.58	1.9
		Ave	5.8			Av.	4.2

TABLE XIII (Cont'd.)

L_2, cm.	c, g./cc.	$10^9 K_{2av}$, $cm.^2$	Av. Dev., %
	Sample 7		
0.177	0.296	434	5.5
0.150	0.348	209	1.6
0.125	0.419	60.0	5.5
0.108	0.481	55.9	1.6
0.0987	0.530	25.0	3.8
0.0835	0.626	7.09	1.2
		Av.	3.2
	Sample 9		
0.203	0.373	266	7.5
0.177	0.428	121	6.1
0.150	0.504	44.5	8.5
0.125	0.605	14.2	8.3
0.108	0.696	3.70	8.4
0.101	0.746	1.72	8.3
		Av.	7.8
	Sample 11		
0.203	0.295	574	1.5
0.177	0.338	380	6.2
0.150	0.399	231	9.2
0.125	0.478	106.0	1.0
0.108	0.551	65.7	4.4
0.0987	0.605	38.6	4.2
0.0846	0.707	9.35	5.6
		Av.	4.6

L_2, cm.	c, g./cc.	$10^9 K_{2av}$, $cm.^2$	Av. Dev., %
	Sample 8		
0.222	0.337	362	6.9
0.203	0.368	253	3.0
0.177	0.423	95.5	4.9
0.150	0.498	34.8	1.4
0.125	0.598	15.2	4.5
0.108	0.688	2.51	4.7
0.101	0.738	1.17	9.0
		Av.	4.9
	Sample 10		
0.177	0.310	336	10.5
0.150	0.366	179	1.9
0.125	0.439	63.6	3.3
0.108	0.505	45.4	6.8
0.0987	0.556	27.1	6.4
0.0835	0.658	4.45	6.0
		Av.	5.8

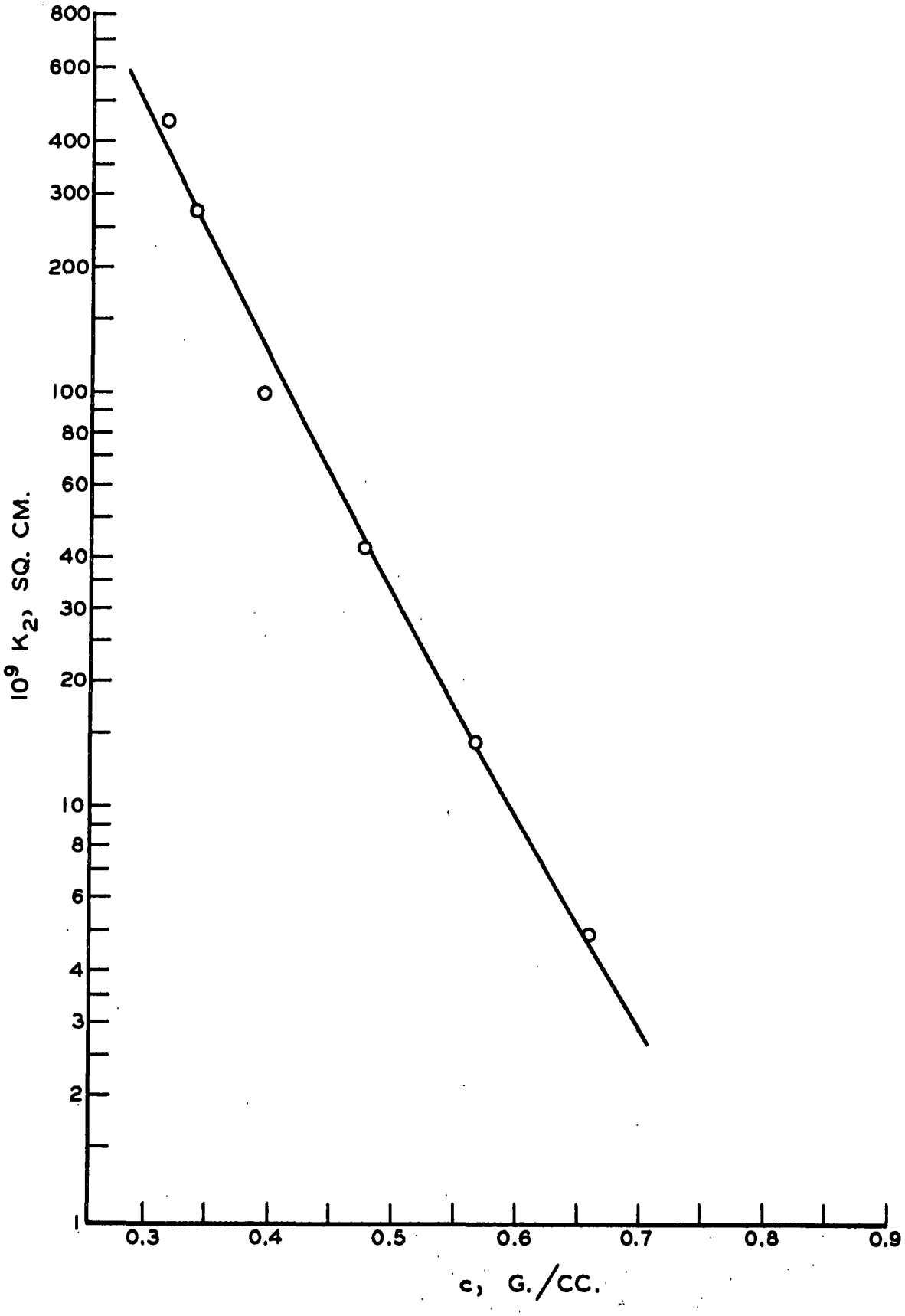

Figure 41. Lateral Permeability
(Sample 1)

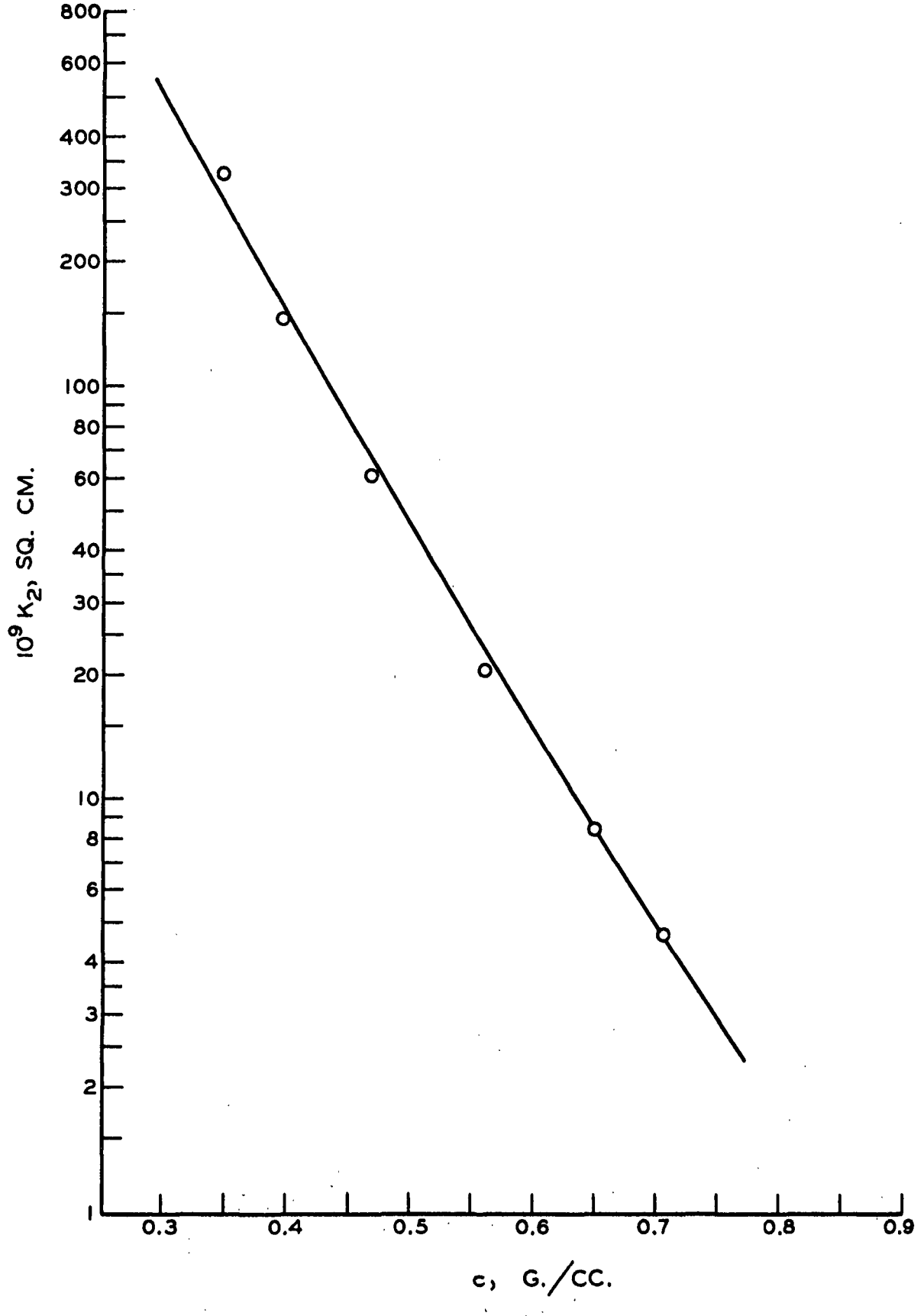

Figure 42. Lateral Permeability
(Sample 2)

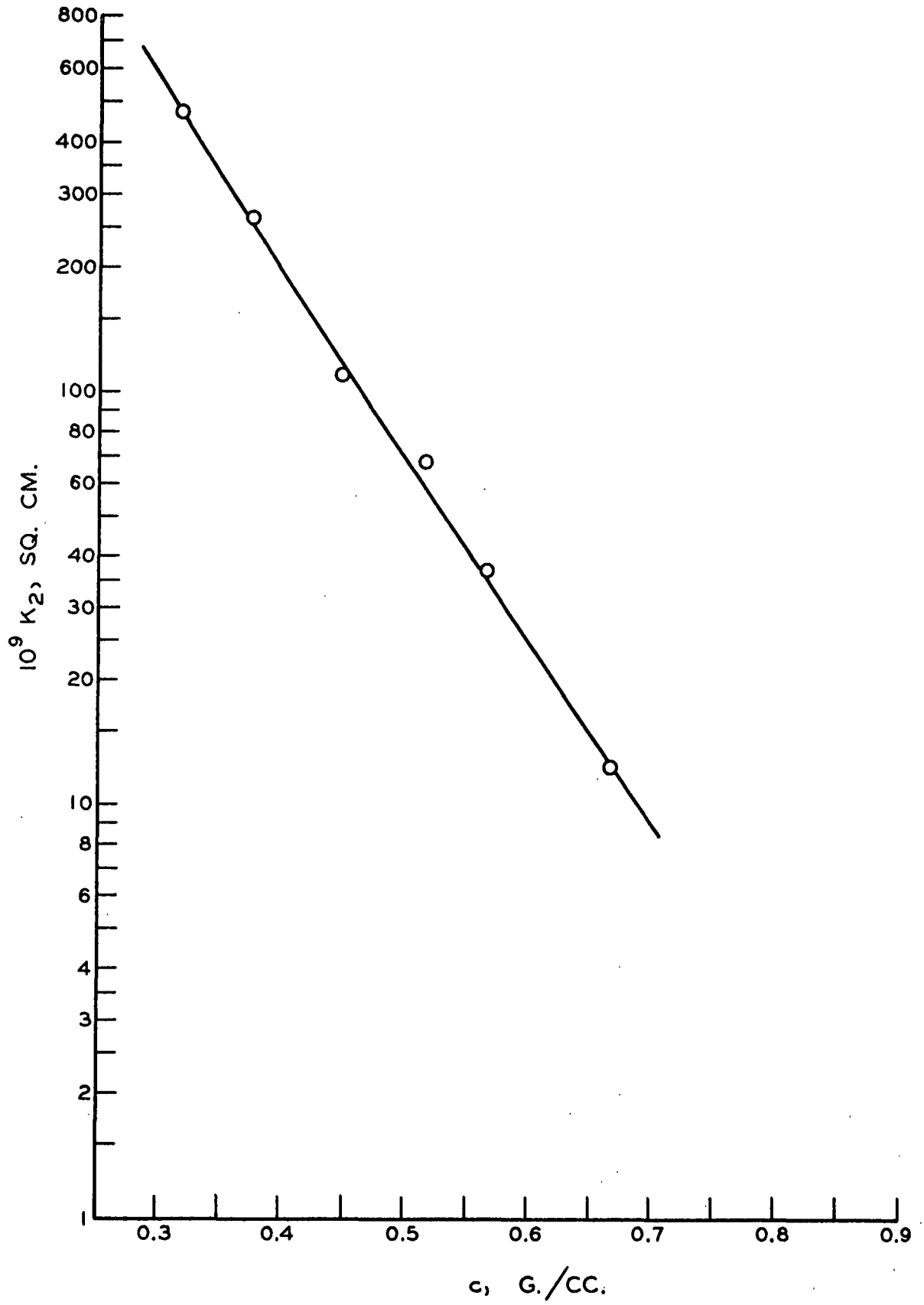

Figure 43. Lateral Permeability
(Sample 3)

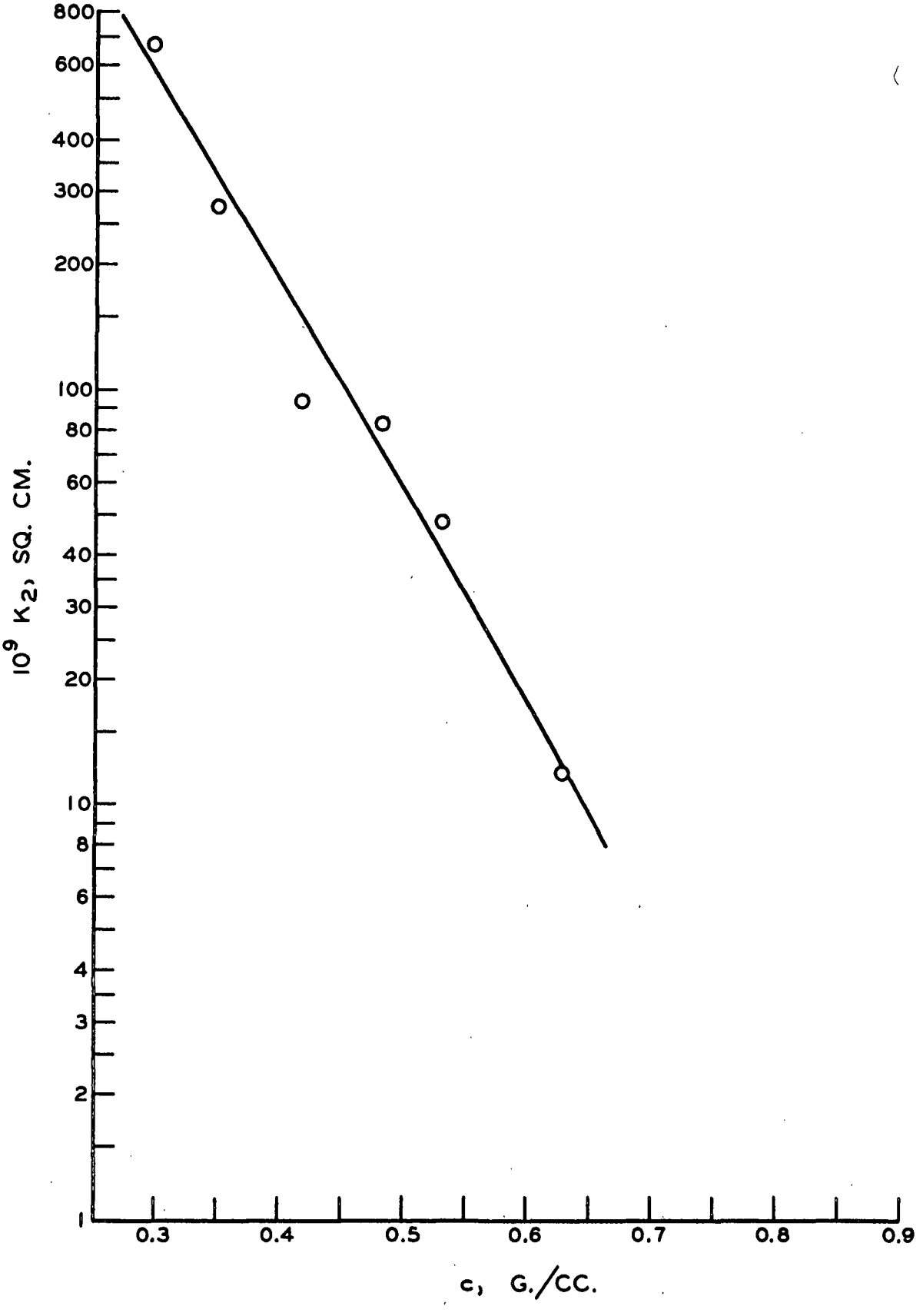

Figure 44. Lateral Permeability
(Sample 4)

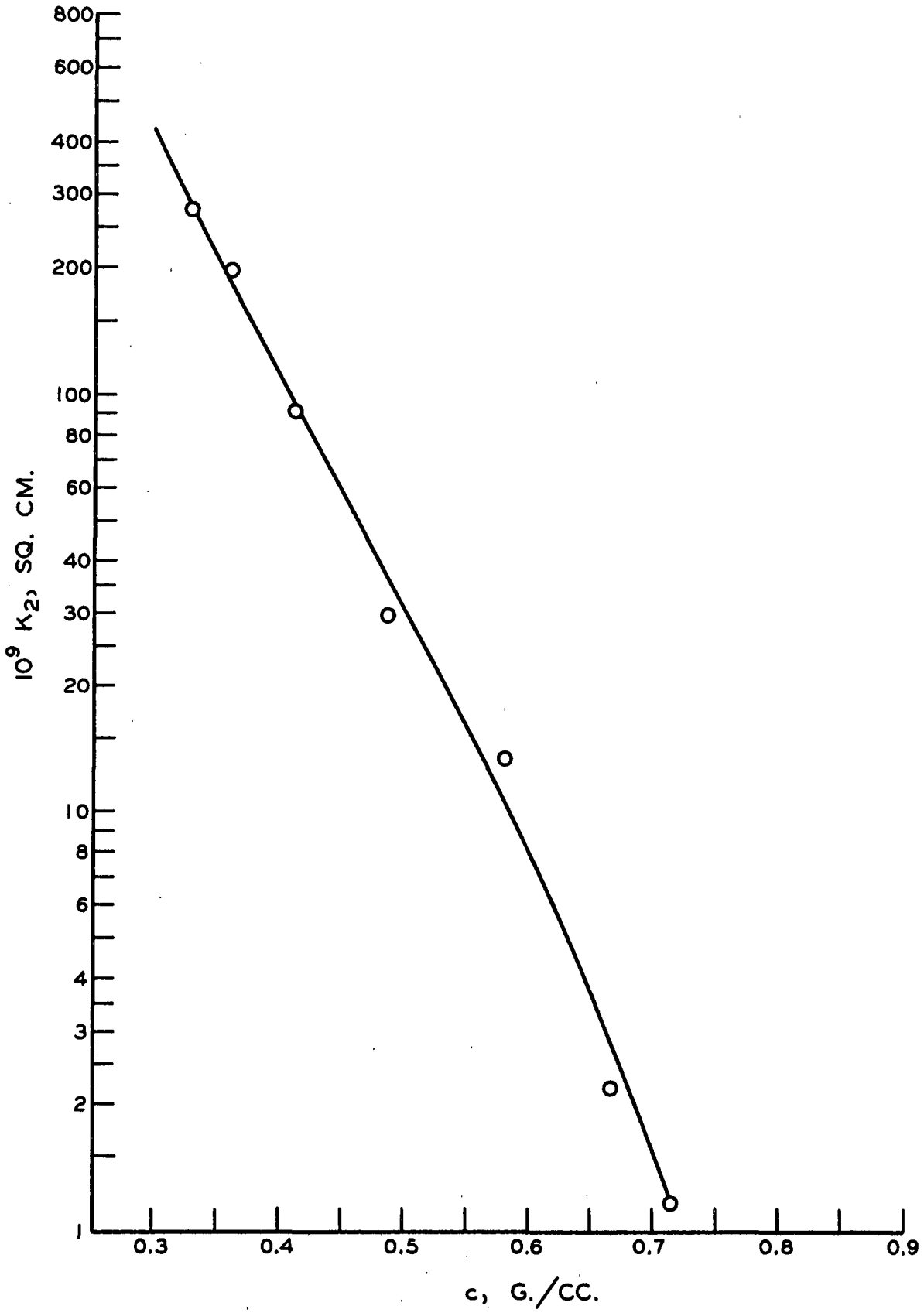

Figure 45. Lateral Permeability
(Sample 5)

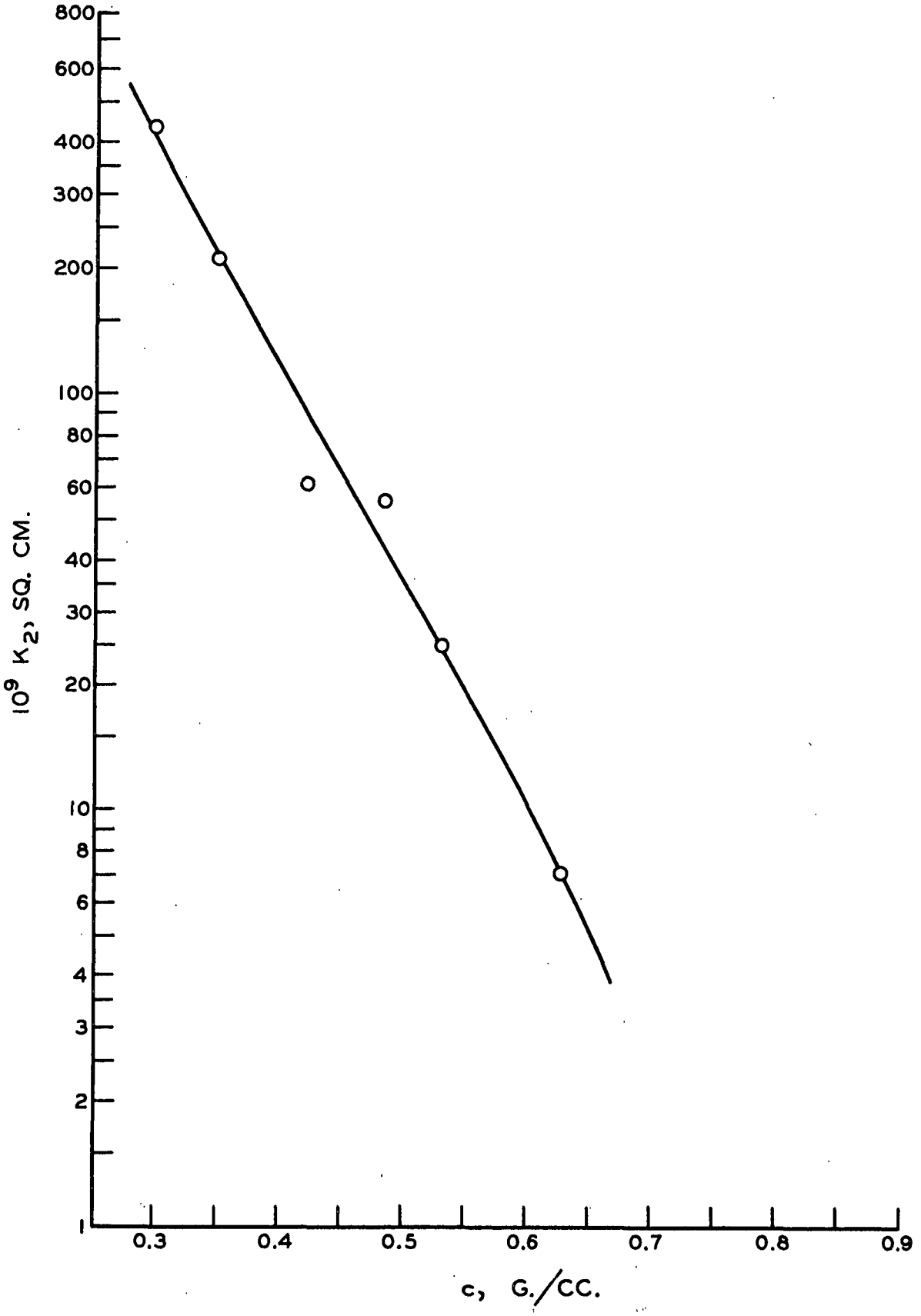

Figure 46. Lateral Permeability
(Sample 7)

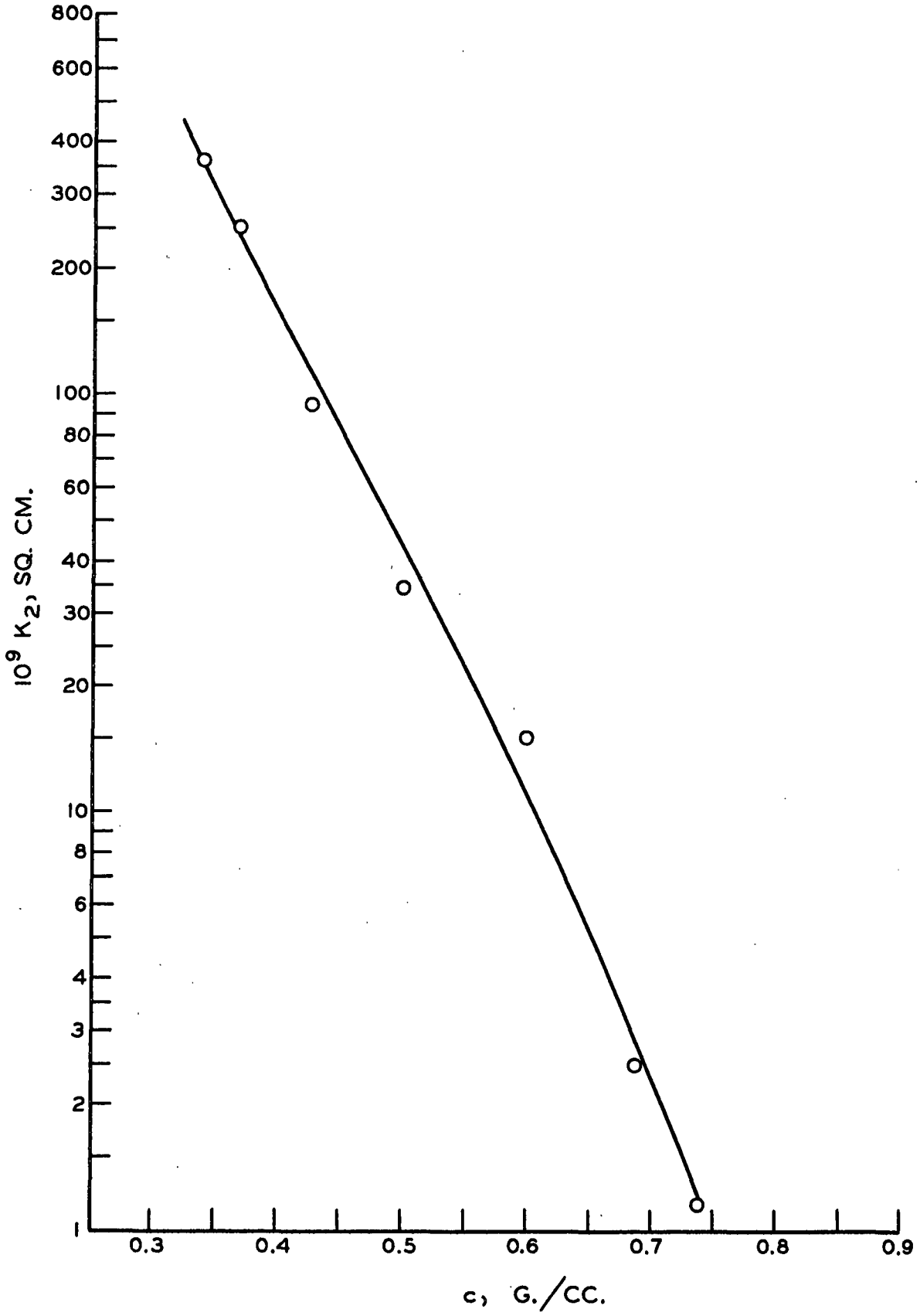

Figure 47. Lateral Permeability
(Sample 8)

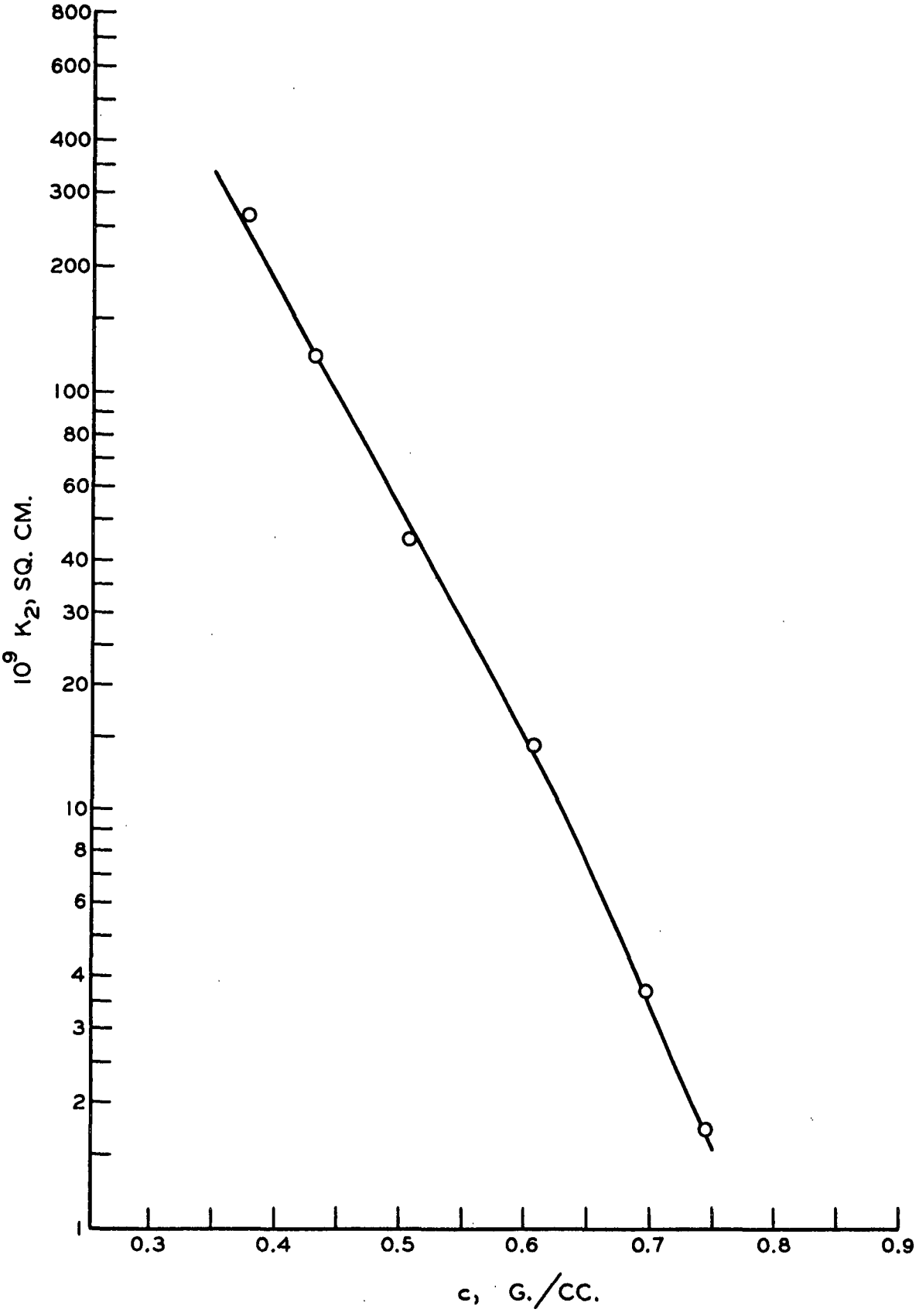

Figure 48. Lateral Permeability
(Sample 9)

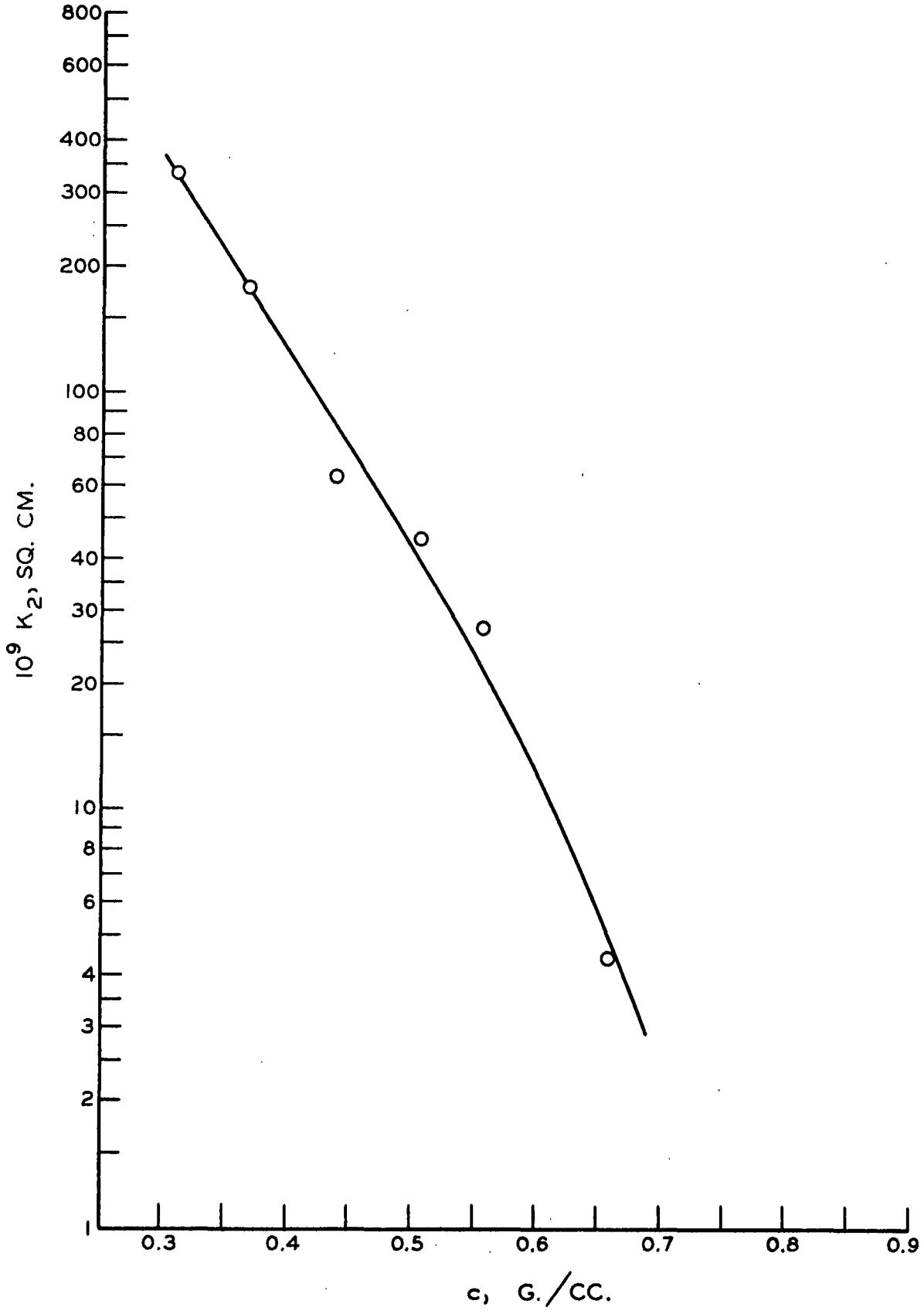

Figure 49. Lateral Permeability
(Sample 10)

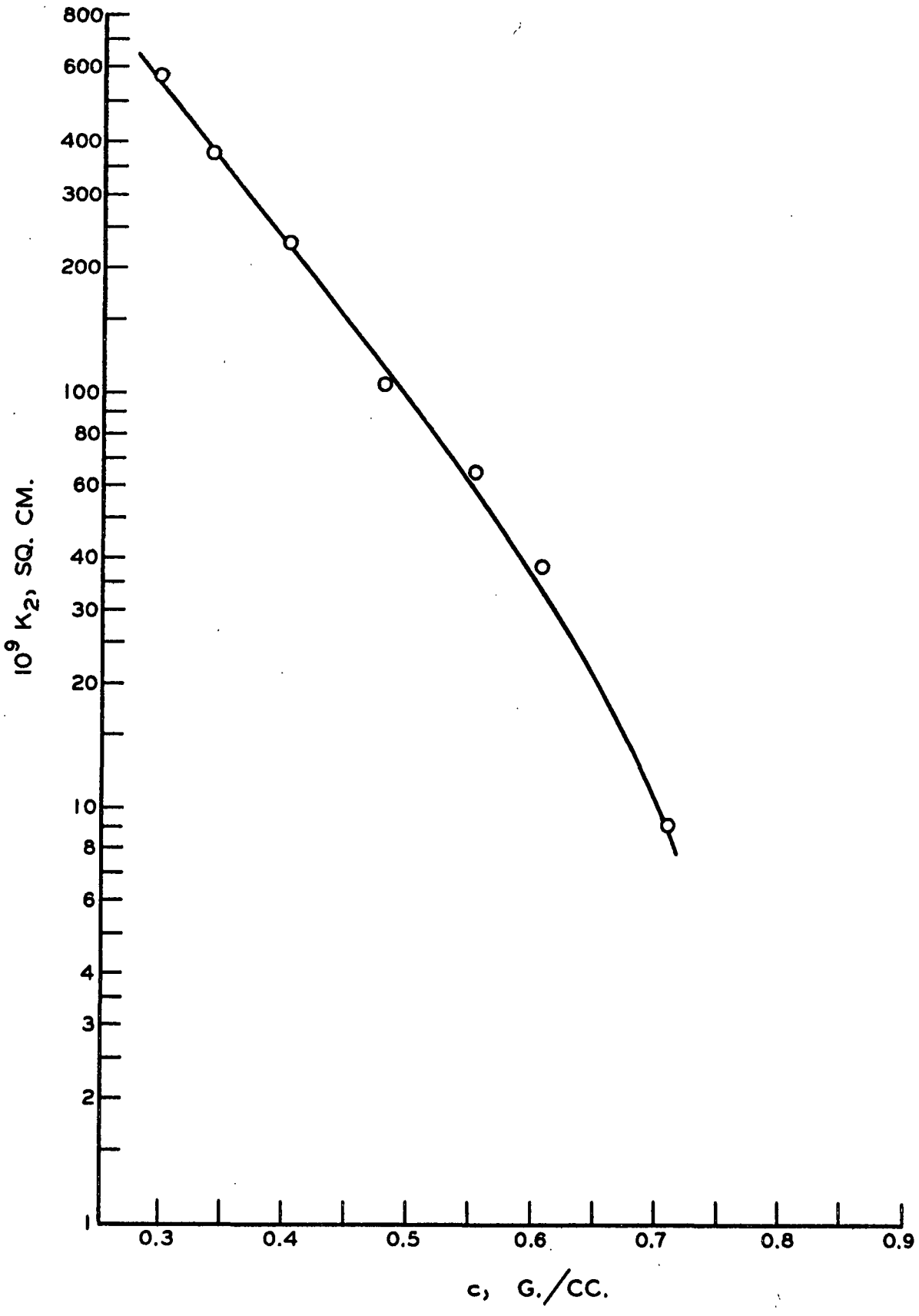

Figure 50. Lateral Permeability
(Sample 11)